

Palacký University, Olomouc

Diploma thesis

Olomouc 2023

Bc. Ľuboslava Ferková

Palacký University, Olomouc
Faculty of Science
Department of Cell Biology and Genetics



**Chromosome organization in cycling and
endoreduplicated nuclei of barley embryo and
endosperm tissues**

Diploma thesis

Bc. Ľuboslava Ferková

Study programme: Molecular and Cellular Biology

Form of study: Full-time

Olomouc 2023

Supervisor: Anna Nowicka, PhD.

UNIVERZITA PALACKÉHO V OLMOUCI

Přírodovědecká fakulta

Akademický rok: 2021/2022

ZADÁNÍ DIPLOMOVÉ PRÁCE

(projektu, uměleckého díla, uměleckého výkonu)

Jméno a příjmení: **Bc. Luboslava FERKOVÁ**
Osobní číslo: **R21925**
Studijní program: **N0511A030046 Molekulární a buněčná biologie**
Téma práce: **Organizácia chromozómov v jadrách deliacich sa mitózou a endoreduplikovaných jadrách embrya a endospermu jačmeňa**
Zadávací katedra: **Katedra buněčné biologie a genetiky**

Zásady pro vypracování

1. Searching and studying literature regarding chromatin organization and its modifications in nuclei of cereal tissue.
2. Growing the plant material and harvesting the seeds on suitable days after pollination.
3. Preparation the material (samples) for sorting nuclei on microscope slides.
4. Analysis of chromatin organization and its modifications in nuclei using fluorescence *in situ* hybridization and immunostaining.
5. Optimization of oligopainting protocol for barley chromosomes and nuclei.
6. Mastering the work with a confocal microscope.
7. Mastering the work with software for microscopic image analysis (e.g. 3D visualization, signal colocalization, fluorescence intensity analysis, Imaris, ImageJ, Photoshop).
8. Mastering the work with software for statistical analysis (Minitab, Statistica).

Rozsah pracovní zprávy:

Rozsah grafických prací:

Forma zpracování diplomové práce: **tištěná**

Jazyk zpracování: **Angličtina**

Seznam doporučené literatury:

- Nowicka A., Kovačik M., Tokarz M., Vrána J., Zhang Y., Weigt D., Doležel J., Pečinka A. (2021): Dynamics of endoreduplication in developing barley seeds. *Journal of Experimental Botany* 72: 268–282, 2021, doi: 10.1093/jxb/eraa453
- Schubert V., Klatt M., Pecinka A., Meister A., Jasencakova Z., Schubert I. (2006): Sister chromatids are often incompletely aligned in meristematic and endopolyploid interphase nuclei of *Arabidopsis thaliana*. *Genetics* 172: 467–475, doi: 10.1534/genetics.105.048363
- Baroux C., Pecinka A., Fuchs J., Kreth G., Schubert I., Grossniklaus U. (2017): Non-random chromosome arrangement in triploid endosperm nuclei. *Chromosoma* 126:115–124, doi: 10.1007/s00412-016-0578-5
- Fuchs J., Demidov D., Houben A., Schubert I. (2006): Chromosomal histone modification patterns – from conservation to diversity. *Trends in Plant Science* 11: 1360–1385, doi: 10.1016/j.tplants.2006.02.008
- Bourdon M., Pirrello J., Cheniclet C., Coriton O., Bourge M., Brown S., Moise A., Peypelut M., Rouyere V., Renaudin J.-P., Chevalier C., Frangne, N. (2012): Evidence for karyoplasmic homeostasis during endoreduplication and a ploidy-dependent increase in gene transcription during tomato fruit growth. *Development* 139: 3817–3826, doi: 10.1242/dev.084053
- Leitch A. (2020): Higher levels of organization in the interphase nucleus of cycling and differentiated cells. *Microbiology and Molecular Biology Reviews* 64(1): 138–152. doi: 10.1128/mmb.64.1.138-152.2000

Vedoucí diplomové práce: **Mgr. Anna Nowicka, PhD.**
Katedra buněčné biologie a genetiky

Datum zadání diplomové práce: **29. října 2021**
Termín odevzdání diplomové práce: **31. července 2023**

L.S.

doc. RNDr. Martin Kubala, Ph.D.
děkan

prof. RNDr. Zdeněk Dvořák, DrSc.
vedoucí katedry

V Olomouci dne 17. března 2023

Bibliographical identification

Author's first name and surname: Luboslava Ferková

Title: Chromosome organization in cycling and endoreduplicated nuclei of barley embryo and endosperm tissues

Type of thesis: Master

Department: Department of Cell Biology and Genetics, FS UP in Olomouc

Supervisor: Anna Nowicka, Ph.D.

The year of presentation: 2023

Keywords: barley, embryo, endoreduplication, endosperm, fluorescence *in situ* hybridization, immunostaining, nucleolus, Rab1 chromatin organization, seed, sister chromatids

Number of pages: 61

Number of appendices: 1

Language: English

Abstract: Cereal seeds are one of the most important sources of energy for humans and domestic animals, owing to their large and nutritious endosperm tissues. The functions of seeds include protection of the embryo, survival in difficult conditions and nutrition of the embryo during germination. Seed development is a very complex process, little is known about the structure and organization of the chromosomes in seed tissues.

The main goal of this master thesis was to analyze chromosome organization in cycling and endoreduplicated nuclei isolated from embryo and endosperm tissues of developing barley seeds. First, on the basis of a comparative karyotype analysis, the appropriate barley accession was selected for further research. Then, using fluorescence *in situ* hybridization, sister chromatid cohesion at *45S* and *5S rDNA* loci was investigated. To investigate the coherence of sister chromatids in specific chromosome segments, attempts were made to optimize the oligo-FISH staining protocol. Further, using FISH-associated immunolabeling, nucleoli changes were studied. Finally, by using FISH combined with image rendering, the Rab1 chromosome organization was investigated.

Altogether showed that endoreduplication alters chromosome and chromatin organization in a tissue- and seed-age-dependent manner, which may be accompanied by programmed cell death.

Bibliografické údaje

Meno a priezvisko autora: Ľuboslava Ferková

Názov práce: Organizácia chromozómov v jadrách deliacich sa mitózou a endoreduplikovaných jadrách embrya a endospermu jačmeňa

Typ práce: diplomová

Pracovisko: Katedra buněčné biologie a genetiky, PřF UP v Olomouci

Vedúci práce: Mgr. Anna Nowicka, Ph.D.

Rok obhajoby práce: 2023

Kľúčové slová: embryo, endoreduplikácia, endosperm, fluorescenčná *in situ* hybridizácia, imunofarbenie, jačmeň, jadierko, Rabl organizácia chromatinu, semeno, sesterské chromatídy

Počet strán: 61

Počet príloh: 1

Jazyk: anglický

Súhrn: Semená obilnín sú jedným z najdôležitejších zdrojov energie pre ľudí a domáce zvieratá vďaka svojmu výživnému tkanivu - endospermu. Medzi funkcie semien patrí ochrana embrya, prežitie v ťažkých podmienkach a výživa embrya počas klíčenia. Na lepšie pochopenie procesu vývoja semien je potrebné vedieť viac o štruktúre a organizácii chromozómov v ich bunkových jadrách.

Hlavným cieľom tejto diplomovej práce bolo analyzovať organizáciu chromozómov v mitoticky sa deliacich a endoreduplikovaných jadrách izolovaných z tkanív embrya a endospermu vyvíjajúcich sa semien jačmeňa. Ako prvé bol na základe porovnávacej analýzy karyotypov vybraný príslušný kultivar jačmeňa. Ďalej bola pomocou fluorescenčnej *in situ* hybridizácie študovaná kohézia sesterských chromatíd na *45S* a *5S rDNA* lokusoch. Na vylepšenie experimentu bol optimalizovaný protokol pre farbenie oligo-FISH na špecifických chromozomálnych segmentoch. Ďalej pomocou imunoznačenia spojeného s FISH bolo možné študovať zmeny jadriek v jadrách. Nakoniec bola pomocou FISH v kombinácii s vykreslením obrazu skúmaná Rabl organizácia chromozómov.

Celkovo sa ukázalo, že endoreduplikácia mení organizáciu chromozómov a chromatinu v závislosti od typu tkaniva a veku semien. Daný proces môže byť sprevádzaný programovanou bunkovou smrťou.

Declaration

I declare that this diploma thesis was written independently with the help of my supervisor, Anna Nowicka, PhD., and using the sources listed in the reference.

In Olomouc

.....

Luboslava Ferková

Acknowledgement

I would like to thank my supervisor Anna Nowicka, PhD. for time, patience, professional guidance, and valuable advice that helped me complete this work. I would also like to thank the whole scientific team under the leadership of Aleš Pečinka, PhD. for help and patience during my presence in the laboratory. I would like to thank Mahmoud Said, PhD. for sorting the nuclei on slides and Ms. Zdeňka Dubská for cell synchronization.

TABLE OF CONTENT

ABBREVIATIONS	viii
FIGURES	ix
TABLES.....	x
1 INTRODUCTION	1
2 AIMS OF THE THESIS	2
3 LITERATURE REVIEW.....	3
3.1 BARLEY TAXONOMY, MORPHOLOGY, AND IMPORTANCE.....	3
3.2 SEED DEVELOPMENT	3
3.2.1 Embryo development	5
3.2.2 Endosperm development.....	5
3.2.3 Seed maternal tissues	7
3.3 CELLULAR PROCESSES ACCOMPANIED SEED DEVELOPMENT	8
3.4 GENOME ARCHITECTURE: DOMAIN ORGANIZATION OF INTERPHASE CHROMOSOMES.....	9
3.4.1 Barley mitotic chromosomes.....	9
3.4.2 Major chromosomal landmarks.....	9
3.4.3 Interphase chromosome configuration.....	11
3.5 METHODS USED TO STUDY THE ORGANIZATION OF CHROMOSOMES IN INTERPHASE	13
3.5.1 Fluorescence <i>in situ</i> hybridization.....	13
3.5.2 Immunostaining.....	15
3.5.3 ImmunoFISH	15
3.5.4 Image collection and analysis	16
4 MATERIALS AND METHODS	17
4.1 PLANT MATERIAL	17
4.2 MATERIALS AND EQUIPMENT	17
4.2.1 Laboratory equipment	17
4.2.2 Small laboratory equipment	19
4.2.3 Software	20

4.2.4 Chemicals.....	20
4.2.5 Preparation of stock solutions	22
4.2.6 Preparation of working solutions	23
4.3 PLANT GROWTH CONDITIONS AND ESTIMATING DAYS AFTER POLLINATION	26
4.4 EXPERIMENTAL SETUP AND EVALUATION PROCEDURES	26
4.4.1 Mitotic chromosome preparation	27
4.4.2 Nuclei isolation and flow-sorting.....	28
4.4.3 Fluorescence <i>in situ</i> hybridization.....	29
4.4.4 ImmunoFISH	31
4.4.5 Microscopy.....	31
4.4.6 Image analysis.....	32
4.4.7 Statistical analysis	33
5 RESULTS	34
5.1 SELECTION GENOTYPE AND CHROMOSOMAL LANDMARKS FOR FURTHER EXPERIMENTS	34
5.2 STUDY OF LOCUS-SPECIFIC SISTER CHROMATID ALIGNMENT IN MITOTICALLY DIVIDING AND ENDOREDUCATED NUCLEI	35
5.3 OPTIMALIZATION OF OLIGOPAINTING-FISH TO STUDY SISTER CHROMATID COHESION AT SPECIFIC CHROMOSOMAL SEGMENTS.....	38
5.4 CHARACTERIZATION OF NUCLEOLI IN CYCLING AND ENDOREDUCATED NUCLEI.....	39
5.5 STUDY OF RABL CHROMOSOME CONFIGURATION IN SEED NUCLEI	43
6 DISCUSSION	47
6.1 Selection the genotype and cytogenetic markers	47
6.2 Sister chromatid cohesion at <i>45S</i> and <i>5S rDNA</i> loci	47
6.3 Testing the chromosome-arm-specific oligopainting probes	48
6.4 Nucleoli organization study	49
6.5 Rabl chromosome configuration in mitotically active and endoreduplicated nuclei	50
7 CONCLUSION.....	51

8 REFERENCES.....	52
9 APPENDICES	61

ABBREVIATIONS

AGPase	ADP-glucose pyrophosphorylase
AL	aleurone layer
ANOVA	analysis of variance
BETL	basal endosperm transfer layer
BSA	bovine albumin serum
CSE	central starchy endosperm
CV.	cultivar
DAG	days after germination
DAP	days after pollination
DFC	dense fibrillar component
dTTP	deoxythymidine triphosphate
ESR	embryo-surrounding region
FC	fibrillar centers
FISH	fluorescence <i>in situ</i> hybridization
FITC	fluorescein isothiocyanate
GC	granular component
PCD	programmed cell death
RAM	root apical meristem
RMS	radial microtubular system
RT	room temperature
SAL	subaleurone layer
SC	sister chromatid

FIGURES

Figure 1: Seed development in maize.	4
Figure 2: Structure and phenotype of development barley seeds, cultivar Compana	5
Figure 3: Stages and timing of barley endosperm development.	6
Figure 4: Schematic drawing showing the differences between the mitotic cycle and endocycle 8	
Figure 5: Structural and functional domains of the nucleolus	11
Figure 6: Interphase chromosome configurations	12
Figure 7: Schematic drawing showing two types of probe labeling	14
Figure 8: Explanation of the principle of immunostaining in the detection of a specific protein 15	
Figure 9: Schematic drawing of experimental setup used in this master thesis	27
Figure 10: Karyotypes of four barley accessions	35
Figure 11: Sister chromatid cohesion at 5S and 45S rDNA loci of barley seed nuclei.....	37
Figure 12: Fluorescence <i>in situ</i> hybridization with oligo-probes hybridizing to three regions on 6H barley chromosome	38
Figure 13: Microscopic characteristics of the nucleoli in cycling and endoreduplicated nuclei. 40	
Figure 14: Nucleoli organization in cycling and endoreduplicated embryo and endosperm nuclei	41
Figure 15: Location of FIBRILLARIN protein in nucleoli.....	42
Figure 16: Metaphase chromosomes of RAM after FISH with centromeric and telomeric probes	43
Figure 17: Three phenotypes of chromosome organization at interphase nuclei of barley seeds 44	
Figure 18: Graphs for Rab1 chromosome organization.....	46

TABLES

Table 1: Preparation of hybridization mix 30

1 INTRODUCTION

Seeds represent an enveloped embryonic stage unique to angiosperms and gymnosperms. Seed development is initiated by the act of double fertilization, during which the two nuclei in the pollen grain migrate to the embryo sac in the ovule. One nucleus fuses with the egg cell, while the second fuses with the diploid central nucleus. Subsequently, a diploid embryo (2x, one female and one male genome copies) and a triploid endosperm (3x, two female and one male genome copies) are formed. The developing embryo and endosperm are surrounded by seed maternal tissues of maternal origin (2x).

While passing through different stages of the cell cycle, chromosomes have to perform manifold functions including replication, transcription or repair. To optimally conduct these operations, chromatin is folded at different levels and precisely organized with respect to each other and cellular environment. The arrangement of chromatin within interphase nuclei seems to depend on tissue and developmental stage. We hypothesized, that endocycle which is alternative cell cycle, will trigger changes in chromatin reorganization. To test this, sister chromatids alignment, nucleoli organization, and Rab1 chromosome organization in mitotically dividing and endoreduplicated nuclei isolated from embryo and endosperm tissues were investigated.

2 AIMS OF THE THESIS

The following work objectives were set for the preparation of the master thesis:

- Searching and studying literature regarding chromatin organization and its modifications in nuclei of cereal tissue.
- Growing the plant material and harvesting the seeds on suitable days after pollination.
- Preparation the material (samples) for sorting nuclei on microscope slides.
- Analysis of chromatin organization in nuclei using fluorescence *in situ* hybridization (FISH) and immunostaining combined with FISH.
- Optimalization of oligopainting protocol for barley chromosomes and nuclei.
- Mastering the work with a confocal microscope.
- Mastering the work with software for microscopic image analysis (e.g., 3D visualization, signal colocalization, fluorescence intensity measurements, Imaris, ImageJ, Photoshop).
- Mastering the work with software for statistical analysis (Minitab, Statistica).

3 LITERATURE REVIEW

3.1 BARLEY TAXONOMY, MORPHOLOGY, AND IMPORTANCE

Cultivated barley (*Hordeum vulgare* subsp. *vulgare*, $2n = 2x = 14$, HH, 4.88 Gbp/1C) was domesticated about 10,000 years ago from its progenitor wild barley (*H. vulgare* subsp. *spontaneum*, $2n = 2x = 14$). Genus *Hordeum*, like wheat and rye, belongs to the *Triticeae* tribe of grasses, most conspicuously characterized by their inflorescence that is a spike instead of the panicle that occurs in most other grasses (Blattner, 2018). Both cultivated and wild barleys are annuals. There are two main types of barley cultivars, i.e., winter barleys require a period of cold stimulus (vernalization/6-8 weeks) to initiate floral development, and spring barleys do not require vernalization (Ibrahim *et al.*, 2018). Wild barley represents intermediate phenotype, called facultative type, and requires short time of cold (3 weeks) to induce flowering. Barley is a model experimental system for cereals because of its short life cycle (5-6 months for spring type) and morphological, physiological, and genetic characteristics. It ranks fourth in world cereal crop production and is used for animal feed (70%), brewing malts (21%), human food (6%) (Tricase *et al.*, 2018). Furthermore, there is a growing interest in using barley for biofuel, cosmetics, and molecular farming (3%) (Hicks *et al.*, 2014; Holásková *et al.*, 2018).

3.2 SEED DEVELOPMENT

Seeds of Angiosperms (= flowering plants) enclose the embryonic stage of their life cycle, survive long periods of unfavorable conditions, serve as propagation units for colonization of new sites and provide the embryo with nutrition during the first days after germination (Bewley *et al.*, 2006). Seeds allowed vascular plants conquering the land, by maximizing the success of embryo development (reviewed in Pires, 2014). Long storability together with high-energy and nutrition content made seeds the prime source of food for humans and domestic animals. In most flowering plants, including barley, the female gametophyte is the seven-celled embryo sac, containing haploid egg cell, diploid central cell, two haploid synergids and three haploid antipodes. The male gametophyte is a mature pollen grain, which consists of tri-cellular structure containing two haploid sperm cells and one haploid vegetative cell (Mascarenhas, 1989). Seed development in Angiosperm is initiated by the act of double fertilization, which occurs in two events (Figure 1a). The first fertilization happens, when one sperm cell from pollen grain fuses with an egg cell which generates diploid ($2n$) zygote. In parallel, the second sperm cell merges with central cell, giving rise to triploid ($3n$) cell (Sabelli and Larkins, 2009). The zygote proliferates into an embryo, while the triploid cell develops to an endosperm. The endosperm functions consist of control of seed development, nourishing the embryo, preventing premature germination, and providing energy to the germinating plant (Berger *et al.*, 2008). The amount of

endosperm in mature seeds varies greatly between species. Many dicots, including model species *Arabidopsis thaliana* (*Arabidopsis*), represent example where developing embryo consumes most of the endosperm prior to the seed maturation. In contrast, grasses (*Poaceae*) have generally large endosperm, and especially cereals including barley have been bred for its high nutritional value (Sabelli and Larkins, 2009).

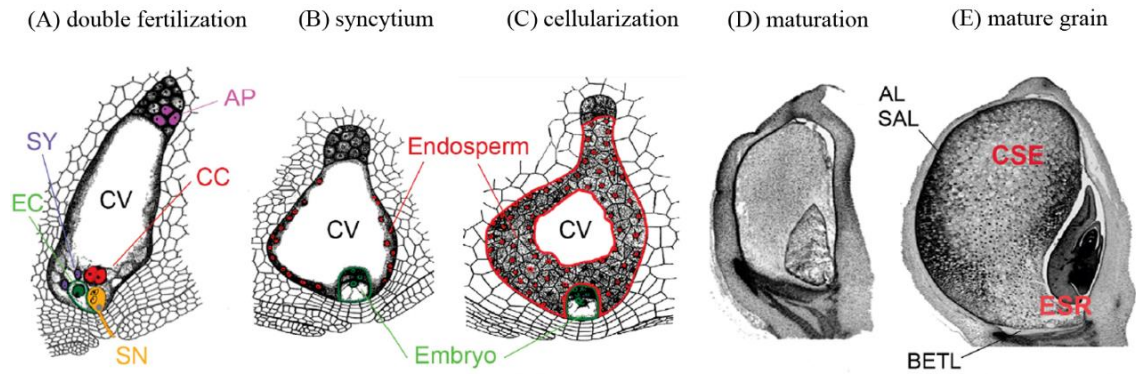


Figure 1: Seed development in maize.

(A) **Double fertilization:** two sperm nuclei (SN, yellow) move via the pollen tube into the ovule, where they fuse with the egg cell nucleus (EC, dark green) and the central cell nucleus (CC, red). The synergids (SY, violet) and antipodals (AP, pink) do not participate in fertilization. Central vacuole (CV) occupies a large part of the mature embryo sac. (B) **Syncytium:** endosperm nuclei (red) are pushed to the cell wall by CV. Embryo starts dividing. (C) **Cellularization:** cell walls are established between endosperm nuclei and these nuclei further divide. This stage is associated with highly dynamic microtubule organization. (D) By further growth the seed reaches **maturing** and finally (E) **mature grain** stage with fully developed embryo and five endosperm domains: the central starchy endosperm (CSE), the subaleurone layer (SAL), the aleurone layer (AL), the basal endosperm transfer layer (BETL) and the embryo-surrounding region (ESR). According to Sabelli and Larkins, 2009 with modifications.

In cereals, seed development is usually divided into three partially overlapping stages: an early-development (stage I) is initiated by double fertilization and followed by cell proliferation and slight weight gain; mid-development (stage II) includes differentiation of the main tissue types, large weight increase accompanied by accumulation of storage compounds, and late-development (stage III) characterizes the maturation, reduction of seed weight associated with desiccation and finally reaching the physiological maturation and dormancy (Sabelli and Larkins, 2009). After that, seed is ready for a quiescent period and germination (Angelovici *et al.*, 2010; Sreenivasulu *et al.*, 2010; Dante *et al.*, 2014). Barley grain development lasts around 7 weeks (Figure 2; Nowicka *et al.*, 2021).

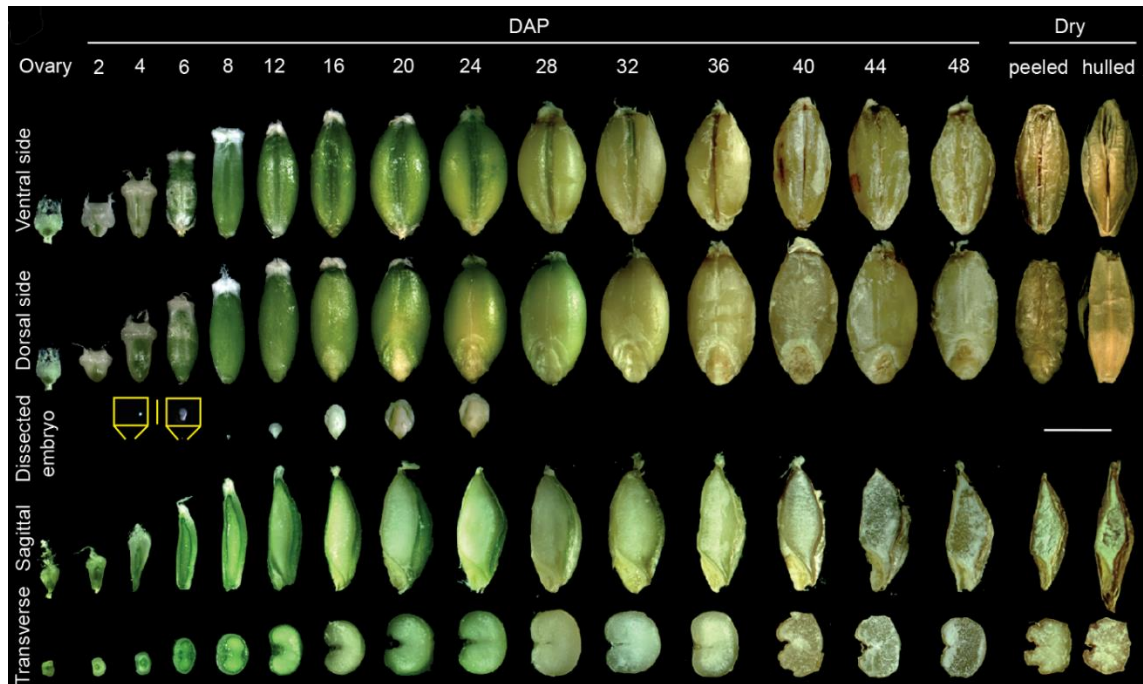


Figure 2: Structure and phenotype of development barley seeds, cultivar Compana. Seed developmental series from 0 (ovary) up to 48 days after pollination (DAP) and in dry seeds. For analysis of sagittal and transverse sections, the seeds were cut into half. Scale bar=5 mm. The yellow insets show early-stage embryos with scale bar=500 μm . According to Nowicka *et al.*, 2021 with modifications.

3.2.1 Embryo development

Zygote undergoes a transverse division to form apical and basal cells of approximately equal size, which develop into proper embryo and suspensor, respectively (Norstog, 1972). Then, the embryo continues cell proliferation and differentiation. The mature embryo comprises the embryonic axis with coleorhiza surrounding the radicle (embryonic root) and coleoptile enclosing the shoot apical meristem and plumule (primary leaf), and the scutellum (cotyledon) (Rodríguez *et al.*, 2015; Liew *et al.*, 2019). The embryo encloses all compartments necessary for a new plant development (Dante *et al.*, 2014).

3.2.2 Endosperm development

Endosperm development includes several, partially overlapping phases. The proliferation of endosperm begins with syncytial (also known as coenocyte) stage, where synchronously dividing nuclei are pushed to the periphery by the central vacuole (Figure 1b; Figure 3). It is an evolutionary strategy for the endosperm tissue to grow and prepare for storage compounds production without spending a lot of energy (Sabelli and Larkins, 2009; Dante *et al.*, 2014). Syncytium stage takes up to 6 days after pollination (DAP) (Brown *et al.*, 1994). The next phase, cellularization (Figure 1c; Figure 3), is initiated by formation of radial microtubular systems

(RMS). It's a system of microtubules emanating from the nucleolar membrane, gradually forming the cell wall. The tube-like structures, called alveoli, are formed around each nucleus. They start to divide in a periclinal division plane, which is followed immediately by cytokinesis (Brown *et al.*, 1994; Olsen, 2001; Olsen, 2004). After 5 or 6 divisions, the central vacuole is completely gone and replaced by cellular endosperm. In barley, the cellularization event takes place at 6 – 8 DAP (Sabelli and Larkins, 2009; Olsen, 2004), and fully cellularized endosperm contains ~2 000 nuclei (Bennett *et al.*, 1975).

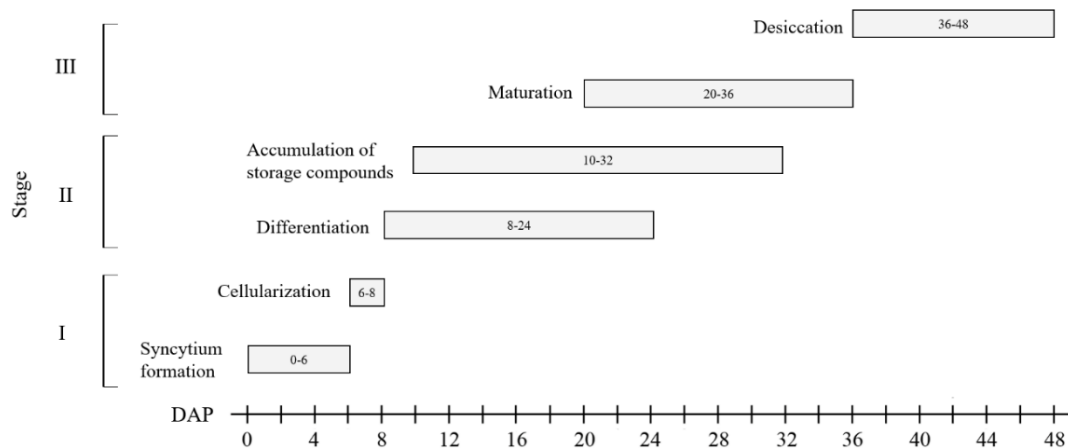


Figure 3: Stages and timing of barley endosperm development. Time period expressed in days after pollination (DAP). According to Brown *et al.*, 1994 with modifications.

The differentiation stage is recognized by formation of the five endosperm tissue types. During this time mitotic cell cycle is replaced by endocycles (explained further), and endosperm accumulates the storage compounds (Figure 1c, Figure 3). The mature grain contains five endosperm domains: the embryo-surrounding region (ESR), the basal endosperm transfer layer (BETL), the subaleurone layer (SAL), the aleurone layer (AL), and the central starchy endosperm (CSE) (Figure 1d-e) (Olsen, 2001; Sabelli and Larkins, 2009).

The ESR cells start to differentiate first, at around 4 DAP. It is composed of several cell layers adjacent the embryo. In parallel with embryo growing, the ESR undergoes PCD (programmed cell death) (Sabelli and Larkins, 2009). ESR cells are dense in cytoplasmic composition, they have a lot of small vacuoles and a complex membrane system. The function of ESR is yet unclear, but it is believed, that it separates the embryo from endosperm and at the same time ensures transportation of nutrients between these two components (Olsen 2001; Olsen, 2004; Sabelli and Larkins, 2009).

The BETL cells differentiate before cellularization is completed. They are located near main vascular seed maternal tissue. Transfer cells are used for transporting nutrients, mainly sucrose,

amino acids and monosaccharides between maternal plant and endosperm compartments. This transport is possible due to their extensive cell wall invaginations and plasma membrane surface (Olsen 2001; Olsen, 2004; Sabelli and Larkins, 2009).

The SAL and AL cover the whole perimeter of the endosperm except for the transfer layer. In barley, the differentiation of the three layers of AL start during cellularization. The AL is visible by accumulation of small vacuoles and dense cytoplasm (Sabelli and Larkins, 2009). There are a lot of aleurone grains present, which are vacuoles (lytic or protein-storage) with inclusion bodies. In contrast to other cereals, in barley AL cells do not undergo endocycles (Olsen, 2001; Nowicka *et al.*, 2021). The function of this layer is to mobilize storage nutrients such as starch and proteins. They produce hydrolases, glycanases and proteinases after hormone stimulation from the embryo (Olsen, 2004). Towards the end of maturation stage, the seed/ endosperm undergoes desiccation, but only AL nuclei remain alive (Olsen 2001; Olsen, 2004).

The SCE is the largest part of endosperm. These cells contain one important enzyme called ADP-glucose pyrophosphorylase (AGPase), that contributes to the synthesis of starch. In the presence of sucrose, the AGPase in cytosol can facilitate starch biosynthesis. Thanks to three more enzymes that are stored in amyloplasts, the starch is then produced and packed into granules. Starchy endosperm cells also produce prolamin storage proteins (Olsen, 2001; Sabelli and Larkins, 2009). In barley, the SCE cells undergoes two rounds of endoreduplication (Nowicka *et al.*, 2021).

3.2.3 Seed maternal tissues

Seed maternal tissues consist of the nucellus, the nucellar projection, the testa and the pericarp (Sreenivasulu *et al.*, 2010; Rodríguez *et al.*, 2015). In the nucellus is embedded the embryo sac, which is progressively degraded after double fertilization, providing space and nutrients for the early endosperm. Only the nucellar region opposite to the main vascular bundle stays alive and differentiates into the nucellar projection, which is responsible for the nutrient transfer inside the seed (Gubatz *et al.*, 2007; Radchuk *et al.*, 2010). The barley grain is enclosed by seed coats created by the nucellar epidermis and the testa preceded by cuticle layers. The pericarp is a multilayered structure with embedded vascular bundles (Sreenivasulu *et al.*, 2010; Rodríguez *et al.*, 2015). During the cellularization of endosperm, the pericarp enlarges by cell elongation and undergoes programmed cell death. Seed coats/pericarp contain a high amount of starch and are protective structures (Sreenivasulu *et al.*, 2010; Sabelli *et al.*, 2013). In addition, the entire barley seed is protected by hulls (consisting of the glumellae – lemma and palea) of maternal origin, that may remain tightly attached to the caryopsis after ripening (Rodríguez *et al.*, 2015).

3.3 CELLULAR PROCESSES ACCOMPANIED SEED DEVELOPMENT

All changes during the whole seed development are accompanied by cellular processes, i.e., mitotic cell cycle, endocycle and PCD.

Mitotic cell cycle consists of 4 phases: a DNA pre-synthetic G1-phase, S-phase where DNA is synthesized, a DNA post-synthetic G2-phase and M-phase, where mitosis takes place. This canonical cell cycle involves duplication of chromosomes, their segregation and cytokinesis into two daughter cells. C-value is the amount of nuclear DNA in one chromosomal set (haploid). A diploid organism has DNA content $2C$ in G1-phase, in S-phase the DNA content is duplicating so we can observe between $2C$ and $4C$. In G2-phase it is $4C$ and after mitosis the DNA content returns to $2C$ (Figure 4) (Joubes and Chevalier, 2000). Mitotic division launches the zygote into the early-embryo proliferation stage. In endosperm, it occurs during mid-stage in CSE, SAL, and AL, and is largely responsible for generating the final population of endosperm cells (Sabelli and Larkins, 2009).

There is a variant of mitotic cell cycle called endocycle. During endocycle, the chromosome segregation and cytokinesis is not present, resulting in endoreduplicated nuclei. Consequently, endoreduplicated nuclei have doubled chromatids without change of the chromosome number (Figure 4) (Larkins *et al.*, 2001; Lee *et al.*, 2009).

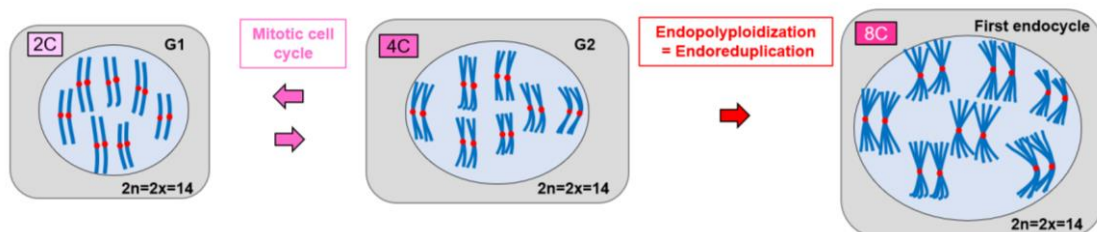


Figure 4: Schematic drawing showing the differences between the mitotic cycle and endocycle. During canonical mitotic cycle all cells ($2C$) replicate the DNA in S phase ($2C \rightarrow 4C$) and divide into two daughter cells in mitosis ($4C \rightarrow 2C$) coupled by karyokinesis and cytokinesis, both phases are preceded by G1 and G2 gap phases, respectively. During endocycle, cells double DNA content in S phase, but do not divide ($4C \rightarrow 8C$ etc.). The number of chromosomes stays the same, only number of chromatids and C-value is doubled.

The endoreduplicated nuclei do not undergo further division and they are present in differentiated cell tissues. For instance, in the diploid tissue, the $4C$ value remains and may enter consecutive endocycles to become $8C \rightarrow 16C \rightarrow 32C$, and so on (de Veylder *et al.*, 2011). Endoreduplication increases ploidy in individual cells, not on the whole plant body. It is a common cycle in plants and animals (Larkins *et al.*, 2001) and is present in tissues with high metabolic activity, such as endosperm, cotyledons, leaf epidermal cells etc. (Joubes and Chevalier, 2000). It is hypothesized

that endoreduplication is a tool for making more DNA templates and thus increasing the gene expression. With endoreduplication, the metabolic activity could be equivalent to that of many diploid cells (Larkins *et al.*, 2001). There is evidence that higher DNA content from endoreduplication correlates with higher transcription yield (Pirrello *et al.*, 2018).

Development of cereal seeds would not be possible without regular cell death. At early-development stage, maternal tissues, i.e., synergid and antipodal cells, the nucellus, the testa, the pericarp, and the nucellar projections undergo a progressive degeneration by PCD (Tran *et al.*, 2014; Radchuk *et al.*, 2017; Domínguez and Cejudo, 2014; An and You, 2004). At the late stage of seed development, mainly two endosperm domains (ESR and CSE) undergo cell death, but the cells remain intact in the mature grain and their contents will not be remobilized until germination. Finally, mature cereal grain consists mainly of dead material, where only the embryo and AL remain viable (Yifang *et al.*, 2012; Domínguez and Cejudo, 2014; Young and Gallie, 2000; Kobayashi *et al.*, 2013; Wu *et al.*, 2016).

3.4 GENOME ARCHITECTURE: DOMAIN ORGANIZATION OF INTERPHASE CHROMOSOMES

3.4.1 Barley mitotic chromosomes

Both cultivated and wild barleys are diploid species with seven pairs of chromosomes ($2n=14$). All mitotic barley chromosomes are metacentric and relatively large, their length in metaphase oscillates between 10-11 μm (Kaduchova *et al.*, submitted to TPJ). Since barley chromosomes are indistinguishable by arm length or ratio, molecular cytogenetics methods, e.g., fluorescence *in situ* hybridization (FISH, explained later) are applied to discriminate these chromosomes. For FISH, either a set of major chromosomal landmarks comprising *rDNA* and telomeric and centromeric sequences or satellite markers e.g. $(\text{GAA})_n$ can be used (Sugiyama *et al.*, 2011; Kapusi *et al.*, 2011; Georgieva and Gecheff, 2013).

3.4.2 Major chromosomal landmarks

Centromeres

The centromere is defined by specific DNA sequence together with proteins that bind to this DNA. On a microscopic picture of metaphase chromosomes, the location of the centromere is marked as a visible gap or narrowing also known as a primary constriction. In metaphase chromosomes, centromeres hold sister chromatids together and provide the site at which microtubules from the mitotic and meiotic II spindle attach to segregate the chromatids to opposite

poles. The structures of centromeres are extremely diverse between different organisms (Hudakova *et al.*, 2001). The major DNA component of barley centromeres is retroelement-like element *CEREBA*. This sequence is present in all seven centromeres of barley chromosomes and is absent in any other chromosome sequence (Zeng and Jiang, 2016). *CEREBA* is G+C-rich satellite sequence with high similarity to the *Ty3/gypsy* group of retrotransposons (Hudakova *et al.*, 2001).

Except for the centromeric DNA sequence, centromere for its function requires the presence of nucleosomes containing histone H3 variant centromere protein A (CENP-A; in plants also known as CENH3). These proteins are defined epigenetically and are specific for most eukaryotes (McKinley and Cheeseman, 2015).

Telomeres

Telomeres are the terminal regions of eukaryotic linear chromosomes, consisting of guanine-rich repeats. Telomere functions include the protection from progressive degradation and repairing DNA caused by mistaking the ends for a double-strand break. Barley, as other higher Angiosperms, has telomeres consisting of thousands of TTTAGGG repeats (also known as Arabidopsis-type telomeres) (Kilian *et al.*, 1995).

Genes encoding ribosomal RNA

Ribosomes are a translational apparatus that synthesize biological proteins in every cell. They consist of two ribosomal subunits and ribosomal RNA (rRNA). Genes encoding ribosomal RNA are called ribosomal DNA (*rDNA*). The *45S rDNA* locus is transcribed by RNA Polymerase I to produce 28S, 5.8S and 18S rRNA (Huang *et al.*, 2012; Tulpová *et al.*, 2022). Unlike *5S rDNA*, the *45S rDNA* locus is associated with nucleolus organizer region (NOR). Both *45S* and *5S rDNA* loci are organized into clusters of tandem repeats of homogenous units (Baum and Johnson, 1994; Tulpová *et al.*, 2022). These tandem repetitive regions are appropriate for detection and study of chromatin arrangement using FISH. On a microscopic picture of metaphase chromosomes, NORs are visible as gaps, therefore they are called as secondary constrictions. The chromosomes bearing *45S rDNA* are also known as satellite chromosomes. In barley, there are two pairs of chromosomes with satellites (pairs 6H and 7H). Active NORs cluster preferentially around the nucleolus (Nicoloff *et al.*, 1977; Linde-Laursen, 1984).

Nucleoli

Nucleolus is a large part of an interphase nucleus, where the rRNA synthesis and ribosome biogenesis takes place. It has been shown that its function also includes cell cycle regulation, growth and development and response to stress (Kalinina *et al.*, 2018). There are three main components of nucleoli, i.e., the fibrillar centers (FCs), the dense fibrillar component (DFC) and the granular component (GC) (Figure 5). The FCs are areas containing transcription-associated factors, and they can be activated or inactive. They are embedded in DFC, in which the transcription of precursor rRNA takes place. DFC contains proteins called FIBRILLARIN, which is important in rRNA processing (Amin *et al.*, 2007). The final step of assembly of ribosomal subunits occurs in GC (Sirri *et al.*, 2007; Kalinina *et al.*, 2018).

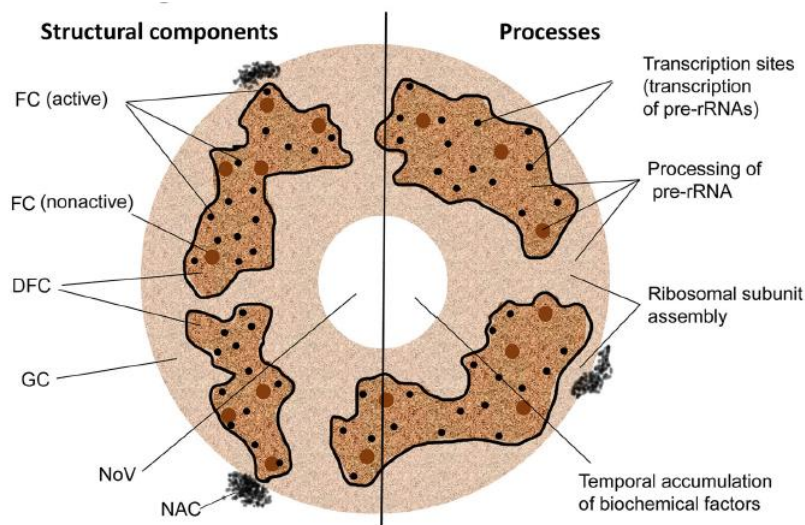


Figure 5: Structural and functional domains of the nucleolus. FC- fibrillar center; DFC- the dense fibrillar component; GC- the granular component; NoV- nucleolar vacuole; NAC- nucleolus-associated chromatin. Adopted from Kalinina *et al.*, 2018.

3.4.3 Interphase chromosome configuration

There are three main patterns of interphase chromosome configuration: (A) Rabl, (B) non-Rabl, and (C) rosette-like organization (i.e., nucleolus-associated clustering of telomeres) (Figure 6). A lot of crop species with large genome have Rabl pattern, named after the scientist Carl Rabl, who first observed this on nuclei of *Caudata* (Rabl, 1885). In this case, centromeres and telomeres are located at opposite poles of the nucleus, and chromosome arms lie next to each other (Rabl, 1885; Santos and Shaw, 2004). Although a lot of species with large genome size contain Rabl configuration, which can lead to a conclusion that Rabl correlates with genome size, there are also some exceptions. For example, *Brachypodium distachyon* (0.35 Gbp/1C) with a small genome size shows Rabl configuration (Idziak *et al.*, 2015). Other species, like maize (*Zea mays*) has large

genome, but does not exhibit Rabl organization at all (Tiang *et al.*, 2011). There is a hypothesis, that Rabl pattern is the result of anaphase configuration. When a nucleus enters interphase, the chromosomes are in a conformation resembling the Rabl pattern. Some species have interphase conformation resembling anaphase configuration and that is how the Rabl organization is created (Santos and Shaw, 2004).

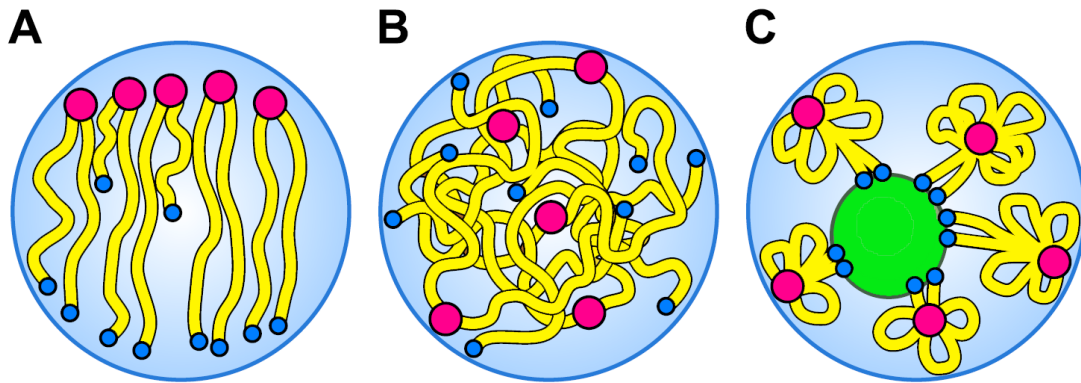


Figure 6: Interphase chromosome configurations. (A) Rabl configuration. (B) Non-Rabl configuration. (C) Rosette-like configuration (nucleolus-associated telomere clustering). Centromeres are shown in purple, telomeres in blue, chromosome arms in yellow, and the nucleolus in green. Adopted from Lysak, 2022.

The rosette-like configuration occurs in plant species with a small and repeat-sequences poor genome, e.g., *Arabidopsis*. Heterochromatin in *Arabidopsis* is confined into small, condensed regions called chromosome territories. In the nuclei, the (peri)centromeric regions cluster at the nucleus periphery and the euchromatic chromosomal arms are emanating from these heterochromatic regions. The telomeres are clustered around the nucleolus (Fransz *et al.*, 2002; Pecinka *et al.*, 2004; Nowicka *et al.*, 2023).

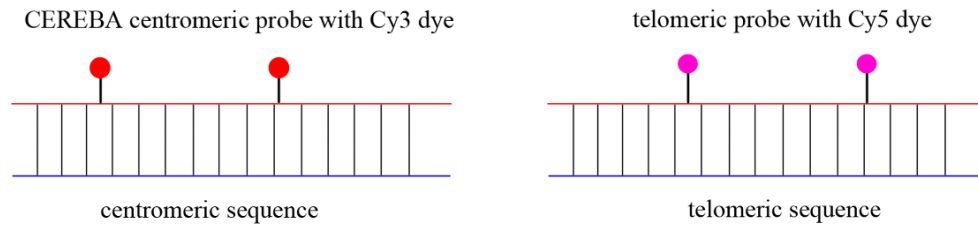
Some plants do not show Rabl nor rosette-like chromosome configuration. When the centromeres and telomeres are randomly distributed in the nuclei, and chromosome arms are not arranged along one axis, this case is named non-Rabl chromosome configuration (Lysak, 2022).

3.5 METHODS USED TO STUDY THE ORGANIZATION OF CHROMOSOMES IN INTERPHASE

3.5.1 Fluorescence *in situ* hybridization

The most known molecular cytogenetics method is fluorescent *in situ* hybridization (FISH). It is used to reveal presence or absence of complementary DNA sequences in cells or tissues. A DNA probe has incorporated labelled nucleotides and this sequence can hybridize to targeted DNA (Cui *et al.*, 2016; Speicher and Carter, 2005). The probe can be labeled directly by fluorophore or indirectly with small molecules called hapten (Figure 7). To detect probe labeled by hapten, specific anti-hapten antibodies conjugated with fluorophore are used. Direct approach is applied for labeling shorter probes. On the contrary, indirect labelling is used when a stronger signal is required (Speicher and Carter, 2005). Probes can be either commercially synthesized and labeled, or in-house prepared using PCR or nick translation. Labelling by PCR requires nucleotides conjugated with a fluorophore or a hapten. It runs the same as classic PCR, but deoxythymidine triphosphate (dTTP) is partially replaced by hapten-dUTP-labeled nucleotide. In turn, nick translation is a reaction based on using two enzymes. First enzyme, DNase I randomly introduces nicks into the DNA strand, and second enzyme DNA Polymerase I synthesizes a new strand with fluorophore or hapten-labeled nucleotides. The hybridization mix and the DNA double-strand must be first denatured to hybridize together.

(A) Direct labelling



(B) Indirect labelling

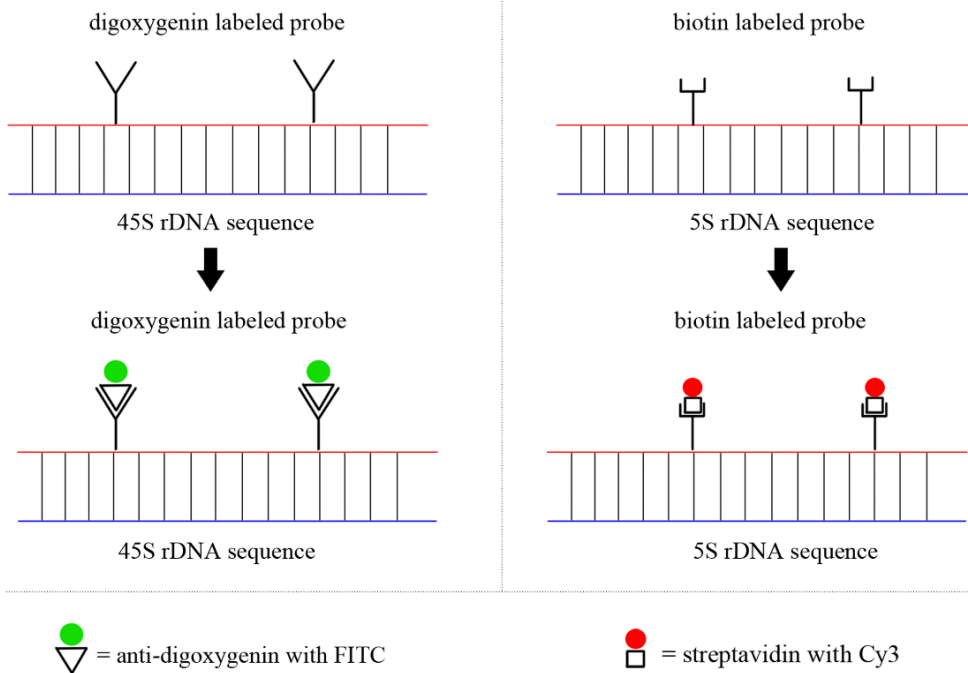


Figure 7: Schematic drawing showing two types of probe labeling.

(A) Direct labelling with fluorochromes. Examples of *CEREBA*-centromeric repeat labelled with Cy3 fluorescent dye and telomeric probe was bound with Cy5 fluorescent dye. This type of labeling was used for the research performed in the frame of this master thesis. Both oligo-probes were commercially synthesized. (B) Indirect labelling with haptens. Examples of *45S rDNA* probe labeled with digoxigenin and detected with anti-digoxigenin antibody conjugated with fluorescein isothiocyanate (FITC). The *5S rDNA* sequence labeled with biotin and detected with streptavidin conjugated with Cy3 dye. Both types of labeling were applied in this research.

3.5.2 Immunostaining

Immunostaining uses specific antibodies to detect a single target protein within individual cells or tissues. In the case of direct labelling, a primary antibody is conjugated with an enzyme or fluorophore, and if there is indirect labelling, both primary and secondary antibodies with conjugated enzyme/fluorophore are used (Figure 8). Enzymes, such as horseradish peroxidase or alkaline phosphatase catalyze reactions that give a chemiluminescent product. Fluorophores can be detected using epifluorescence or confocal microscopy.

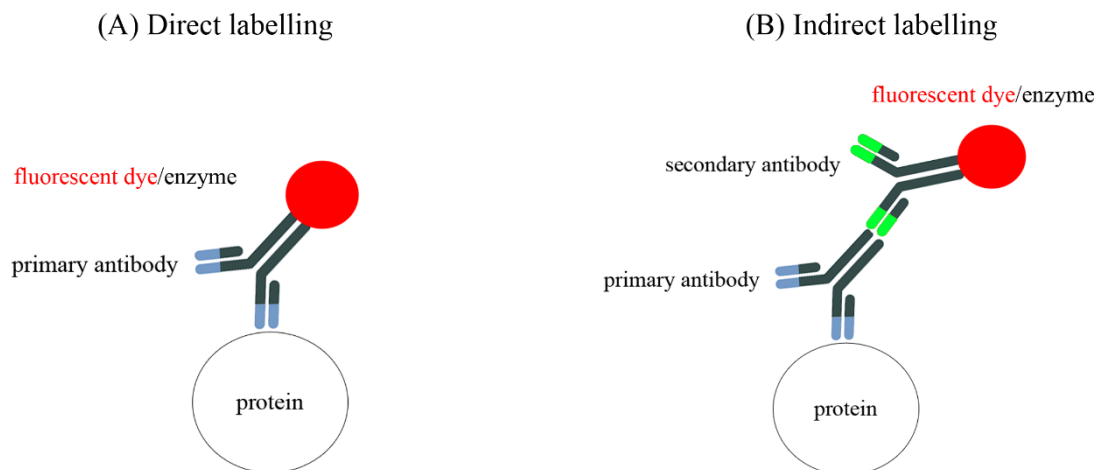


Figure 8: Explanation of the principle of immunostaining in the detection of a specific protein.

(A) Direct labelling with a single primary antibody conjugated with a fluorescent dye or an enzyme.
(B) Indirect labelling where primary antibody is used with a secondary antibody conjugated with fluorescent dye or an enzyme.

3.5.3 ImmunoFISH

For detecting distribution of proteins and specific DNA sequence simultaneously in a nucleus both immunolabelling with conjugated fluorophore and FISH can be combined – this method is called immunoFISH (Sepsi *et al.*, 2018). This protocol starts with immunostaining (described above). Before FISH, slides must be post-fixed, washed and the protocol continues with the FISH steps (explained above), (Sepsi *et al.*, 2018; Nowicka *et al.*, 2023).

3.5.4 Image collection and analysis

Epifluorescence or laser scanning microscopies are used to visualize and collect high-resolution three-dimensional (3D) image stacks (Sepsi *et al.*, 2018). Nucleus and interphase chromosome organization studies rely on image analysis, which allow to convert microscopic pictures (1) to quantitative data on signal intensity level or (2) advanced qualitative pictures showing e.g., details of shapes and distribution patterns in space (Dumur *et al.* 2019; Randall *et al.* 2022). Quantitative image analysis requires specific programs for image rendering, segmentation, setting measurement points and exporting data to numerical format. Image processing can be done using commercial software e.g., Imaris (Bitplane, Zurich, Switzerland) or publicly available software e.g., FIJI (<https://imagej.nih.gov/ij/download.html>).

4 MATERIALS AND METHODS

4.1 PLANT MATERIAL

- Cultivated barley (*Hordeum vulgare* ssp. *vulgare*, 2n=14), spring type, two-rowed elite cultivar (cv.) Compana (PI 539111)
- Cultivated barley (*H. vulgare* ssp. *vulgare*, 2n=14), spring type, six-rowed elite cv. Morex (BCC 906)
- Ethiopian landrace (*H. vulgare* ssp. *vulgare*, 2n=14), facultative type, intermediate-rowed (HOR 10350)
- Wild barley (*H. vulgare* ssp. *spontaneum*, 2n=14), facultative type, two-rowed (HOR 12560)

The seeds of the cv. Compana were obtained from National Small Grains Collection of the National Plant Germplasm System of the United States Department of Agriculture-Agricultural Research Service. The seeds of the remaining accessions were received from Leibniz Institute of Plant Genetics and Crop Plant Research (IPK), Gatersleben, Germany.

4.2 MATERIALS AND EQUIPMENT

In the following subchapters will be listed laboratory equipment, software, materials, chemicals, and solutions used for this work.

4.2.1 Laboratory equipment

The following equipment was used:

- analytical scales (Sartorius)
- automatic pipets (Nichipet EXII, Nichiryo)
- automatic shaker (Heidolph Reax)
- AxioImager Z2 (Zeiss) epifluorescence microscope equipped with a DSD2 spinning disk confocal imaging module and monochromatic Zyla 4.2 camera (both Andor)
- centrifuge myFuge Mini (Benchmark Scientific)
- confocal microscope Leica TCS SP8 STED3X equipped with an HC PL APO CS2 63×/1.40 Oil objective, hybrid detectors (HyD) (all Leica Microsystems)
- electrophoretic chamber Wide Mini-Sub Cell GT Cell (Bio-Tech)

- flow cytometer and sorter (FACSAria II, SORP)
- freezers
- fume hood (Merci)
- gel imaging and analysis system (Syngene)
- growth chamber fytotron (Weiss Technik)
- hybridizer Slide Moat (Boekel Scientific)
- ice maker (MF26, Scotsman)
- magnetic stirrer (Variomag)
- pH meter Inolab (WTW)
- phase-contrast microscope (Primo Star, Zeiss)
- Polytron PT1300D homogenizer (Kinematica AG)
- refrigerators
- source for electrophoresis PowerPac (Bio-Rad)
- standard analog shaker (VWR)
- stereomicroscope (SZX16, Olympus)
- Thermal Cycler C1000 Touch (Bio Rad)
- thermocycler Mastercycler nexus (Eppendorf)
- thermostat (Biological Thermostat, BT 120)
- vacuum system (Labobase)
- water bath (Mettler)

4.2.2 Small laboratory equipment

The following small laboratory equipment was used:

- beakers
- Coplin jar
- diamond pen
- disposable plastic stick (SP BEL-ART)
- Erlenmeyer flask
- filter diameter Ø 0.22 µm
- flowerpots (15×15×15 cm)
- glass plate for cutting
- humid box of Styrofoam
- nylon mesh with pore size 30 and 50 µm
- Pasteur pipet
- Petri dish (diameter Ø 60 and 90 mm)
- Poly-L-Lysine Slides (Menzel Gläser, J2800AMNZ)
- pellet pestle
- preparation needles
- razor blades
- small flowerpots (5×5×5 cm, Jiffy)
- Superfrost Plus Slides (Menzel Gläser, J1810AMNZ)
- tubes 0.2; 0.5; 1.5; 2 ml (Eppendorf)
- tubes 5ml Polypropylene for flow cytometry (Fisher Scientific)
- tweezers

4.2.3 Software

- Adobe Photoshop CS5 6.0 (Adobe Systems Corporation, San Jose, CA)
- GeneSnap (Syngene)
- Imaris File Converter 9.2.1 (Bitplane, Oxford instruments)
- Imaris 9.7 (Bitplane)
- FIJI (public ownership)
- Inkscape (public ownership)
- iQ 3.6.1 (Andor)
- Leica Application Suite X (LAS-X) version 3.5.5 (Leica)
- Microsoft Excel (Microsoft)
- Minitab (Minitab Inc.)

4.2.4 Chemicals

The following chemicals were used:

- 10X BlueJuice Gel Loading Buffer (Invitrogen, cat. no. 10816015)
- 37% formaldehyde (Sigma-Aldrich, cat. no. F8775)
- 37% hydrochloric acid (Sigma-Aldrich, cat. no. 435570)
- 4',6-diamidino-2'-phenylindole dihydrochloride, DAPI (Sigma-Aldrich, cat. no. 10236276001)
- $\geq 99.9\%$ ethanol absolute (EtOH; cat. no. Merck MFCD00003568)
- 96% EtOH (Lachner, cat. no. 20025-A96-M1000-1)
- acetic acid (Lachner, cat. no. 61019-001-P0000-1)
- agarose (Meridian, cat. no. BIO-41025)
- biotin-11-dUTP (Roche, cat. no. 11093070910)
- blocking reagent (Roche, cat. no. 11096176001)
- bovine albumin serum, BSA (Sigma-Aldrich, cat. no. A3294-100G)

- Cellulase Onozuka R-10 (Yakult Pharmaceutical Industry, cat. no. 150422-01)
- deionized formamide (Millipore, cat. no. S4117)
- dextran sulfate (Carl Roth, cat. no. 9042-14-2)
- dATP Solution (100 mM; Thermo Scientific, cat. no. R0141)
- dCTP Solution (100 mM; Thermo Scientific, cat. no. R0151)
- dGTP Solution (100 mM; Thermo Scientific, cat. no. R0161)
- dTTP Solution (100 mM; Thermo Scientific, cat. no. R0171)
- DIG-Nick translation Mix (Roche, cat. no. 11745816910)
- disodium EDTA dihydrate (Merck, cat. no. ED2SS)
- double distilled water (ddH₂O)
- GeneRuler 1 kb Plus DNA Ladder (Thermo Scientific, cat. no. SM1331)
- genomic DNA (cv. Compana)
- horse serum (Sigma-Aldrich, cat. no. H0146-5ML)
- magnesium chloride (Sigma-Aldrich, cat. no. 208337)
- methanol (MeOH; Merck, cat. no. MFCD00004595)
- Pectolyase Y23 (Duchefa, cat. no. 9033-35-6)
- Phusion High-Fidelity DNA Polymerase (2 U·μl⁻¹; Thermo Scientific, cat. no. F-530XL)
- potassium chloride (Sigma-Aldrich, cat. no. 30076-AP0)
- RNase A (10 mg·ml⁻¹; Thermo Scientific, cat. no. EN0531)
- salmon sperm (10 mg·ml⁻¹; Invitrogen, cat. no. AM9680)
- sodium dihydrogen citrate (Roth, cat. no. R.HN13.1)
- sodium chloride (Lachner, cat. no. 30093-AP0)
- sterile ddH₂O
- sucrose (Millipore, cat. no. 107687)
- tris-hydroxymethyl-aminomethane (Tris; Sigma-Aldrich, cat. no. 77-86-1)

- Triton X100 (Sigma-Aldrich, cat. no. T8787)
- Tween-20 (Sigma-Aldrich, cat. no. P9416)
- Vectashield with DAPI (Vector Laboratories, cat. no. H-1000-10)
- Primary antibodies
 - mouse monoclonal anti-FIBRILLARIN (Abcam, cat. no. ab4566)
- Secondary antibodies
 - anti-digoxigenin fluorescein isothiocyanate (FITC, Roche, cat. no. 11207741910)
 - avidin-Texas Red (Vector Laboratories, cat. no. NC9172942)
 - goat anti-avidin-biotin (Vector Laboratories, cat. no. NC9256157)
 - goat anti-mouse-Alexa Fluor 488 (Molecular Probes, cat. no. A-32723)
 - goat anti-mouse-Alexa Fluor 547 (Invitrogen, cat. no. A-11003)
 - streptavidin-Cy3 (Molecular Probes, cat. no. SA1010)
- Oligo-probes
 - 6H-1-Texas Red – chromosome 6H top arm-specific probe
 - 6H-6-Cy5 – chromosome 6H pericentromeric-specific probe
 - 6H-13-digoxigenin – chromosome 6H bottom arm-specific probe
 - centromeric *CEREBA* probe
 - telomeric TEL probe

4.2.5 Preparation of stock solutions

- 1M Tris-HCl pH=7.0 ($M_{\text{Tris}}=121.15 \text{ g}\cdot\text{mol}^{-1}$): Dissolve 60.5 g in 400 ml of ddH₂O, adjust the pH to 7.0 using 37% HCl, add ddH₂O to 500 ml. Autoclave. Store at room temperature (RT).
- 1M Tris-HCl pH=7.5 ($M_{\text{Tris}}=121.15 \text{ g}\cdot\text{mol}^{-1}$): Dissolve 60.5 g in 400 ml of ddH₂O, adjust the pH to 7.5 using 37% HCl, add ddH₂O to 500 ml. Autoclave. Store at RT.

- 1M MgCl₂ ($M_{\text{MgCl}_2}=95.21 \text{ g}\cdot\text{mol}^{-1}$): Dissolve 47.6 g in 500 ml of ddH₂O. Autoclave. Store at RT.
- 1M NaCl ($M_{\text{NaCl}}=58.44 \text{ g}\cdot\text{mol}^{-1}$): Dissolve 29.2 g in 500 ml of ddH₂O. Autoclave. Store at RT.
- 1M KCl ($M_{\text{KCl}}=74.55 \text{ g}\cdot\text{mol}^{-1}$): Dissolve 37.3 g in 500 ml of ddH₂O. Autoclave. Store at RT.
- 10 × PBS (1.37 M NaCl, 27 mM KCl, 100 mM Na₂HPO₄, 18 mM KH₂PO₄, pH=7.4), ($M_{\text{NaCl}}=58.44 \text{ g}\cdot\text{mol}^{-1}$, $M_{\text{KCl}}=74.55 \text{ g}\cdot\text{mol}^{-1}$, $M_{\text{Na}_2\text{HPO}_4}=141.96 \text{ g}\cdot\text{mol}^{-1}$, $M_{\text{KH}_2\text{PO}_4}=136.086 \text{ g}\cdot\text{mol}^{-1}$). Dissolve 80 g NaCl, 2 g KCl, 17.8 g Na₂HPO₄·2H₂O, 2.4 g KH₂PO₄ in 1000 ml ddH₂O. Filter through a ϕ 0.22 μm filter. Store at RT.
- 20× SSC (3 M NaCl, 300 mM C₆H₇NaO₇), ($M_{\text{NaCl}}=58.44 \text{ g}\cdot\text{mol}^{-1}$, $M_{\text{C}_6\text{H}_7\text{NaO}_7}=214.10 \text{ g}\cdot\text{mol}^{-1}$). Dissolve 175.3 g of NaCl and 64.2 g of C₆H₇NaO₇ in 1000 mL of ddH₂O. Autoclave. Store at RT.
- 0.5M EDTA pH=8.0 ($M_{\text{EDTA}}=372.24 \text{ g}\cdot\text{mol}^{-1}$): Dissolve 18.61 g in 80 ml of ddH₂O, adjust the pH to 8.0 using NaOH salt, add ddH₂O to 100 ml. Autoclave. Store at RT.
- 0.5M EDTA pH=4.0 ($M_{\text{EDTA}}=372.24 \text{ g}\cdot\text{mol}^{-1}$): Dissolve 18.61 g in 80 ml of ddH₂O, adjust the pH to 4.0 using NaOH salt, add ddH₂O to 100 ml. Autoclave. Store at RT.

4.2.6 Preparation of working solutions

- Tris buffer (100 mM Tris-HCl pH=7.0; 5 mM MgCl₂, 85 mM NaCl, 0.1% Triton X100). Mix 10 ml of 1M Tris-HCl pH=7.0, 500 μl of 1M MgCl₂, 8.5 ml of 1M NaCl and 100 μl of Triton X100. Add water to 100 ml. Mix on a magnetic stirrer. Always prepare fresh and store at 4°C until use. Used for nuclei isolation and fixation solution.
- Fixation solution for fixation of plant material (4% formaldehyde in Tris buffer). Mix 5.4 ml of 37% formaldehyde and 50 ml of Tris buffer. Always prepare fresh.
- Fixation solution for fixing nuclei on slides (3.7% formaldehyde in 1× PBS). Mix 5 ml of 37% formaldehyde and 5 ml of 10× PBS. Add water to 50 ml. Always prepare fresh.
- Nuclei Isolation and Sorting Buffer (NISB; 100 mM Tris pH=7.0, 50 mM KCl, 2 mM MgCl₂, 0.05% Tween-20, 5% sucrose). Dissolve 2.5 g sucrose in 5 ml 1M Tris pH=7.0, 2.5 ml 1M KCl, 0.1 ml 1M MgCl₂ and 25 μl Tween. Add water to 50 ml. Filter through a ϕ 0.22 μm filter and store at 4°C until use.

- 1× PBS (pH=7.4), (137 mM NaCl, 2.7 mM KCl, 10 mM Na₂HPO₄, 1.8 mM KH₂PO₄). Mix 10 ml of 10× PBS with 90 ml of ddH₂O. Always prepare fresh. Used for FISH and ImmunoFISH.
- 4× SSC with Tween-20 (600 mM NaCl, 60 mM C₆H₇NaO₇, 0.01% Tween-20). Mix 20 ml 20× SSC with 80 ml ddH₂O and 10 µl Tween 20. Mix on a magnetic stirrer. Autoclave. Store at RT. Used for FISH and ImmunoFISH.
- 2× SSC with Tween-20 (300 mM NaCl, 30 mM C₆H₇NaO₇, 0.01% Tween-20). Mix 10 ml 20× SSC with 90 ml ddH₂O and 10 µl Tween 20. Mix on a magnetic stirrer. Autoclave. Store at RT. Used for FISH and ImmunoFISH.
- 0.1× SSC (15 mM NaCl, 1.5 mM C₆H₇NaO₇). Mix 0.5 ml 20× SSC with 99.5 ml ddH₂O. Autoclave. Store at RT. Used for FISH and ImmunoFISH.
- Blocking buffer (BL; 3% BSA, 10% horse serum, 1× PBS). Dissolve 0.3 g BSA in 1 ml horse serum, 1 ml 10× PBS and 8 ml ddH₂O. Filter through a ø 0.22 µm filter and store at -20°C until use. Used for ImmunoFISH.
- AK buffer (1% BSA, 10% horse serum, 1× PBS, 0.1% Tween-20). Dissolve 0.1 g BSA in 1 ml horse serum, 1 ml 10× PBS and 8 ml ddH₂O. Add 10 µl of Tween-20. Filter through a ø 0.22 µm filter and store at -20°C until use. Used for ImmunoFISH.
- TNB buffer (100 mM Tris-HCl pH=7.5, 150 mM NaCl, 0.5% blocking reagent). Dissolve 0.05 g of blocking reagent in 1 ml of 1 M Tris-HCl pH=7.5, 1.5 ml of 1 M NaCl and 7.5 ml of ddH₂O. Filter through a ø 0.22 µm filter and store at -20°C until use. Used for ImmunoFISH.
- TNT buffer (100 mM Tris-HCl pH=7.5, 150 mM NaCl, 0.1% Tween-20). Mix 5 ml 1M Tris-HCl pH=7.5, 7.5 ml of 1M NaCl and 50 µl of Tween 20. Add ddH₂O to 50 ml. Mix on a magnetic stirrer. Always prepare fresh. Used for ImmunoFISH.
- Incubation buffer (IB; 1% BSA, 0.1% Tween-20, 4× SSC). Dissolve 0.1 g BSA in 2 ml 20× SSC and 8 ml ddH₂O. Add 10 µl of Tween-20. Filter through a ø 0.22 µm filter and store at -20°C until use. Used for FISH.
- Blocking buffer (BB; 5% BSA, 0.2% Tween-20, 4× SSC). Dissolve 0.5 g BSA in 2 ml 20× SSC and 8 ml ddH₂O. Add 20 µl of Tween-20. Filter through a ø 0.22 µm filter and store at -20°C until use. Used for FISH.

- 1× KCl buffer (75 mM KCl, 7.5 mM EDTA, pH=4.0). Mix 750 µl of 1M KCl and 75 µl of 0.5M EDTA pH=4.0. Add ddH₂O to 10 ml. Store at RT. Used for chromosome preparation.
- 4% cellulase Onozuka R-10 with 1% pectolyase Y-23. Dissolve 0.2 g cellulase and 0.05 g pectolyase enzyme powder in 5 ml 1×KCl buffer. Used for chromosome preparation.
- 90% EtOH. Mix 93.75 ml of 96% EtOH and 6.25 ml of ddH₂O. Store at RT until use. Used for FISH.
- 70% EtOH. Mix 73 ml of 96% EtOH and 27 ml of ddH₂O. Store at RT until use. Used for FISH.
- 70% EtOH. Mix 73 ml of 96% EtOH and 27 ml of ddH₂O. Store at 4°C until use. Used for root fixation.
- 90% acetic acid. Mix 90 ml of 100% acetic acid and 10 ml of ddH₂O. Store at 4°C until use. Used for root fixation.
- TE buffer (Tris-EDTA buffer, pH=7.6) (0.1M Tris, 0.01M EDTA). Dissolve 15.759 g Tris and 2.92 g EDTA in 800 ml of ddH₂O, adjust the pH to 7.6 using 37% HCl, add ddH₂O to 1000 ml. Autoclave. Store at RT. Used for chromosome preparation.
- 9:1 ice-cold acetic acid: MeOH. Mix 9 ml acetic acid and 1 ml MeOH, keep on ice until use. Used for chromosome preparation.
- LB01 buffer (15 mM Tris-HCl pH 7.5, 2 mM Na₂EDTA, 0.5 mM spermine tetrahydrochloride, 80 mM KCl, 20 mM NaCl and 0.1% Triton X-100). Dissolve 363.4 mg Tris, 148.9 mg Na₂EDTA, 34.8 mg spermine tetrahydrochloride, 1.193 g KCl, 233.8 mg NaCl in 200 ml of ddH₂O. Add 200 µl of Triton X-100. Filter through a 0.22 µm filter and store at -20°C until use. Used for nuclei isolation.

4.3 PLANT GROWTH CONDITIONS AND ESTIMATING DAYS AFTER POLLINATION

For seed germination a Petri dish (\varnothing 90 mm) with filter paper soaked with ddH₂O was used. Barley seeds (approx. 15 seeds) were evenly placed on the filter paper, stratified at 4°C for 48 hours (the seed coat in seed dormancy stage softens, and the development of the embryo starts). The Petri dish was transferred to a thermostat set for darkness at 25°C for 48 hours. Subsequently, the sprouting seedlings were transferred to small pots (5×5×5 cm, Jiffy) filled with a mixture of soil and sand (3:1; v/v) and were left for one week in a phytochamber (phytotron) under controlled long day conditions (16 hours a day – 8 hours night; temperature: 20 °C/day – 16 °C/night; light intensity 200 $\mu\text{mol}\cdot\text{m}^{-2}\cdot\text{s}^{-1}$; humidity 60%). After a week, the plants were transferred to 15×15×15 cm pots and left in the phytotron for two months under the same conditions as above. Day of pollination was set using the morphology of stigma and anthers according to the Waddington scale [W10] (Waddington et al., 1983) as established previously (Kovacik *et al.*, 2020; Nowicka *et al.*, 2021). Seeds were collected at 8 and 24 DAP. At some experimental points, the root apical meristem (RAM) at 2 days after germination (DAG) were used as a somatic tissue control.

4.4 EXPERIMENTAL SETUP AND EVALUATION PROCEDURES

The experiment setup used in this master thesis included five tasks (Figure 9):

- (A) Selection the genotype and chromosomal landmarks for further research
- (B) Study of sister chromatid cohesion at *5S* and *45Sr DNA* loci
- (C) Study of sister chromatid cohesion at specific chromosomal segments
- (D) Study of nucleoli organization
- (E) Study of Rab1 chromosome organization.

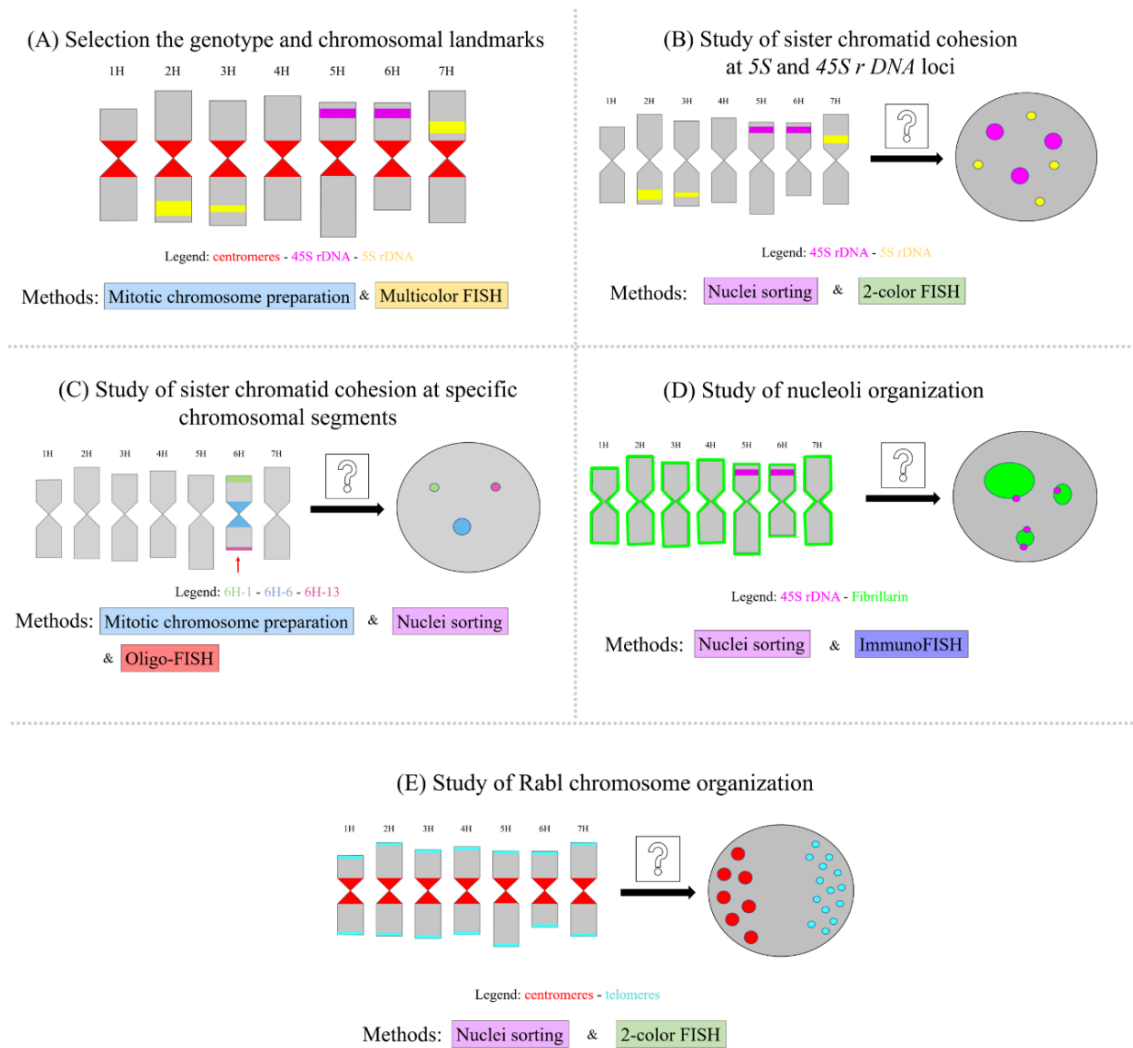


Figure 9: Schematic drawing of experimental setup used in this master thesis.

4.4.1 Mitotic chromosome preparation

Synchronized root tips were used for preparation of metaphase chromosomes (Lysak *et al.*, 1999). The cell synchronization was performed by Ms. Zdeňka Dubská. Then the root tips at 2 DAG were fixed in ice-cold 90% acetic acid for 10 min followed by three washes in 70% ethanol and stored in 70% ethanol at -20 °C. Metaphase chromosomes were prepared using the drop technique (Danilova *et al.*, 2012). Root tips were washed three times in water, then in 1× KCl buffer for 5 minutes. Then, the root tips were cut off approximately 1 mm from the tip and put into mixture of 4% cellulase Onozuka R-10 with 1% pectolyase Y-23 in KCl buffer, and incubated for 58 minutes in water bath at 37 °C. The reaction was stopped by TE buffer and the root tips were washed three times in 100% EtOH. Ice cold acetic acid with MeOH (9:1, v/v) was added and the roots tips were broken by a blunt end of plastic inoculation loop. The slides were placed

in Styrofoam humid box and 7 μ l of prepared mixture was dropped on the slides from a significant height. The quality of spread chromosomes was controlled with phase-contrast microscope (Primo Star, Zeiss). For further experiments the slides with at least five metaphases were used. Slides prepared using this method were used in tasks A and C.

4.4.2 Nuclei isolation and flow-sorting

Nuclei were isolated from RAM, embryo, and endosperm tissues.

Root nuclei isolation

Approximately 70 roots of 2 DAG seeds were cut 1 cm from the apex and put on drop of distilled water on ice. Fixation was performed in 4% formaldehyde in Tris buffer. The roots were kept on ice for 15 minutes. Subsequently, the fixation continued in the same solution for 5 min by vacuum infiltration on ice. Next, the roots were washed two times for 5 minutes in Tris buffer, cut 1 mm from the tip and homogenized in 500 μ l LB01 buffer for 13 s at 15 000 rpm using a Polytron PT1300D homogenizer.

A detailed description of isolation for embryo and endosperm of different DAP is described in my bachelor thesis (Ferkova, 2021). Here, only the brief description is given.

Embryo nuclei isolation

For 8 DAP seeds, approximately 80 embryos and for 24 DAP seeds, 30 embryos were manually dissected using an SZX16 binocular microscope (Olympus). Fixation of 8 DAP embryos was performed in 4% formaldehyde in Tris buffer for 15 minutes on ice and then for 5 minutes by vacuum infiltration on ice. After washing in Tris buffer, embryos were homogenized with a pellet pestel in NISB buffer. Fixation for 24 DAP embryos was performed in 4% formaldehyde in Tris buffer for 40 minutes on ice and then for 30 minutes by vacuum infiltration on ice. After washing in Tris buffer, embryos were homogenized by chopping with a razor blade on a Petri dish in 500 μ l NISB buffer.

Endosperm nuclei isolation

For 8 DAP and 24 DAP seeds, approximately 80 and 60 seeds were used, respectively. Seeds before fixation in 4% formaldehyde were cut with razor blade into smaller pieces. 8 DAP endosperm samples were fixated for 40 minutes on ice and then for 20 minutes by vacuum infiltration on ice. In turn, 24 DAP endosperm samples were fixated for 40 minutes on ice and then followed by 30 minutes by vacuum infiltration on ice. After washing in Tris buffer, samples were homogenized by chopping with a razor blade on a Petri dish in 2 ml of NISB buffer.

Nuclei flow sorting

The crude homogenates of all samples were filtered through 50 µm pore size mesh. Nuclei suspension was stained with 2 µg·ml⁻¹ DAPI. For 8 DAP embryo and RAM 2C and 4C nuclei populations, for 24 DAP embryo 2C, 4C and 8C populations were established. For 8 DAP endosperm there were 3C, 6C and 12C nuclei fractions, for 24 DAP endosperm there were 3C, 6C, 12C and 24C nuclei (Nowicka *et al.*, 2021). Approximately 500 nuclei (for each C-value) per population were sorted onto microscope slides into a 2 µl drop of NISB buffer using a FACSaria II SORP flow cytometer and sorter (BD Biosciences, Santa Clara). Slides were air-dried for 1 hour at RT and stored at -20 °C until use. Super frost slides and polylysine slides were used for FISH and ImmunoFISH, respectively. Nuclei sorting was performed by Dr. Mahmoud Said. Slides with sorted nuclei were used in tasks B-E.

4.4.3 Fluorescence *in situ* hybridization

Probe preparation and labeling

The probes, which were used for the experiments are described in detail in (Nowicka *et al.*, 2023). Here, in brief, for barley centromeric detection, a synthetic 28-mer oligonucleotide (5'-AGGGAGA-3')₄ probe was applied. The probe corresponds to a barley centromeric retroelement-like element *CEREBA* (Hudakova *et al.*, 2001). For barley telomeres detection, a synthetic 28-mer oligonucleotide probe (5'-CCCTAAA-3')₄ corresponding to the Arabidopsis-type telomeric repeat was used. Both probes were synthesized commercially and labeled at the 5' end with Cy3 or Cy5 (Eurofins). Probe for *45S rDNA* was labeled by nick translation using as a template the pTa71 plasmid containing a 9.1 kb fragment of rDNA sequence from bread wheat (Gerlach and Bedbrook, 1979). *45S rDNA* probe was labeled with digoxigenin-11-dUTP using nick translation kit according to the manufacturer's instructions. The *5S rDNA* probe was amplified during PCR from cv. Compana genomic DNA using biotin-dUTP. The following primers were used for amplification: 5'-GGATGCGATCATACCAGCAC-3' and 5'-GACATGCAACTATCTATTTGT-3'. Above mentioned probes were used in tasks A, B, D and E.

All three 6H probes were designed by dr. Eva Hřibová and labeled by dr. Denisa Beránková according to protocols described by Šimoníková *et al.* (2019). In brief, sets of 20,000 oligomers (45 bp) covering 6H chromosome segments were synthesized as immortal libraries by Arbor Biosciences (Ann Arbor, MI, USA) and then labeled by Texas Red, Cy5 and digoxigenin according to Han *et al.* (2015). These oligoprobes were used in task C.

Fluorescence in situ hybridization

Slides were air-dried and washed in 2× SSC for 5 minutes in a Coplin jar. Then, they were treated with RNase A (50 µg·ml⁻¹ in 2× SSC) for 30 minutes in humid chamber at 37 °C. Slides were washed twice in 2× SSC and after that in 1× PBS. Fixation of the slides were performed in 4% formaldehyde in 1× PBS at RT for 20 minutes in a fume hood. After that, the slides were rinsed three times in 1× PBS. The hybridization mix contained two or three probes, sheared salmon sperm DNA, deionized formamide, dextran sulfate, and 2× SSC (Table 1). For biotin-dUTP and digoxigenin-11-dUTP labeled probes, the hybridization mixture was denaturated for 4 minutes at 95 °C in a thermocycler and cooled on ice. After adding the mix on the slides, they were denaturated again for 4 minutes at 80 °C in Mastercycler nexus. For oligo-probes, the step of hybridization mixture pre-denaturation was skipped. The slides were incubated in 37 °C overnight in a hybridizer Slide Moat (Boekel Scientific). Next day, the following washes were performed: at 42 °C (in water bath) – twice for 7 minutes in 2× SSC, 10 minutes in 0.1× SSC, 5 minutes in 2× SSC, and at RT twice for 7 minutes in 4× SSC. Next, the slides were blocked in a Blocking Buffer (BB) for 30 minutes in a humid chamber in 37 °C. Subsequently, the slides were incubated with antibodies, streptavidin-Cy3 in Incubation Buffer (IB) (1:200, v/v) for biotin labeled probes and anti-digoxigenin-FITC in Incubation Buffer (IB) (1:200, v/v) for digoxigenin labeled probes. The incubation lasted for 1 hour at 37 °C in a humid chamber. Then the slides were washed three times for 5 minutes in 4× SSC at 37 °C. Dehydration of the slides was performed in a Coplin jars with EtOH series as follows 70%, 90% and 96%, each washing for 2 minutes. The slides were counterstained with DAPI in Vectashield. FISH was the basic method used in all experiments performed in this master thesis.

Table 1: Preparation of hybridization mix

Component	Stock concentration	Final concentration	20 µl/nuclei population
Deionized formamide	100%	50%	10 µl
SSC	20×	2×	2 µl
Dextran sulfate	50%	10%	4 µl
Probe #1	variable*	400 ng/µl	variable**
Probe #2	variable*	400 ng/µl	variable**
Probe #3	variable*	400 ng/µl	variable**
Salmon sperm	10 mg/mL	0.5 µg	1 µl
Sterile H₂O	-	-	Up to 20 µl

*stock concentration of probes varied between 100 to 200 µg/µl

**volume of the individual probes varied between 0.4 to 2 µl, depending on stock concentration

4.4.4 ImmunoFISH

Slides were air-dried at RT for 10 minutes and fixed in 4% formaldehyde in 1× PBS at RT for 15 minutes in a fume hood. Subsequently, they were washed three times at RT each for 5 minutes in 1× PBS. Then, the slides were blocked with Blocking Buffer (BL) for 30 minutes at 37 °C in humid chamber and incubated with anti-FIBRILLARIN primary antibody in AK buffer (1:50, v/v) in humid chamber in 4 °C overnight.

The next day, the slides were rinsed three times in 1× PBS followed one wash in TNT (all at RT). Subsequently, they were incubated with secondary antibody anti-mouse Alexa-Fluor 547 in TNB buffer (1:200, v/v) at 37 °C in humid chamber for 90 minutes. After incubation, the slides were three times washed in 1× PBS and one time washed in TNT (all in the dark).

Before FISH, slides were fixed for 10 minutes in 96% ethanol in acetic acid (3:1, v/v), followed by 10 minutes fixation with 3.7% formaldehyde in 1× PBS. Slides were washed three times with 1× PBS. FISH steps were performed as described in previous section, using *45S rDNA* probe, excluding RNase A treatment. ImmunoFISH was performed in task D.

4.4.5 Microscopy

The details of microscopic evaluation and analysis are described in (Nowicka *et al.*, 2023). In brief, Axioimager Z2 (Zeiss) epifluorescence microscope equipped with a DSD2 confocal module and Zyla camera 4.2 (both Andor) was used for visualization of fluorescent signals. Pictures in the z-axis were acquired separately for each fluorochrome, using the given excitation (DAPI $\lambda = 390/40$ nm, GFP $\lambda = 482/18$ nm, RFP $\lambda = 561/14$ nm, Cy5 = 640/14 nm) and emission (DAPI $\lambda = 452/45$ nm, GFP $\lambda = 525/45$ nm, RFP $\lambda = 609/54$ nm, Cy5 = 676/29 nm) filters with iQ 3.6.1 (Andor) software. For each nucleus, image stacks of 40-80 slides depending on the C-value of the nucleus, on average, with 0.2 μm z-step were acquired and subsequently merged into a 3D maximum intensity projections (mip) models. DSD2 microscope was used in all experiments performed in this master thesis. In addition, for task C imaging was performed with a Leica confocal microscope TCS SP8 (Leica 265 Microsystems) and HC PL PAO CS2 63×/1.4 OIL objective equipped with Leica LAS-X software (Leica). Images were captured separately for each fluorochrome by using 546 (Texas red), 488 (Alexa Fluor 488), and 405 (DAPI) nm laser lines for excitation and appropriate emission filters.

4.4.6 Image analysis

All photos were converted into *.ims* format using the Imaris converter 9.2.1 (Bitplane, Oxford Instruments). Subsequent analyzes were performed using the extended version of Imaris 9.7 (Bitplane, Oxford Instruments).

Preparation of karyotype and idiogram

To prepare karyotypes, homologous chromosomes were paired based on the position of *rDNA* loci and *CEREBA* FISH signals. The classification of individual chromosomes was made according to (Kapousi *et al.*, 2012). The karyotypes and idiograms were constructed in Adobe Photoshop CS5 6.0. (Task A).

Estimation the number of FISH signals

Number of *45S rDNA*, major and minor signals *5S rDNA* FISH signals was quantified in FIJI with the ‘Multipoint’ tool using *mip .tif* images (Task B).

Nucleoli organization analysis

The ratio nucleolus area/nucleus area was obtained based on the measurements performed in FIJI using *mip .tif* images. First, the scale was set up for each image, using ‘Set scale’ function. Then, using freehand selection, the nucleus was covered, the area was automatically measured. The same pipeline was applied for individual nucleoli measurements. Ratio nucleolus area/nucleus area was calculated in Microsoft excel. The correlation (Rr) value was obtained in Microsoft Excel using Data Analysis Tool plugin. The percentage of individual nucleolus was calculated (nucleolus/nucleus area) and the nucleoli were sorted into five categories – very small (I), small (II), medium (III), large (IV), very large (V). This analysis was performed in Microsoft excel using Logical functions. The fluorescence intensity of FIBRILLARIN signals was measured in FIJI, making a straight line through the region of interest. The ‘Plot profile’ tool was used for generating the graphs (Task D).

Visualization of nucleus surface and signals

For rendering the surface of DAPI-stained nuclei and for getting the 3D nucleus images, the ‘Surface’ function of Imaris 9.7 was used. For modeling the centromere/telomere signals, the ‘Spots’ function in Imaris was applied. For imaging the distribution of centromeric and telomeric spots inside the nucleus space the ‘Clipping plane’ function of Imaris was used (Task E).

Rabl configuration analysis

The 'Shortest Distance to Spots' values were obtained from each analyzed nucleus containing centromeric and telomeric FISH signals. The values were gained by marking both segmented objects (centromeric and telomeric spots), going to the Statistics tab and clicking on the 'export' button. Excel files were generated for each individual nucleus. The nucleus diameter was measured using Imaris 'Measurement point' in pair mode. The distance measurement between centromeres and telomeres was calculated by dividing minimal distance between spots/longest nucleus diameter (Task E).

4.4.7 Statistical analysis

One-way analysis of variance (ANOVA) was used to determine the variability in the obtained data set. Tukey's post hoc test with a confidence interval of $p=0.05$ was used to compare relevant values. All statistical analysis was performed in Minitab (Minitab Inc.).

5 RESULTS

5.1 SELECTION GENOTYPE AND CHROMOSOMAL LANDMARKS FOR FURTHER EXPERIMENTS

To study chromosome organization in embryo and endosperm nuclei, it was necessary to choose an accession for which chromosomal landmarks would be easily recognizable. The studies were carried out on two cultivars: Compana and Morex, one landrace originating from Ethiopia and one accession of wild barley. As chromosomal landmarks three major tandem repetitive regions *5S rDNA*, *45S rDNA* and *CEREBA* centromeric repeats were selected. Barley possesses a haploid complement of 7 chromosomes, where the number of *5S rDNA* and *45S rDNA* loci is variable and stable between different genotypes, respectively (Fukui *et al.*, 1994).

Figure 10 shows, that the number and position of *45S rDNA* loci did not differ between genotypes. The *45S rDNA* loci were located in the distal region of the short arms of chromosomes 5H and 6H.

Further, it was confirmed that the number and position of *5S rDNA* loci differed between the examined accessions (Figure 10). For all genotypes, the bottom arm of chromosome 2H had a distinguishable large locus visible as strong FISH signal (hereafter called as *5S major rDNA*). Further, cv. Morex, landrace and wild barley had another *5S major rDNA* locus at the bottom arm of chromosome 3H, whereas in cv. Compana this locus was smaller (the FISH signal is weaker). In all accessions, the pericentromeric regions of the upper arms of chromosome 7H carried weak *5S rDNA* signals (hereafter called as *5S minor rDNA*). In the Ethiopian landrace 1 additional strong locus on chromosome 4H and 2 weak loci on chromosome 5H and 6H were recognized. In turn, cv. Compana possessed *5S minor rDNA* loci (very weak FISH signals) at pericentromeric regions of chromosomes 4H and 6H.

To summarize, as cv. Compana had only 1 major and several minor *5S rDNA* loci, this cultivar was selected for further experiments.

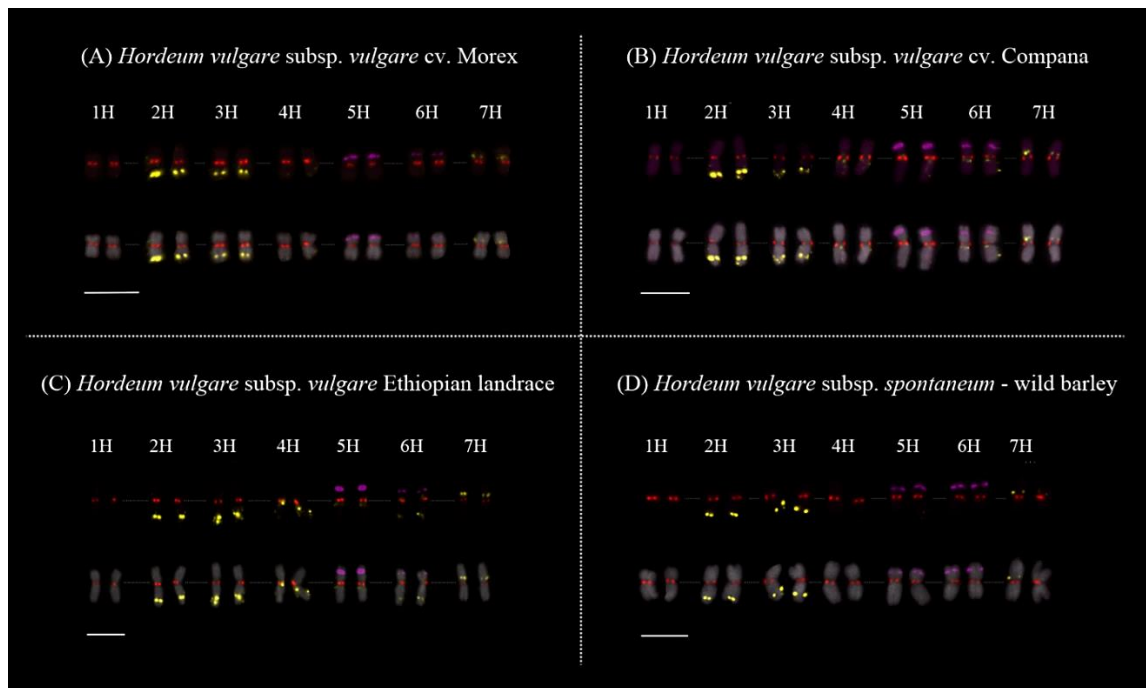


Figure 10: Karyotypes of four barley accessions. Fluorescence *in situ* hybridization was performed on RAM metaphase chromosomes using *CEREBA*-centromeric (red), *45S* (purple) and *5S* (yellow) *rDNA* probes. DNA was counterstained with DAPI (grey). Scale bars=10 μ m.

5.2 STUDY OF LOCUS-SPECIFIC SISTER CHROMATID ALIGNMENT IN MITOTICALLY DIVIDING AND ENDOREDUPLICATED NUCLEI

Sister chromatid cohesion in interphase embryo and endosperm nuclei was analyzed using FISH with *rDNA* probes. Populations of nuclei were sorted from seeds collected at 8 DAP and 24 DAP, as these days represent early and late phases of seed development, respectively. For embryo and RAM (both diploid tissues), the populations of 2C (G1 phase) and 4C (G2 phase) nuclei were sorted. These populations represent mitotically cycling nuclei. For 24 DAP embryo, except from above fractions, there was also population of 8C nuclei representing the first level of endoreduplicated nuclei (one round of endocycle). For endosperm, the populations of cycling 3C (G1 phase) and 6C (G2 phase) nuclei were collected. Endoreduplicated nuclei 12C were sorted for both 8 and 24 DAP time points, and 24C nuclei were collected for 24 DAP seeds. The populations of 12C and 24C nuclei represented the first and second rounds of endocycles, respectively.

As it was established in the previous subchapter, cv. *Compana* had 1 major and 4 minor *5S rDNA* loci, which after FISH should be visible as strong and weak signals, respectively (Figure 11A). One signal reflects full sister chromatids alignment. Therefore, in the case of *5S major rDNA* locus, it was expected to observe 2 and 3 strong FISH signals for diploid and triploid nuclei,

respectively. More signals reflect sister chromatids separation. For *5S minor rDNA* loci, 4 and 6 weak signals should appear for diploid and triploid nuclei, respectively. For *45S rDNA* loci, it was assumed to have 4 signals for diploid and 6 signals for triploid nuclei.

Both 2C embryo and RAM nuclei displayed on average 2 strong *5S major rDNA* FISH signals per nucleus (Figure 11B). However, in 4C and 8C nuclei isolated from 24 DAP seeds, the average number of signals increased to 3 and 5, respectively. For endosperm, the number of *5S major* signals was 3 for 3C nuclei. This number increased with increasing C-value. For example, 24 DAP 12C nuclei had on average 11 signals and 24 DAP 24C showed even 21 signals.

The number of *5S rDNA* weak FISH signals for both diploid and triploid nuclei progressively enhanced with increasing C-value and seed age (Figure 11B). In detail, for 2C embryo nuclei there were ~7-10 signals per nucleus. The 4C and 8C contained ~10 and ~20 signals per nucleus. The 3C endosperm nuclei had on average 8 signals. The mean number of signals in 6C nuclei amounted 11 and 14 for populations isolated from 8 and 24 DAP seeds, respectively. Finally, 12C endoreduplicated nuclei showed on average 17 signals in 8 DAP sample and two times more in 24 DAP samples. For 24C/24 DAP nuclei fraction the amount of *minor 5S rDNA* foci reached almost 50.

Analysis of the *45S rDNA* revealed a lower-than-expected number of FISH signals. For diploid samples (both embryo and RAM), there were 3 to 4 signals per nucleus. Endosperm nuclei possessed 5 or 6 signals.

In conclusion, sister chromatid separation at major and minor *5S rDNA loci* significantly increased with rising C-value and seed age. The organization of *45S rDNA* loci remained relatively intact. This suggests a locus-specific control of sister chromatid alignment in barley endoreduplicated seed nuclei.

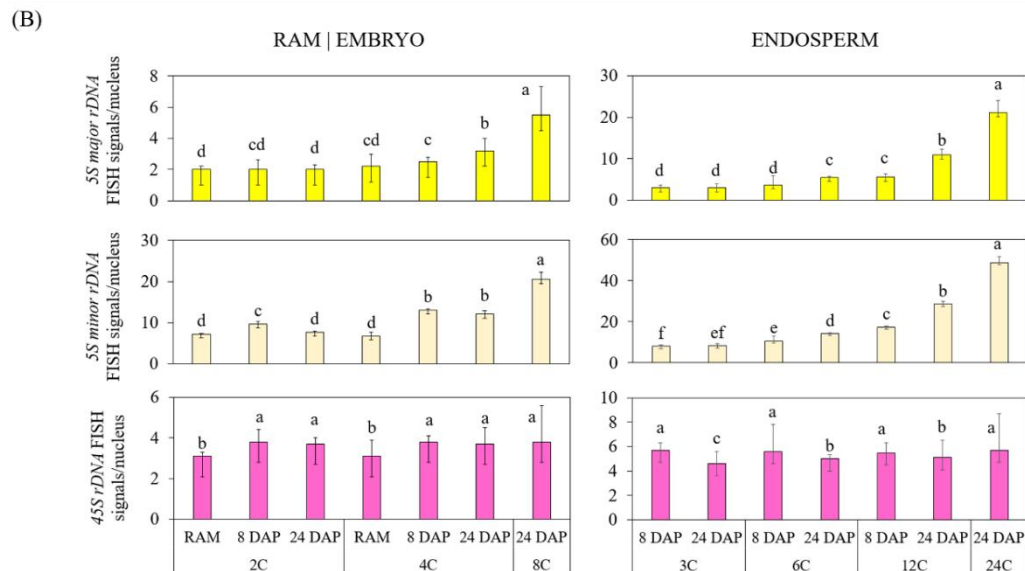
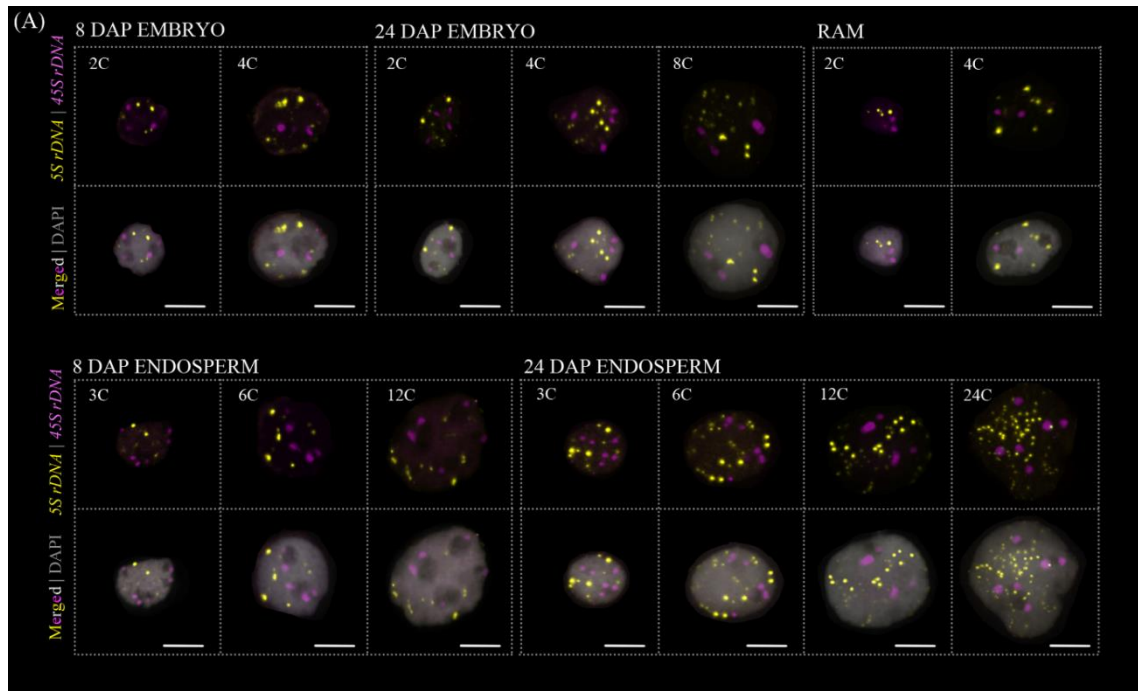


Figure 11: Sister chromatid cohesion at 5S and 45S rDNA loci of barley seed nuclei.

(A) Representative photos of embryo and endosperm nuclei (8 DAP and 24 DAP) with different C-values. Root apical meristem (RAM) nuclei were used as somatic tissue control. Fluorescence *in situ* hybridization was performed to detect 45S (purple) and 5S (yellow) rDNA loci. The larger and brighter 5S rDNA signals correspond to the 5S major rDNA loci. DNA was counterstained with DAPI (grey). Scale bars=10 μm. (B) Graphs showing the number of major and minor 5S rDNA and 45S rDNA FISH signals per nucleus for different tissues, C-values, and DAP. Each sample contained ≥ 70 evaluated nuclei. Values are the averages \pm SD. Different letters indicate significant differences between samples ($p \leq 0.05$, one-way ANOVA, followed by Tukey's post hoc test).

5.3 OPTIMALIZATION OF OLIGOPAINTING-FISH TO STUDY SISTER CHROMATID COHESION AT SPECIFIC CHROMOSOMAL SEGMENTS

The next logical step of the experiments was to analyze sister chromatid cohesion at specific chromosomal segments. This is possible to use method called oligopainting-FISH. For this study, probes were designed to label segments of the upper (6H-1) and lower arms (6H-13) of chromosome 6H as well as its pericentromeric region (6H-6). First, these probes were hybridized to metaphase chromosomes of RAM. The presence of FISH signals at the ends and in the pericentromeric region of the 6H chromosome confirmed the segment-specificity of designed probes (Figure 12). Further, hybridization of the probes to nuclei isolated from embryo and endosperm tissues, did not reveal any FISH signals, even when confocal microscope was used for signal detection. This suggests further need to optimize FISH conditions.

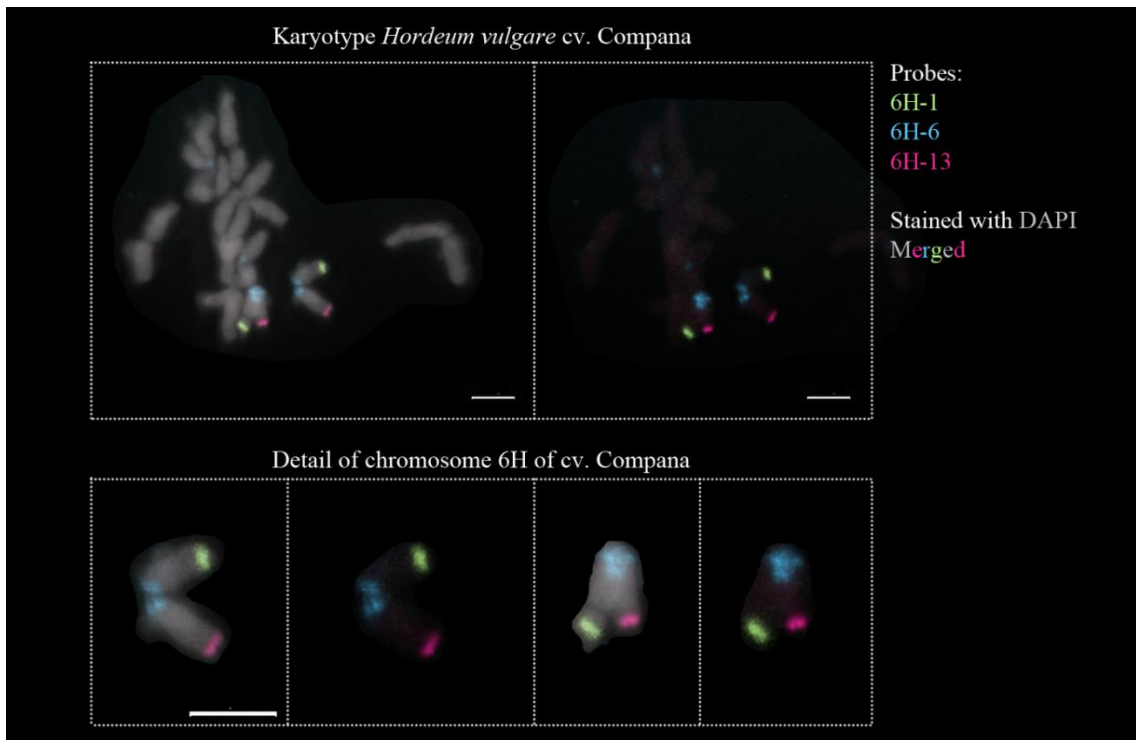


Figure 12: Fluorescence *in situ* hybridization with oligo-probes hybridizing to three regions on 6H barley chromosome. Karyotype of cv. Compana showing the localization of 6H-1 (light green), 6H-6 (light blue) and 6H-13 (burgundy) barley chromosome segments. DNA was counterstained with DAPI (grey). Scale bars=5 μm .

5.4 CHARACTERIZATION OF NUCLEOLI IN CYCLING AND ENDOREDUPLICATED NUCLEI

For the study of nucleoli organization, FIBRILLARIN and *45S rDNA* immuno-FISH was performed (Figure 13 – Representative photos). FIBRILLARIN protein localized in nucleoli and genes encoding *45S ribosomal RNA* are associated with NOR and are clustering preferentially around the nucleolus. In this experiment, the nuclei sorted from seeds collected 8 and 24 DAP were used. Analogously to previous parts of this thesis, the same populations of nuclei were collected.

First, for each nucleus its area and the total nucleoli area were measured. For these parameters the Pearson correlation coefficient (R_r) was calculated. It is a number between -1 and 1 that measures the strength and direction of the relationship between two variables. The percentage of total nucleoli area/nucleus area and the R_r were decreasing with increasing C-value and sample age (Figure 14A). The only exception were 2C/24 DAP embryo nuclei, where there was no correlation between nucleus and nucleoli size ($R_r=-0.04$). Interestingly, although the nucleoli were decreasing, the *45S rDNA* loci were always attached with nucleoli (Figure 13).

Second, each individual nucleolus within nucleus was categorized into one of five established classes: I – very small nucleolus; II – small nucleolus; III – medium nucleolus; IV – large nucleolus; V – very large nucleolus. The categories were established based on the percentage area of each individual nucleolus relative to the total area of the nucleus (Figure 14B). For example, average 2C/8 DAP embryo nucleus had 4 nucleoli: 2 very small, 1 small and 1 medium. This slightly changed with increasing the sample age, because 2C/24 DAP embryo nucleus showed in total 3 nucleoli: 2 very small and 1 medium. Importantly, all 2C, 4C and 8C embryo nuclei possessed only very small to medium-sized nucleoli. In the case of endosperm, 3C/8 DAP nucleus contained on average 5 nucleoli: 3 very small, 1 medium and 1 large. Then, 3C/24 DAP and 6C/8 and 24 DAP nuclei had also in total a few small to medium-sized nucleoli. Interestingly, in endoreduplicated 12C and 24C nuclei isolated from old seeds, the number of very small nuclei increased to reach around 10 and 20 per nucleus, respectively. This indicates the tendency to dispersion of nucleoli in endoreduplicated nuclei.

Figure 14C shows the average nucleolus area relative to the total area of the nucleus. In embryo cycling nuclei (2C and 4C), the average nucleolus occupied 2 – 3% of the nucleus area. In 8C endoreduplicated nucleus, the average nucleolus decreased to 1.13% of the nucleus area. In endosperm cycling nuclei (3C and 6C) isolated from 8 DAP seeds, the average nucleolus area was ~4%. In endoreduplicated 12C/8 DAP nucleus, the average nucleoli size was reduced twice (~2.11%) as compared to cycling nuclei. Interestingly, the average nucleolus area in 3C and 6C/24 DAP endosperm nuclei occupied less than 2% of the nucleus area. Endoreduplication

decreased the average nucleolus area even more. The 12C and 24C/24 DAP showed tiny nucleoli, individual nuclei occupying less than 1% of the nucleus area. To summarize, the endoreduplication and sample age caused decreasing nucleoli area.

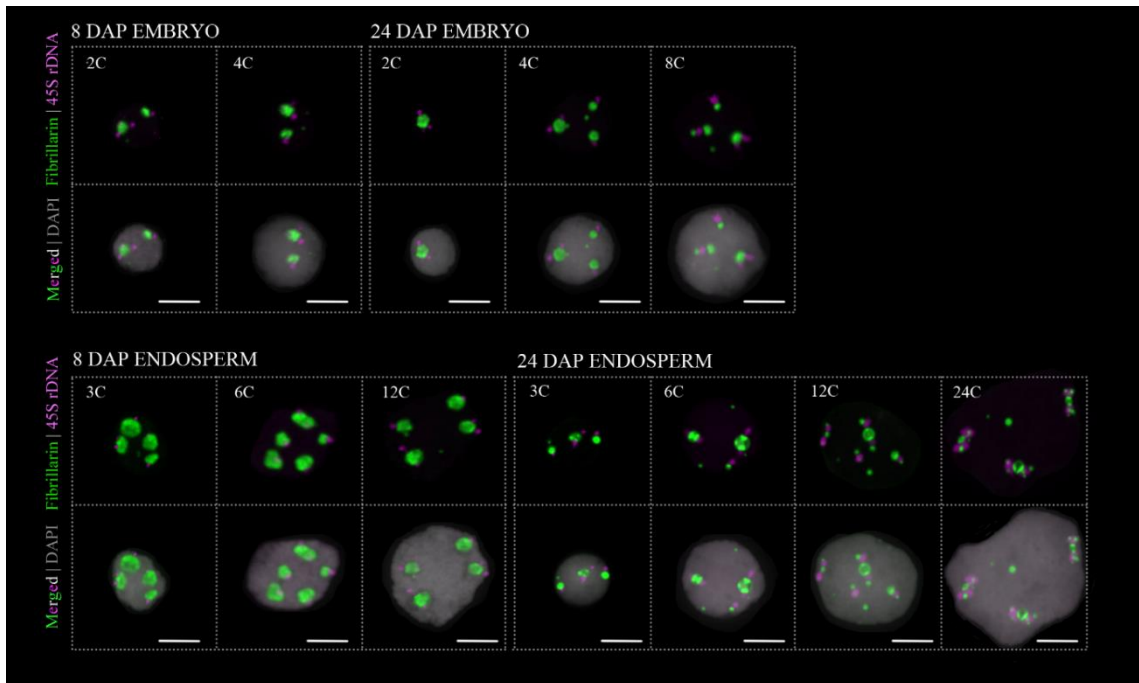


Figure 13: Microscopic characteristics of the nucleoli in cycling and endoreduplicated nuclei.

Representative photos of embryo and endosperm nuclei (8 DAP and 24 DAP) with different C-values after ImmunoFISH with *45S* (purple) *rDNA* probe and anti-FIBRILLARIN antibody (green). DNA was counterstained with DAPI (grey). Scale bar=10 μm .

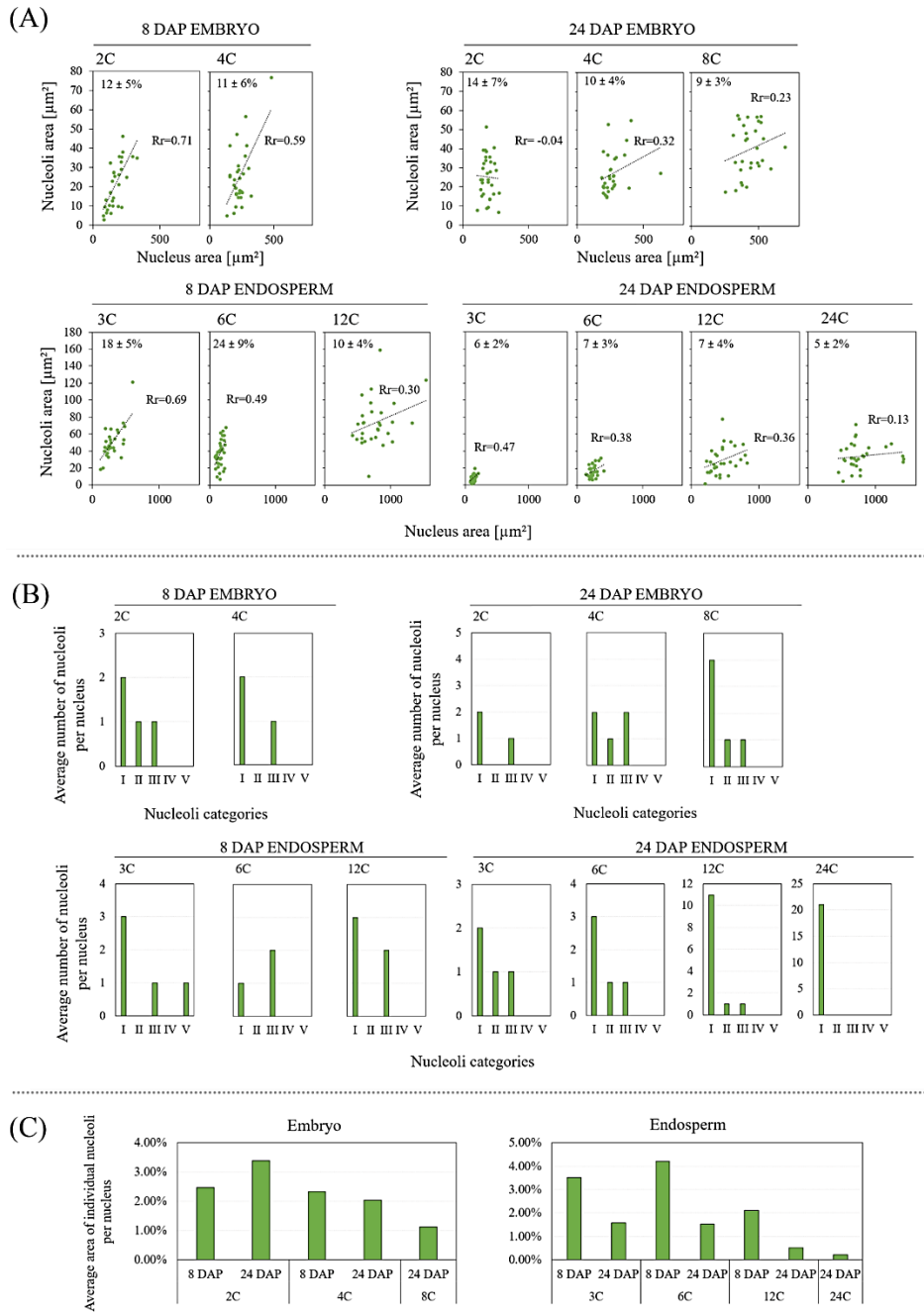


Figure 14: Nucleoli organization in cycling and endoreduplicated embryo and endosperm nuclei.

(A) Graphs showing the values of total nucleoli area depending on nuclei area for embryo and endosperm tissue, C-value, and DAP. At least 30 nuclei were analyzed for each C-value. The total nucleoli area/nucleus area in percentage is shown in a left corner of each graph. R_r = Pearson correlation coefficient was calculated for total nucleoli area versus nucleus area. (B) Graphs showing the average number of nucleoli per nucleus. Nucleoli were categorized into 5 classes. The categories were established according to the following criteria (by their ratio nucleoli/nucleus): $<1\%$ = I; $1-2\%$ = II; $2-8\%$ = III; $8-10\%$ = IV and $>10\%$ = V. Each graph shows average value. (C) Graphs showing the average nucleolus area relative to nucleus size.

Next, to analyze the detailed localization of FIBRILLARIN protein in the nucleoli, the fluorescence intensity of the immunostaining signal was measured (Figure 15A). The quantification was based under assumption that the fluorescence intensity of signals should directly reflect the amount of FIBRILLARIN protein. The nuclei were prepared as it is described in the previous subchapter.

It was found that the fluorescence signals were stronger at the periphery of the nucleoli and weaker in the center (Figure 15B). In addition, there were one or two fluorescence intensity peaks, indicating that FIBRILLARIN accumulated either on one or on both sides of the nucleolus.

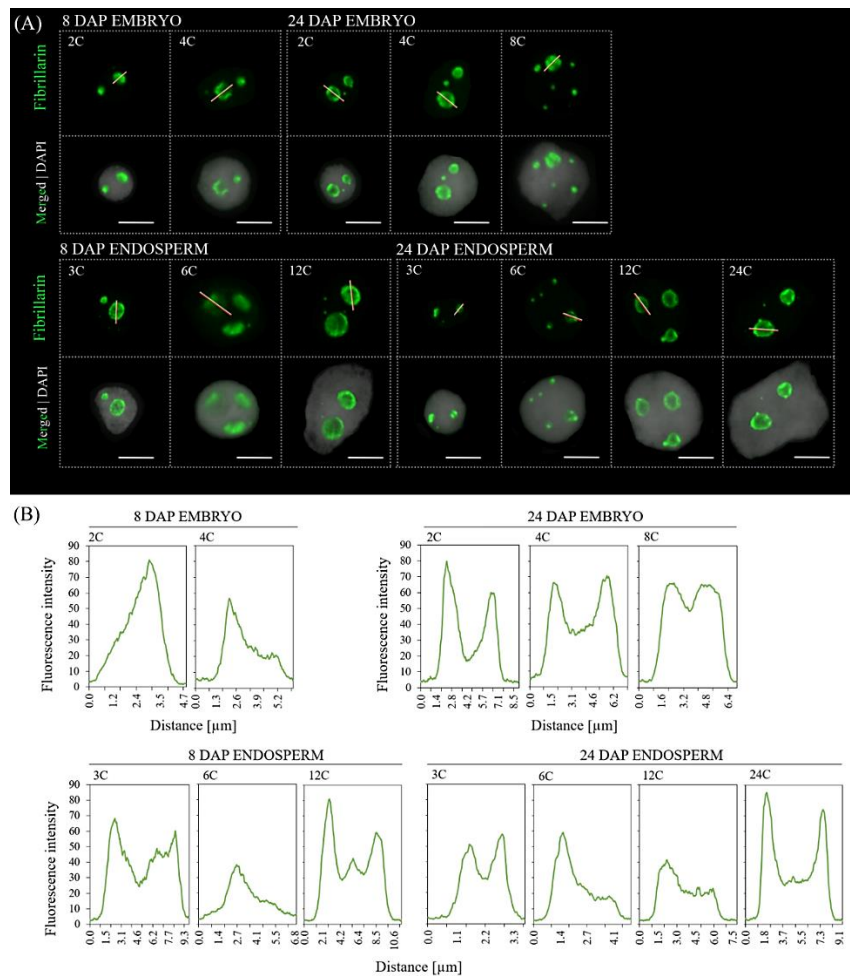


Figure 15: Location of FIBRILLARIN protein in nucleoli.

(A) Representative photos of embryo and endosperm nuclei (8 DAP and 24 DAP) with different C-values. Immunostaining with anti-FIBRILLARIN antibody. DNA was counterstained with DAPI (grey). Scale bars=10 μ m. The white-red straight lines indicate the place where the fluorescence intensity was measured. (B) Fluorescence intensity plot profiles of FIBRILLARIN. The analyzed nucleolus was chosen randomly.

5.5 STUDY OF RABL CHROMOSOME CONFIGURATION IN SEED NUCLEI

To study Rabl chromosome organization, FISH with *CEREBA* centromeric probe and telomeric probe was performed. First, the probes were tested using metaphase chromosomes of RAM (Figure 16). Recent study confirmed the regular Rabl configuration in meristem cells of barley root tips (Němečková *et al.*, 2020). Here, we asked the question if embryo and endosperm nuclei fractions will retain Rabl configuration and how it will be affected by the increasing seed age?

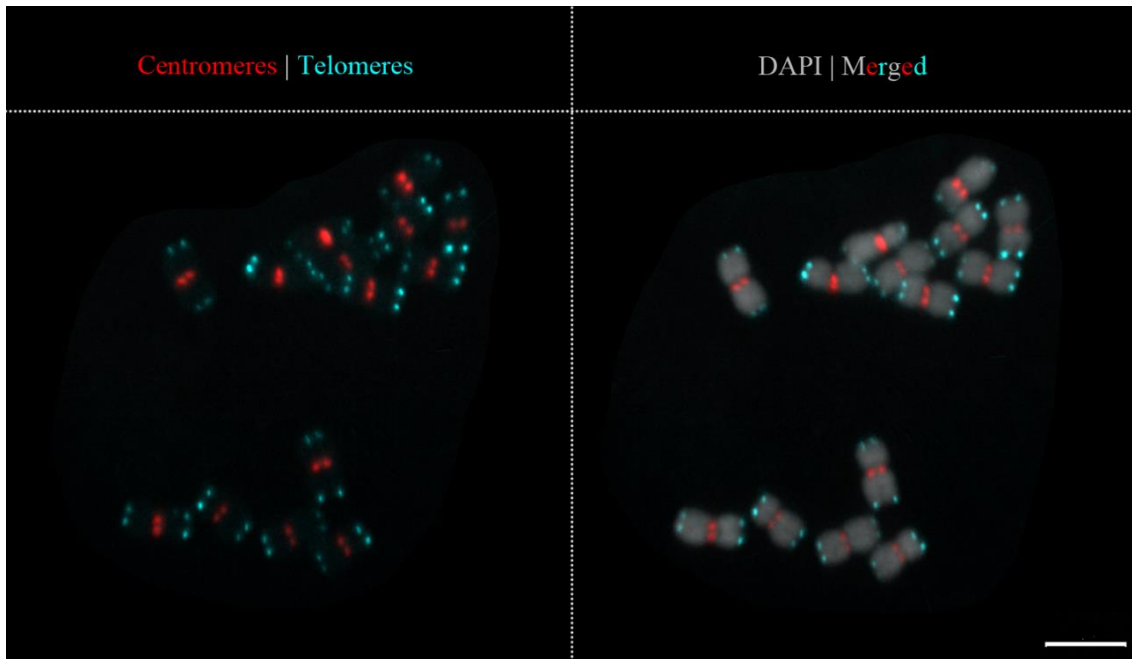


Figure 16: Metaphase chromosomes of RAM after FISH with centromeric and telomeric probes. Centromeres in red, telomeres in turquoise. DNA was counterstained with DAPI (grey). Scale bar=7 μm .

Analogously to the previous experiments, both mitotically dividing and endoreduplicated nuclei of embryo and endosperm tissues were flow-sorted from seeds collected at 8 and 24 DAP. Based on location of centromeric and telomeric FISH signals (Figure 17), three categories of the nuclei were distinguished, (i) bearing Rabl chromosome pattern with centromeres and telomeres at the opposite sides of the nucleus, (ii) nuclei with centromeres and telomeres moved from nucleus poles, but not touching each other (intermediate phenotype), and (iii) nuclei with mixed centromeric and telomeric FISH signals (non-Rabl). To quantify these three established categories, the shortest distance between centromeres and telomeres was measured and then this value was normalized to the nucleus diameter (Figure 18A).

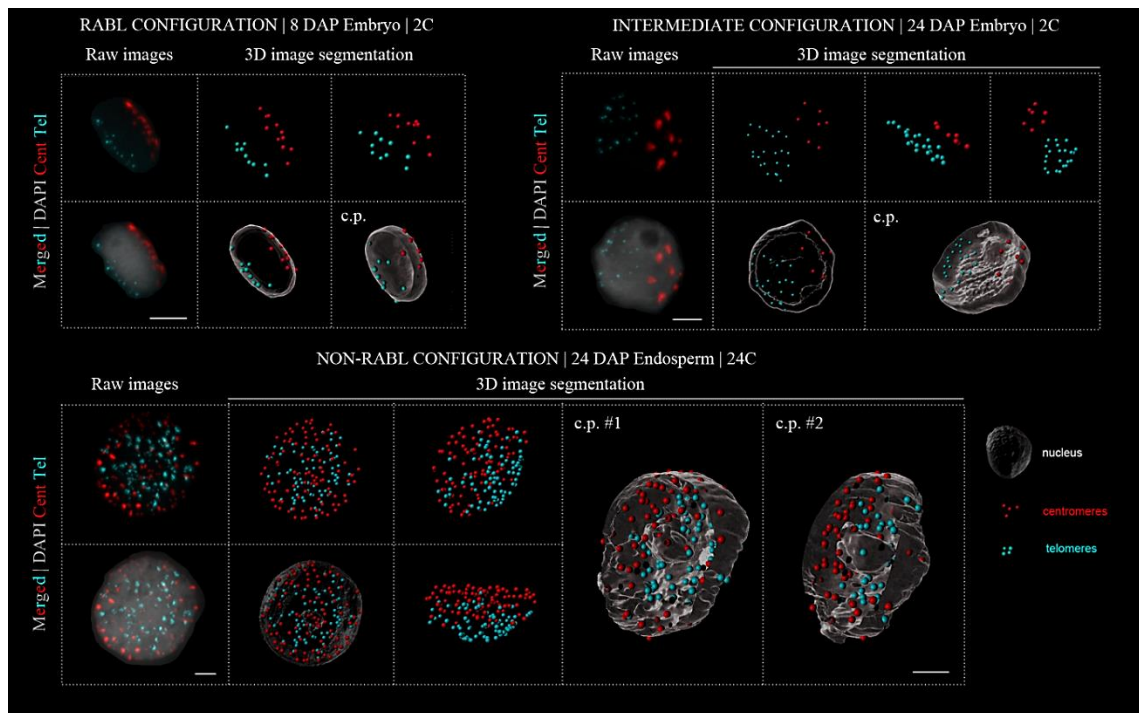


Figure 17: Three phenotypes of chromosome organization at interphase nuclei of barley seeds. Representative raw photos of embryo and endosperm nuclei. Fluorescence *in situ* hybridization with *CEREBA* centromeric (red) and telomeric (turquoise) probes. DNA was counterstained with DAPI (grey). The 3D image segmentation pictures showing nucleus surface, FISH signals and their distribution within the nucleus. Clipping planes (c.p.) show the interior of 3D modeled nuclei. Scale bars=10 μ m.

In embryo, the mean values of shortest centromere to telomere distance (Figure 18A) were not significantly different for 2C and 4C nuclei, ranging between 0.3-0.4. In 8C nuclei, the value was lower, 0.07, indicating shift of centromeres and telomeres to the middle of the nucleus. In endosperm tissues, this parameter was significantly different between C-value and seed age. There was a gradual decrease from 0.29 (3C/8 DAP) to 0.06 (24C/24 DAP) with C-value and age. For 12C and 24C endosperm nuclei collected at 24 DAP, the centromeres and telomeres moved from nuclei poles and occupied the whole space of the nuclei. From these values, three categories of nuclei were established: Rabl 0.30-0.60, intermediate 0.15-0.29, and non-Rabl 0.02-0.14 (Figure 18B).

The frequency of these categories was assessed in all experimental points (Figure 18C). In embryo, the nuclei had mostly Rabl configuration – from 77% (8C/24 DAP) to 95% (2C/8 DAP). The intermediate configuration ranged from 5% (2C/8 DAP) to 23% (8C/24 DAP) nuclei. In embryo samples, non-Rabl nuclei were not observed. There were significant differences in the proportions of nuclei classes in endosperm samples as compared to embryo. The number of nuclei with Rabl configuration were decreased in 12C and 24C/24 DAP endoreduplicated nuclei (15%

and 0%, respectively). It was clearly visible that the number of non-Rabl nuclei was gradually increasing with C-value and age. From 2 – 8% in cycling nuclei to 31% and 49% for 12C and 24C/24 DAP endoreduplicated nuclei, respectively.

Collectively, both qualitative and quantitative analysis show that there is a loss of Rabl chromosome configuration in the embryo and endosperm endoreduplicated nuclei.

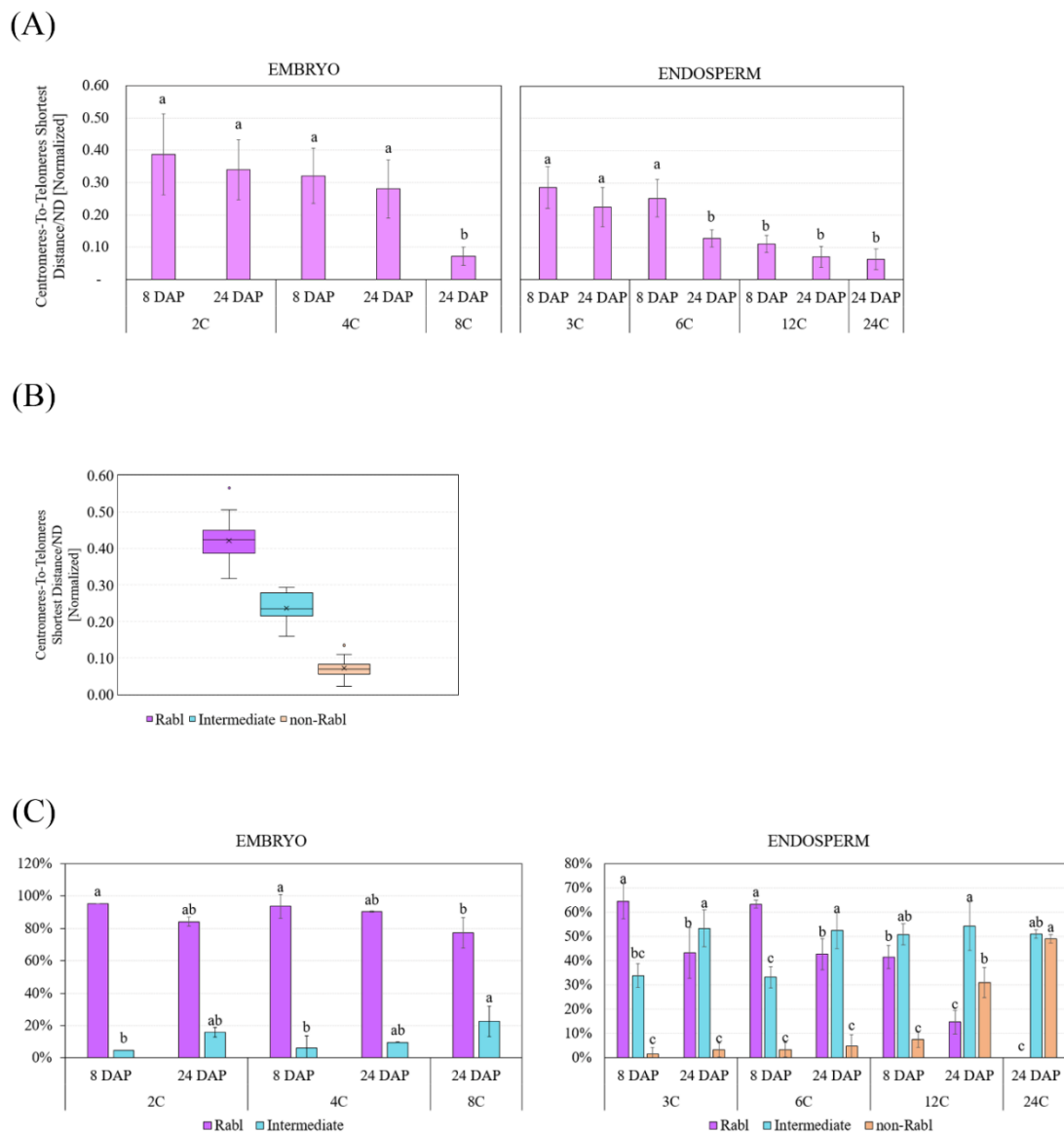


Figure 18: Graphs for Rab1 chromosome organization.

(A) Graphs showing the shortest distance between centromeres and telomeres normalized to nucleus diameter (ND). Each sample had 6 – 7 evaluated nuclei. The graph shows mean value \pm SD for each tissue, C-value, and DAP. Statistics was performed for embryo and endosperm separately. Different letters indicate significant differences between samples ($p \leq 0.05$, one-way ANOVA, followed by Tukey's post hoc test).

(B) Boxplots showing the shortest distance between centromeres and telomeres normalized to nucleus diameter (ND). The lower and upper hinges of the boxplot correspond to the first and third quartiles of the data and the black lines within the boxes mark the median. There were in total 42 evaluated nuclei.

(C) Percentage of nuclei with Rab1, intermediate and non-Rab1 chromosome organization. Values are the means \pm SD from 3 biological replicates (microscopic slides), each with ≥ 25 evaluated nuclei. Statistics was made for each category (Rab1, Intermediate, Non-Rab1) and embryo and endosperm separately. Different letters indicate significant differences ($p \leq 0.05$, one-way ANOVA, followed by Tukey's post hoc test).

6 DISCUSSION

6.1 Selection the genotype and cytogenetic markers

The main goal of this study was to analyze chromosome organization in mitotically cycling and endoreduplicated nuclei isolated from embryo and endosperm tissues of developing barley grains. Therefore, the first step of the research was to screen several barley accessions in order to select the one in which cytogenetic markers would be easy to recognize. This analysis was performed on metaphase chromosomes of RAM, which is a diploid somatic tissue. I focused on genes encoding ribosomal RNA (rRNA). *rDNA* are the most abundant genes in the eukaryotic genome. They reside in tandem repetitive clusters, in some cases totaling hundreds of copies (Kobayashi, 2011). In barley, the position and number of *45S rDNA* loci is stable in all accessions, while the *5S rDNA* loci are variable. I wanted to select the genotype, where the major and minor *5S rDNA* loci will be clearly visible and distinguishable. As a reference, I used cv. Golden Promise, where there are two *5S major rDNA* loci cluster on at the bottom arm of chromosome 2H and pericentromeric region of chromosome 7H (Kapusi *et al.*, 2011). Here, I tested four barley genotypes cv. Morex, Compana, Ethiopian landrace and one wild barley accession. Cultivar Morex is the reference strain, which means that its genome was already sequenced and the reference map was prepared (Mascher, 2021). Cultivar Compana was used in the study of endoreduplication dynamics during barley seed development (Nowicka *et al.*, 2021). Ethiopian landrace and wild barley the genotypes sequenced within the barley pangenome project (Jayakodi *et al.*, 2020). After performing FISH with *45S* and *5S rDNA* as probes, I observed that cv. Compana had one major *5S rDNA* locus located on chromosome 2H, and the other accessions had two major *5S rDNA* loci - one on chromosome 2H and one on chromosome 3H. When it comes to the minor *5S rDNA* loci, the same as in cv. Golden Promise, all genotypes studied here had several of them. I could clearly distinguish *5S major* and *5S minor rDNA* loci in cv. Compana, visible as strong and weak FISH signals, respectively, therefore this cultivar was selected for all the upcoming experiments performed using flow-sorted embryo and endosperm nuclei.

6.2 Sister chromatid cohesion at *45S* and *5S rDNA* loci

Sister chromatid (SC) cohesion is defined as the colinear alignment of chromatids from one chromosome (Schubert *et al.*, 2005). Here, I found that SC association along replicated chromatids is position-specific (*5S* and *45S rDNA* loci), C-value- and age-dependent. When it comes to *45S rDNA* loci, I noticed, that in both in embryo and endosperm nuclei, the number of *45S rDNA* FISH signals remained the same and was non-affected by increasing C-value- and seed age. Absence of SCs dissociation at *45S rDNA* loci was previously shown in all types of plant body tissues (Schubert *et al.*, 2005; Bourdon *et al.*, 2012; Baroux *et al.*, 2016). As it was explained earlier, during endocycle, the chromatids are replicated, but not segregated, resulting in

chromosomes with many chromatids called polytene chromosomes (D'amato, 1964). The presence of 4 and 6 *45S rDNA* FISH signals in embryo and endosperm nuclei, respectively, first confirmed that chromosome number was not affected by endoreduplication, and second demonstrated the occurrence of polytenic chromosomes (Bourdon *et al.*, 2012).

In turn, the analysis of *5S rDNA* loci revealed, that the SCs there were strongly dissociated with increasing age and C-value both in embryo and endosperm nuclei. While the nucleus is dividing, the chromosome condensation is mediated by chromosomal cohesion sites, where 'glue' molecules hold sister chromatids together. Between individual cohesion sites there are symmetric loops, and their size determines the degree of SC compaction (Koshland and Guacci, 2000). It is possible, that in the case of *5S rDNA* loci various degree of dissociation, may depend on non-uniform chromosomal distribution of cohesion sites (Schubert *et al.*, 2005). The number of cohesion sites in cells with polytene chromosomes may not be changed (as compared to cycling cells) resulting in larger loops between the sites. This possibly causes positional separation along SCs (Schubert *et al.*, 2005). The second possible explanation of position-specific SC cohesion is the higher transcriptional activity in endoreduplicated nuclei (Bourdon *et al.*, 2012). The various degree of chromatin condensation potentially makes genes encoding *5S rRNA* more accessible for the transcription machinery (Schubert *et al.*, 2012). These data revealed that further comparative studies of other chromosomal regions are needed to verify the hypothesis of whether transcriptional activity affects barley SC cohesion.

6.3 Testing the chromosome-arm-specific oligopainting probes

In plants, advanced cytogenetic studies are limited by the lack of DNA probes useful for labeling individual chromosomes. The solution for this problem was developing BAC (Bacterial Artificial Chromosome) probes. This probe contains large fragments of the genome that should mark part or even the entire chromosome (Pecinka *et al.*, 2004). However, BAC-probes are not applicable to plants with huge genome with lots of repetitive sequences, like for example barley (Šimoníková *et al.*, 2019). Here, the alternative solution could be the method called oligopainting-FISH (Han *et al.*, 2015). This approach enabled an alternative and affordable preparation of probes for plants with larger genomes. It is based on identification of large numbers of short (45-50 bp) and single copy sequences in individual chromosomes and synthesis of oligonucleotides. Then these oligonucleotides can be labeled by fluorescent dyes and used as a probe for FISH (Šimoníková *et al.*, 2019). The oligopainting-FISH has not yet been done in barley. As part of the research conducted in this thesis, I tested three chromosome-arm-specific oligopainting designed specifically for 6H barley chromosome segments (probes were designed by dr. Eva Hříbová and labeled by dr. Denisa Beránková). I observed that all probes hybridized specifically to segments of 6H chromosome, but in both cycling and endoreduplicated nuclei, the FISH signals

were not present. So far, in other plant species, the oligopainting approach has only been performed on mitotic chromosomes (Šimoníková *et al.*, 2019; Šimoníková *et al.*, 2020), where chromatin is more condensed than in interphase nuclei. This protocol requires further optimization, e.g., adjusting the number of probes added to the hybridization mix, changing the hybridization and detection conditions (e.g., stringency) or using a microscope with higher resolution. The application of oligo-probes specific for chromosome arms could answer the question posed in the previous section about controlling SC cohesion, not only at specific loci, but also at larger regions of the chromosomes.

6.4 Nucleoli organization study

There is at least one nucleolus in each eukaryotic nucleus, whose size and organization depends on ribosome production. Besides that, nucleolus also plays role in stress response, production of ribonucleoproteins and in humans also several diseases (Hernandez-Verdun, 2011). As it was explained earlier, the nucleolus is formed from FC, DFC and GC, where in each compartment different processes takes place. At the border FC-DFC the initiation of *rDNA* transcription occurs, in the DFC early processing of the rRNAs and in the GC late processing of the rRNAs takes place. At the beginning of mitosis, the nucleolus starts to disassembly. This is followed by repression of RNA polymerase I transcription in the late prophase (Hernandez-Verdun, 2011) and the ribosomal RNA is no longer transcribed and created. The results obtained in this thesis revealed, that endoreduplicated nuclei had smaller and more dispersed nucleoli than in cycling nuclei. It might be caused by the absence of mitosis during endocycle, where the correct disassembly/assembly of nucleolus takes place. The small nucleoli in endoreduplicated nuclei may indicate decreasing of ribosomal RNA transcription. At the end of mitosis, the assembly of small nucleoli occurs at each active NOR, and as interphase progresses, the nucleoli form a single nucleolus (Kalinina *et al.*, 2018). Since there is no M phase during endocycle, the signals for the formation of one whole nucleolus may be corrupted, leading to dispersion. On the other hand, the collapsing of nucleoli in endoreduplicated nuclei isolated from old seed could be the marker of PCD, which accompanied the seed maturation (Nowicka *et al.*, 2021).

There are three major nucleolar proteins - FIBRILLARIN, NUCLEOLIN and B23. After RNA polymerase I transcription, the pre-rRNA takes form of *45S rRNA*, which can be processed by snoRNPs (small nucleolar ribonucleoproteins). FIBRILLARIN is a key component of snoRNP particles and important in pre-rRNA processing and splicing of snoRNA (Kalinina *et al.*, 2018; Perutka *et al.*, 2021). The fluorescent measurements of FIBRILLARIN signals showed, that the pre-rRNA processing is located at the nucleolus periphery in both cycling and endoreduplicated nuclei.

6.5 Rabl chromosome configuration in mitotically active and endoreduplicated nuclei

Rabl chromosome configuration is still a topic for discussion, even now, 130 years after its discovery (Rabl, 1885; Santos and Shaw, 2004). The presence of Rabl configuration differs in different species, and between tissues and developmental stages of the organism (Idziak *et al.*, 2015; Němečková *et al.*, 2020; Shan *et al.*, 2021). Moreover, Rabl pattern is present in some cells during interphase and in other cells is maintained during the next mitosis (Cowan *et al.*, 2001). The one explanation of Rabl architecture is the correlation with genome size and chromosome length of the organism. While this is truthful in the majority of organisms, there are some exceptions, where plants with giant genomes do not show the Rabl pattern (Tiang *et al.*, 2011; Fujimoto *et al.*, 2005). This suggests that genome size alone cannot serve as a universal rule defining the Rabl organization.

Therefore, the recent studies focused on different approach of explaining the Rabl organization and why its presence/absence differ between various organisms. Some studies hypothesized that the Condensin II complex is responsible for 3D genome organization during interphase. Incomplete sets of Condensin II subunits causes Rabl chromosome organization in animals (Hoencamp *et al.*, 2021). However, in plants, this rule is not applicable, because all plants sequenced to date contain a full set of Condensin II subunits (Schubert, 2009). This theory still needs further investigation.

One of the goals of this study was finding the tool for precise distinguishing Rabl and non-Rabl configuration in barley seed nuclei. For this purpose, Z-stack images were acquired with semi-confocal epifluorescence microscope. Images were segmented on the channels reporting on FISH signals to create spot objects corresponding to centromeres and telomeres, and the shortest distance between telomeres and centromeres inside the nucleus was automatically measured. These measurements revealed that distance between telomeres and centromeres was shortened with increasing seed age and C-value. This could be caused by disconnection of centromeres and telomeres from nuclear envelope, which has been confirmed in human cell lines by studying the expression level of nuclear lamina proteins (Hoencamp *et al.*, 2021). The centromere disconnection with nuclear lamina was linked with disruption of lamina-related genes. These results are confirming that interactions between centromeres, telomeres and the nuclear envelope are responsible for maintenance of the Rabl chromosome pattern.

I found, that in barley, the Rabl organization depends on the tissue, the seed developmental stage (DAP) and endoreduplication (C-value). The correlation between loss of Rabl organization and endoreduplication suggest, that Rabl configuration is established during mitotic cell divisions (Santos and Shaw, 2004). However, the exact molecular mechanisms controlling the clustering of centromeres and telomeres on opposite sides of the nucleus are currently unknown.

7 CONCLUSION

In conclusion, the analysis performed in my master thesis focused on characterization of chromosome organization in cycling and endoreduplicated barley embryo and endosperm nuclei. Analysis of sister chromatid separation at *45S* and *5S rDNA* loci showed that there is a locus-specific control of sister chromatid alignment in endoreduplicated nuclei. Although it was impossible to study the coherence of sister chromatids across chromosome segments, some suggestions have been made to optimize the oligopainting method. Studies of nucleoli revealed that endoreduplication caused nucleoli disassembly. The polar chromosome organization was progressively lost in endoreduplicated nuclei. All observed changes were accompanied not only by a change in the C value, but also by the age of the sample.

The data presented in this master thesis made a very important contribution to the preparation of the already published manuscript: Nowicka A., Ferkova L., Said M., Kovacik M., Zwyrtková J., Baroux C., Pecinka A. (2023): Non-Rabl chromosome organization in endoreduplicated nuclei of barley embryo and endosperm tissues. *Journal of Experimental Botany* 74(8): 2527–2541.

The manuscript is submitted at the end of this work as Appendix I.

8 REFERENCES

- Amin M. A., Matsunaga S., Ma N., Takata H., Yokoyama M., Uchiyama S., Fukui K. (2007): FIBRILLARIN, a nucleolar protein, is required for normal nuclear morphology and cellular growth in HeLa cells. *Biochemical and Biophysical Research Communications* 360(2): 320–326.
- An L.-H., You R.-L. (2004): Studies on nuclear degeneration during programmed cell death of synergid and antipodal cells in *Triticum aestivum*. *Sexual Plant Reproduction* 17(4): 195–201.
- Angelovici R., Galili G., Fernie A. R., Fait A. (2010): Seed desiccation: a bridge between maturation and germination. *Trends in Plant Science* 15(4): 211–218.
- Baroux C., Pecinka A., Fuchs J., Kreth G., Schubert I., Grossniklaus U. (2016): Non-random chromosome arrangement in triploid endosperm nuclei. *Chromosoma* 126(1): 115–124.
- Bennett M. D., Smith J. B., Barclay I. (1975): Early Seed Development in the Triticeae. *Philosophical Transactions of the Royal Society B: Biological Sciences* 272(916): 199–227.
- Berger F., Hamamura Y., Ingouff M., Higashiyama T. (2008): Double fertilization – caught in the act. *Trends in Plant Science* 13(8): 437–443.
- Bewley J. D., Black M., Halmer P. (2006): *The encyclopedia of seeds: science, technology and uses*. CABI Publishing Series.
- Blattner F. R. (2018): Taxonomy of the Genus *Hordeum* and Barley (*Hordeum vulgare*). *The Barley Genome*: 11–23.
- Bourdon M., Pirrello J., Cheniclet C., Coriton O., Bourge M., Brown S., Moïse A., Peypelut M., Rouyère V., Renaudin J. P., Chevalier Ch., Frangne, N. (2012): Evidence for karyoplasmic homeostasis during endoreduplication and a ploidy-dependent increase in gene transcription during tomato fruit growth. *Development* 139(20): 3817–3826.
- Brown R. C. (1994): Endosperm Development in Barley: Microtubule Involvement in the Morphogenetic Pathway. *The Plant Cell Online* 6(9): 1241–1252.
- Cowan C. R. (2001): The Polar Arrangement of Telomeres in Interphase and Meiosis. *Rabl Organization and the Bouquet*. *Plant Physiology* 125(2): 532–538.
- Cui C., Shu W., Li P. (2016): Fluorescence In situ Hybridization: Cell-Based Genetic Diagnostic and Research Applications. *Frontiers in Cell and Developmental Biology* 4.

- D'Amato F. (1964): Endopolyploidy as a Factor in Plant Tissue Development. *Caryologia* 17(1): 41–52.
- Danilova T. V., Friebe B., Gill B. S. (2012): Single-copy gene fluorescence in situ hybridization and genome analysis: Acc-2 loci mark evolutionary chromosomal rearrangements in wheat. *Chromosoma* 121: 597–611.
- Dante R. A., Larkins B. A., Sabelli P. A. (2014): Cell cycle control and seed development. *Frontiers in Plant Science* 5.
- De Veylder L., Larkin J. C., Schnittger A. (2011): Molecular control and function of endoreplication in development and physiology. *Trends in Plant Science* 16(11): 624–634.
- Domínguez F., Cejudo F. J. (2014): Programmed cell death (PCD): an essential process of cereal seed development and germination. *Frontiers in Plant Science* 5.
- Dumur T., Duncan S., Graumann K., Desset S., Randall R. S., Scheid O. M., Prodanov D., Tatout Ch., Baroux C. (2019): Probing the 3D architecture of the plant nucleus with microscopy approaches: challenges and solutions. *Nucleus* 10(1): 181–212.
- Ferkova L. (2021): Spatial and temporal analysis of chromatin organization and modifications in embryo and endosperm nuclei of developing barley seed. Bachelor thesis. Faculty of Science, Palacký University Olomouc.
- Fransz P., de Jong J. H., Lysak M., Castiglione M. R., Schubert I. (2002): Interphase chromosomes in *Arabidopsis* are organized as well defined chromocenters from which euchromatin loops emanate. *Proceedings of the National Academy of Sciences* 99(22): 14584–14589.
- Fujimoto S., Yonemura M., Matsunaga S., Nakagawa T., Uchiyama S., Fukui K. (2005): Characterization and dynamic analysis of *Arabidopsis* condensin subunits, AtCAP-H and AtCAP-H2. *Planta* 222(2): 293–300.
- Fukui K., Kamisugi Y., Sakai F. (1994): Physical mapping of 5S rDNA loci by direct-cloned biotinylated probes in barley chromosomes. *Genome* 37(1): 105–111.
- Georgieva M., Gecheff K. (2013): Molecular Cytogenetic Characterization of a New Reconstructed Barley Karyotype. *Biotechnology & Biotechnological Equipment* 27(1): 3577–3582.
- Gerlach W. L., Bedbrook J. R. (1979): Cloning and characterization of ribosomal RNA genes from wheat and barley. *Nucleic Acids Research* 7(7): 1869–1885.

- Gubatz S., Dercksen V. J., Brüß C., Weschke W., Wobus U. (2007): Analysis of barley (*Hordeum vulgare*) grain development using three-dimensional digital models. *The Plant Journal* 52(4): 779–790.
- Han Y., Zhang T., Thammaphichai P., Weng Y., Jiang J. (2015): Chromosome-Specific Painting in Cucumis Species Using Bulked Oligonucleotides. *Genetics* 200(3): 771–779.
- Hernandez-Verdun D. (2011): Assembly and disassembly of the nucleolus during the cell cycle. *Nucleus* 2(3): 189–194.
- Hicks K. B., Montanti J., Nghiem N. P. (2014): Use of Barley Grain and Straw for Biofuels and Other Industrial Uses. *Barley*: 269–291.
- Hoencamp C., Dudchenko O., Elbatsh A. M. O., Brahmachari S., Raaijmakers J. A. , van Schaik T., Sedeño Cacciatore Á., Contessoto V. G., van Heesbeen R. G. H. P., van den Broek B., Mhaskar A. N., Teunissen H., St Hilaire B. G., Weisz D., Omer A. D., Pham M., Colaric Z., Yang Z., Rao S. S. P., Mitra N., Lui C., Yao W., Khan R., Moroz L. L., Kohn A., St Leger J., Mena A., Holcroft K., Gambetta M. C., Lim F., Farley E., Stein N., Haddad A., Chauss D., Mutlu A. S., Wang M. C., Young N. D., Hildebrandt E., Cheng H. H., Knight C. J., Burnham T. L. U., Hovel K. A., Beel A. J., Mattei P. J., Kornberg R. D., Warren W. C., Cary G., Gómez-Skarmeta J. L., Hinman V., Lindblad-Toh K., Di Palma F., Maeshima K., Multani A. S., Pathak S., Nel-Themaat L., Behringer R. R., Kaur P., Medema R. H., van Steensel B., de Wit E., Onuchic J. N., Di Pierro M., Lieberman Aiden E., Rowland B. D. (2021): 3D genomics across the tree of life reveals condensin II as a determinant of architecture type. *Science* 372(6545): 984-989.
- Holásková E., Galuszka P., Mičúchová A., Šebela M., Öz M. T., Frébort I. (2018): Molecular Farming in Barley: Development of a Novel Production Platform to Produce Human Antimicrobial Peptide LL-37. *Biotechnology Journal* 1700628.
- Huang M., Li H., Zhang L., Gao F., Wang P., Hu Y., Yan S., Zhao L., Zhang Q., Tan J., Liu X., He S., Li L. (2012): Plant 45S rDNA Clusters Are Fragile Sites and Their Instability Is Associated with Epigenetic Alterations. *PLoS ONE* 7(4): e35139.
- Hudakova S., Michalek W., Presting G. G., ten Hoopen R., dos Santos K., Jasencakova Z., Schubert I. (2001): Sequence organization of barley centromeres. *Nucleic Acids Research* 29(24): 5029–5035.
- Ibrahim A., Harrison M., Meinke H., Fan Y., Johnson P., Zhou M. (2018): A regulator of early flowering in barley (*Hordeum vulgare* L.). *PLOS ONE* 13(7): e0200722.

- Idziak D., Robaszkiewicz E., Hasterok R. (2015): Spatial distribution of centromeres and telomeres at interphase varies among *Brachypodium* species. *Journal of Experimental Botany* 66(21): 6623–6634.
- Jayakodi M., Padmarasu S., Haberer G., Bonthala V. S., Gundlach H., Monat C., Lux T., Kamal N., Lang D., Himmelbach A., Ens J., Zhang X., Angessa T. T., Zhou G., Tan C., Hill C., Wang P., Schreiber M., Boston L. B., Plott Ch., Jenkins J., Guo Y., Fiebig A., Budak H., Xu D., Zhang J., Wang C., Grimwood J., Schmutz J., Guo G., Zhang G., Mochida K., Hirayama T., Sato K., Chalmers K. J., Langridge P., Waugh R., Pozniak C. J., Scholz U., Mayer K. F. X., Spannagl M., Li C., Mascher M., Stein N. (2020): The barley pan-genome reveals the hidden legacy of mutation breeding. *Nature*.
- Joubès J., Chevalier C. (2000): *Plant Molecular Biology* 43(5/6): 735–745.
- Kaduchová K., Marchetti C., Ovečka M., Galuszka P., Bergougnoux V., Šamaj J., Pecinka A. (2023): Spatial organization and dynamics of chromosomes and microtubules during barley mitosis. Submitted to *The Plant Journal* 18.04.2023.
- Kalinina N. O., Makarova S., Makhotenko A., Love A. J., Taliensky M. (2018): The Multiple Functions of the Nucleolus in Plant Development, Disease and Stress Responses. *Frontiers in Plant Science* 9.
- Kapusi E., Ma L., Teo C. H., Hensel G., Himmelbach A., Schubert I., Mette M. F., Kumlehn J., Houben A. (2011): Telomere-mediated truncation of barley chromosomes. *Chromosoma* 121(2): 181–190.
- Kilian A., Stiff C., Kleinhofs A. (1995): Barley telomeres shorten during differentiation but grow in callus culture. *Proceedings of the National Academy of Sciences* 92(21): 9555–9559.
- Kobayashi T. (2011): Regulation of ribosomal RNA gene copy number and its role in modulating genome integrity and evolutionary adaptability in yeast. *Cellular and Molecular Life Sciences* 68(8): 1395–1403.
- Kobayashi H., Ikeda T. M., Nagata K. (2013): Spatial and temporal progress of programmed cell death in the developing starchy endosperm of rice. *Planta* 237(5): 1393–1400.
- Koshland D. E., Guacci V. (2000): Sister chromatid cohesion: the beginning of a long and beautiful relationship. *Current Opinion in Cell Biology* 12(3): 297–301.
- Kovacik M., Nowicka A., Pecinka A. (2020): Isolation of High Purity Tissues from Developing Barley Seeds. *Journal of Visualized Experiments* 164.

- Larkins B. A., Dilkes B. P., Dante R. A., Coelho C. M., Woo Y., Liu Y. (2001): Investigating the hows and whys of DNA endoreduplication. *Journal of Experimental Botany* 52(355): 183–192.
- Lee H. O., Davidson J. M., Duronio R. J. (2009): Endoreplication: polyploidy with purpose. *Genes & Development* 23(21): 2461–2477.
- Liew L. C., Narsai R., Wang Y., Berkowitz O., Whelan J., Lewsey M. G. (2019): Temporal tissue-specific regulation of transcriptomes during barley (*Hordeum vulgare*) seed germination. *The Plant Journal* 101(3): 700–715.
- Linde-Laursen I. (1984): Nucleolus organizer polymorphism in barley, *Hordeum vulgare* L. *Hereditas* 100(1): 33–43.
- Lysak M. A., Číhalíková J., Kubaláková M., Šimková H., Künzel G., Doležel J. (1999): Flow karyotyping and sorting of mitotic chromosomes of barley (*Hordeum vulgare* L.). *Chromosome Research* 7: 431–444.
- Lysak M. A. (2022): Celebrating Mendel, McClintock, and Darlington: On end-to-end chromosome fusions and nested chromosome fusions. *The Plant Cell* 34(7): 2475–2491.
- Mascarenhas J. P. (1989): The Male Gametophyte of Flowering Plants. *The Plant Cell Online* 1(7): 657–664.
- McKinley K. L., Cheeseman I. M. (2015): The molecular basis for centromere identity and function. *Nature Reviews Molecular Cell Biology* 17(1): 16–29.
- Němečková A., Koláčková V., Vrána J., Doležel J., Hříbová E. (2020): DNA replication and chromosome positioning throughout the interphase in three-dimensional space of plant nuclei. *Journal of Experimental Botany* 71(20): 6262–6272.
- Nicoloff H., Anastassova-Kristeva M., Künzel G., Rieger R. (1977): The behavior of nucleolus organizers in structurally changed karyotypes of barley. *Chromosoma* 62(2): 103–109.
- Norstog K. (1972): Early Development Of The Barley Embryo: Fine Structure. *American Journal of Botany* 59(2): 123–132.
- Nowicka A., Kovacik M., Tokarz B., Vrána J., Zhang Y., Weigt D., Doležel J., Pecinka A. (2021): Dynamics of endoreduplication in developing barley seeds. *Journal of Experimental Botany* 72(2): 268–282.
- Nowicka A., Ferkova L., Said M., Kovacik M., Zwyrtková J., Baroux C., Pecinka A. (2023): Non-Rabl chromosome organization in endoreduplicated nuclei of barley embryo and endosperm tissues. *Journal of Experimental Botany* 74(8): 2527–2541.

- Olsen O.-A. (2001): Endosperm Development: Cellularization and Cell Fate Specification. *Annual Review of Plant Physiology and Plant Molecular Biology* 52(1): 233–267.
- Olsen O.-A. (2004): Nuclear Endosperm Development in Cereals and *Arabidopsis thaliana*. *The Plant Cell* 16(suppl_1): S214-S227.
- Pecinka A., Schubert V., Meister A., Kreth G., Klatte M., Lysak M. A., Fuchs J., Schubert I. (2004): Chromosome territory arrangement and homologous pairing in nuclei of *Arabidopsis thaliana* are predominantly random except for NOR-bearing chromosomes. *Chromosoma* 113(5): 258–269.
- Perutka Z., Kaduchová K., Chamrád I., Beinhauer J., Lenobel R., Petrovská B., Bergougnoux V., Vrána J., Pecinka A., Doležel J., Šebela M. (2021): Proteome Analysis of Condensed Barley Mitotic Chromosomes. *Frontiers in Plant Science* 12: 723674.
- Pires N. D. (2014): Seed evolution: parental conflicts in a multi-generational household. *BioMolecular Concepts* 5(1): 71-86.
- Pirrello J., Deluche C., Frangne N., Gévaudant F., Maza E., Djari A., Bourge M., Renaudin J. P., Brown S., Bowler C., Zouine M., Chevalier C., Gonzalez N. (2018): Transcriptome profiling of sorted endoreduplicated nuclei from tomato fruits: how the global shift in expression ascribed to DNA ploidy influences RNA-Seq data normalization and interpretation. *The Plant Journal* 93(2): 387–398.
- Rabl C. (1885): Uber Zelltheilung. *Morphol. Jahrb.* 10: 214–330.
- Radchuk V., Weier D., Radchuk R., Weschke W., Weber H. (2010): Development of maternal seed tissue in barley is mediated by regulated cell expansion and cell disintegration and coordinated with endosperm growth. *Journal of Experimental Botany* 62(3): 1217–1227.
- Radchuk V., Tran V., Radchuk R., Diaz-Mendoza M., Weier D., Fuchs J., Riewe D., Hensel G., Kumlehn J., Munz E., Heinzl N., Rolletschek H., Martinez M., Borisjuk L. (2017): Vacuolar processing enzyme 4 contributes to maternal control of grain size in barley by executing programmed cell death in the pericarp. *New Phytologist* 218(3): 1127–1142.
- Randall R. S., Jourdain C., Nowicka A., Kaduchová K., Kubová M., Ayoub M. A., Schubert V., Tatout C., Colas I., Kalyanikrishna, Desset S., Mermet S., Boulaflous-Stevens A., Kubalová I., Mandáková T., Heckmann S., Lysak M. A., Panatta M., Santoro R., Schubert D., Pecinka A., Routh D., Baroux C. (2022): Image analysis workflows to reveal the spatial organization of cell nuclei and chromosomes. *Nucleus* 13(1): 277-299.

- Rodríguez M., Barrero J., Corbineau F., Gubler F., Benech-Arnold R. (2015): Dormancy in cereals (not too much, not so little): About the mechanisms behind this trait. *Seed Science Research* 25(2): 99-119.
- Sabelli P. A., Larkins B. A. (2009): The Development of Endosperm in Grasses. *Plant Physiology* 149(1): 14–26.
- Sabelli, P. A. (2012): Seed Development: A Comparative Overview on Biology of Morphology, Physiology, and Biochemistry Between Monocot and Dicot Plants. *Seed Development: OMICS Technologies Toward Improvement of Seed Quality and Crop Yield*: 3–25.
- Sabelli P. A., Liu Y., Dante R. A., Lizarraga L. E., Nguyen H. N., Brown S. W., Klingler J. P., Yua J., LaBranta E., Laytona T. M., Feldmana M., Larkins B. A. (2013): Control of cell proliferation, endoreduplication, cell size, and cell death by the retinoblastoma-related pathway in maize endosperm. *Proceedings of the National Academy of Sciences* 110(19): E1827–E1836.
- Sabelli P. A. (2014): Cell Cycle Regulation and Plant Development: A Crop Production Perspective. In: Pessaraki M. (ed.): *Handbook of Plant and Crop Physiology*, pp. 3-32, CRC Press.
- Santos A. P., Shaw P. (2004): Interphase chromosomes and the Rab1 configuration: does genome size matter? *Journal of Microscopy* 214(2): 201–206.
- Sepsi A., Fábíán A., Jäger K., Heslop-Harrison J. S., Schwarzacher T. (2018): ImmunoFISH: Simultaneous Visualisation of Proteins and DNA Sequences Gives Insight Into Meiotic Processes in Nuclei of Grasses. *Frontiers in Plant Science* 9: 1193.
- Shan W., Kubová M., Mandáková T., Lysak M. A. (2021): Nuclear organization in crucifer genomes: nucleolus-associated telomere clustering is not a universal interphase configuration in Brassicaceae. *The Plant Journal* 108(2): 528-540.
- Schubert V., Klatter M., Pecinka A., Meister A., Jasencakova Z., Schubert I. (2005): Sister Chromatids Are Often Incompletely Aligned in Meristematic and Endopolyploid Interphase Nuclei of *Arabidopsis thaliana*. *Genetics* 172(1): 467–475.
- Schubert V. (2009): SMC Proteins and Their Multiple Functions in Higher Plants. *Cytogenetic and Genome Research* 124(3-4): 202–214.
- Schubert V., Berr A., Meister A. (2012): Interphase chromatin organisation in *Arabidopsis* nuclei: constraints versus randomness. *Chromosoma* 121(4): 369–387.

- Sirri V., Urcuqui-Inchima S., Roussel P., Hernandez-Verdun D. (2007): Nucleolus: the fascinating nuclear body. *Histochemistry and Cell Biology* 129(1): 13–31.
- Speicher M. R., Carter N. P. (2005): The new cytogenetics: blurring the boundaries with molecular biology. *Nature Reviews Genetics* 6(10): 782–792.
- Sreenivasulu N., Borisjuk L., Junker B. H., Mock H. P., Rolletschek H., Seiffert U., Weschke W., Wobus U. (2010): Barley Grain Development. *International Review of Cell and Molecular Biology* 281: 49–89.
- Sugiyama S., Yoshino T., Hirose T., Ohtani T. (2011): Karyotyping of barley chromosomes by a new fluorescence banding technique combined with scanning probe microscopy. *Scanning* 34(3): 186–190.
- Šimoníková D., Němečková A., Karafiátová M., Uwimana B., Swennen R., Doležel J., Hříbová E. (2019): Chromosome Painting Facilitates Anchoring Reference Genome Sequence to Chromosomes In Situ and Integrated Karyotyping in Banana (*Musa Spp.*). *Frontiers in Plant Science* 10: 1503.
- Šimoníková D., Němečková A., Čížková J., Brown A., Swennen R., Doležel J., Hříbová E. (2020): Chromosome Painting in Cultivated Bananas and Their Wild Relatives (*Musa spp.*) Reveals Differences in Chromosome Structure. *International Journal of Molecular Sciences* 21(21): 7915.
- Tiang C.-L., He Y., Pawlowski W. P. (2011): Chromosome Organization and Dynamics during Interphase, Mitosis, and Meiosis in Plants. *Plant Physiology* 158(1): 26–34.
- Tran V., Weier D., Radchuk R., Thiel J., Radchuk V. (2014): Caspase-Like Activities Accompany Programmed Cell Death Events in Developing Barley Grains. *PLoS ONE* 9(10): e109426.
- Tricase C., Amicarelli V., Lamonaca E., Leonardo Rana R. (2018): Economic Analysis of the Barley Market and Related Uses. In: Tadele Z. (ed.): *Grasses as Food and Feed*, IntechOpen.
- Tulpová Z., Kovařík A., Toegelová H., Navrátilová P., Kapustová V., Hříbová E., Vrána J., Macas J., Doležel J., Šimková H. (2022): Fine structure and transcription dynamics of bread wheat ribosomal DNA loci deciphered by a multi-omics approach. *Plant Genome* 15(1): e20191.
- Waddington S. R., Cartwright P. M., Wall P. C. (1983): A Quantitative Scale of Spike Initial and Pistil Development in Barley and Wheat. *Annals of Botany* 51(1): 119–130.


- Wu X., Liu J., Li D., Liu C.-M. (2016): Rice caryopsis development II: Dynamic changes in the endosperm. *Journal of Integrative Plant Biology* 58(9): 786–798.
- Yifang C., Jun Z., Peisong X., Weidong Z., Jianmin C., Cunxu W. (2012): Programmed cell death in wheat starchy endosperm during kernel development. *African Journal of Agricultural Research* 7(49): 6533–6540.
- Young T. E., Gallie D. R. (2000): Programmed cell death during endosperm development. *Plant Molecular Biology* 44(3): 283–301.
- Zeng Z., Jiang J. (2016): Isolation and Proteomics Analysis of Barley Centromeric Chromatin Using PICh. *Journal of Proteome Research* 15(6): 1875–1882.

9 APPENDICES

Appendix I: Nowicka A., Ferkova L., Said M., Kovacik M., Zwyrtková J., Baroux C., Pecinka A. (2023): Non-Rabl chromosome organization in endoreduplicated nuclei of barley embryo and endosperm tissues.

RESEARCH PAPER

Non-Rabl chromosome organization in endoreduplicated nuclei of barley embryo and endosperm tissues

Anna Nowicka^{1,2,*}, Ľuboslava Ferková¹, Mahmoud Said^{1,3}, Martin Kovacik¹, Jana Zwyrková¹,
Célia Baroux⁴ and Ales Pecinka^{1,*}

¹ Centre of Plant Structural and Functional Genomics, Institute of Experimental Botany of the Czech Academy of Sciences, Šlechtitelů 31, 779 00 Olomouc, Czech Republic

² The Polish Academy of Sciences, The Franciszek Górski Institute of Plant Physiology, Niezapominajek 21, 30-239 Krakow, Poland

³ Field Crops Research Institute, Agricultural Research Centre, 9 Gamma Street, Giza, Cairo, 12619, Egypt

⁴ Department of Plant and Microbial Biology, Zürich-Basel Plant Science Center, University of Zürich, Zollikerstrasse 107, 8008 Zürich, Switzerland

* Correspondence: pecinka@ueb.cas.cz or nowicka@ueb.cas.cz

Received 26 October 2022; Editorial decision 16 January 2023; Accepted 25 January 2023

Editor: Zoe Wilson, University of Nottingham, UK

Abstract

Rabl organization is a type of interphase chromosome arrangement with centromeres and telomeres clustering at opposite nuclear poles. Here, we analyzed nuclear morphology and chromosome organization in cycling and endoreduplicated nuclei isolated from embryo and endosperm tissues of developing barley seeds. We show that endoreduplicated nuclei have an irregular shape, less sister chromatid cohesion at 5S rDNA loci, and a reduced amount of centromeric histone CENH3. While the chromosomes of the embryo and endosperm nuclei are initially organized in Rabl configuration, the centromeres and telomeres are intermingled within the nuclear space in the endoreduplicated nuclei with an increasing endoreduplication level. Such a loss of chromosome organization suggests that Rabl configuration is introduced and further reinforced by mitotic divisions in barley cell nuclei in a tissue- and seed age-dependent manner.

Keywords: Barley, CENH3, CEREBA repeat, embryo, endoreduplication, endosperm, *Hordeum vulgare*, nuclear organization, Rabl configuration.

Introduction

Chromosome structure and organization play important roles in replication, transcription, and genome repair (Misteli, 2020). Their organization includes the formation of nucleosomes, as the basic unit of chromatin, and their assembly into higher order domains. These domains represent different chromatin states characterized by specific histone and/or DNA modifications, and vary in their transcription, replica-

tion, or DNA repair patterns (Roudier *et al.*, 2011; Sequeira-Mendes *et al.*, 2014). Individual interphase chromosomes occupy a specific nuclear space known as chromosome territories (CTs) (reviewed in, for example, Schubert and Shaw, 2011; Grob, 2020).

In *Arabidopsis thaliana* (Arabidopsis) with a small and repeat-poor genome, the peri(centromeric) regions form

Abbreviations: CENH3, centromere-specific histone H3; CEREBA, CENTROMERIC RETROELEMENT OF BARLEY; CT, chromosome territory; DAP, days after pollination; FISH, fluorescence *in situ* hybridization; FITC, fluorescein isothiocyanate; mip, maximum intensity projection; msv, middle slide view; NA, nucleus area; NCI, nucleus circularity index; ND, nucleus diameter; NP, nucleus perimeter; ROI, region of interest; SC, sister chromatid.

heterochromatic chromocenters from which euchromatic chromosome arms emanate and the telomeric regions often surround the nucleolus (Fransz *et al.*, 2002, 2003). The CTs of 45S *rDNA*-bearing chromosomes cluster preferentially around the nucleolus, but the CTs of the remaining chromosomes are positioned randomly in roots and leaves (Pecinka *et al.*, 2004) or show pairwise CT associations in the seed endosperm (Baroux *et al.*, 2017). In contrast, plants with large and repeat-rich genomes often harbor Rabl chromosome organization, with the centromeres and telomeres clustering at the opposite nuclear poles (Santos and Shaw, 2004), first described in 1885 by the cytologist and anatomist Carl Rabl based on nuclei of *Caudata* (Rabl, 1885). Because Rabl organization is widespread in cereals with large genomes such as bread wheat (17 Gbp/1C) or barley (5.1 Gbp/1C), and diminishes with a decreasing genome size in, for example, maize (2.4 Gbp/1C) or rice (0.43 Gbp/1C) (Fujimoto *et al.*, 2005a), it has been hypothesized that it is determined by the nuclear genome size (reviewed in, for example, Santos and Shaw, 2004). Although this correlation holds true over distantly related phylogenetic groups such as *Poaceae* and *Brassicaceae* (Němečková *et al.*, 2020; Shan *et al.*, 2021), it is not universal. For example, the majority of root nuclei (but not leaf nuclei) show Rabl in the small genome grass *Brachypodium distachyon* (0.35 Gbp/1C), while some *Liliaceae* species with giant genomes (~35–50 Gbp/1C) lack Rabl organization (Fujimoto *et al.*, 2005a; Idziak *et al.*, 2015). Therefore, other hypotheses suggest that Rabl might be a preserved organization of mitotic chromosomes. However, why this configuration is maintained in some but not other species remains unclear.

To investigate the relationships between occurrence of the Rabl configuration, endoreduplication, and tissue age, we made use of the endosperm and to a smaller extent embryo tissues of barley grains (Nowicka *et al.*, 2021a). In cereals, the endosperm progresses through several stages of development (reviewed in, for example, Olsen, 2001; Sabelli and Larkins, 2009), connected with major changes in transcriptional regulation (Sreenivasulu *et al.*, 2004; Pfeifer *et al.*, 2014). The endosperm forms most of the seed mass and serves as the main energy storage tissue for the embryo during germination. In contrast to vegetative tissues, cereal endosperm shows endoreduplication, a process during which the genome duplicates without mitosis (Sabelli and Larkins, 2009).

Endoreduplication in cereal grains does not contribute to the seed size (Nowicka *et al.*, 2021a), but a study in *Arabidopsis* suggests that it might be linked with high metabolic activity of certain cells (Baroux *et al.*, 2004). Endoreduplicated nuclei allow the study of whether chromosome organization patterns are correlated with ploidy. In *Arabidopsis*, endoreduplicated nuclei from leaves showed loss of positional sister chromatid (SC) cohesion and had generally reduced heterochromatin compaction (Schubert *et al.*, 2006). In rice, endoreduplication forced Rabl chromosome organization in xylem vessel cells (Prieto *et al.*, 2004). Finally, conserved Rabl organization was

observed in endoreduplicated nuclei of bread wheat embryo and endosperm tissues (Wegel and Shaw, 2005).

Here, we studied chromosome organization in mitotically cycling and endoreduplicated nuclei isolated from embryo and endosperm tissues of developing barley grains. Our data suggest that while the chromosomes of embryo nuclei are organized mostly according to a Rabl pattern, the nuclei of endosperm tissues adopt a non-Rabl organization with increasing C-value and number of days after pollination. Collectively, our study provides comprehensive characteristics of embryo and endosperm nuclear processes during the key stages of barley grain development.

Materials and methods

Plant materials and growth conditions

The spring cultivar (cv.) Compana (PI 539111, NSGC of the USDA-ARS, USA) of cultivated barley (*Hordeum vulgare* subsp. *vulgare*) was used in this study. For germination, grains were evenly spread in a Petri dish on filter paper soaked with distilled water, stratified at 4 °C in the dark for 48 h, and germinated in the dark at 25 °C for 3 d. Sprouting seedlings were planted into 5 × 5 × 5 cm peat pots with a mixture of soil and sand (2:1, v/v) and grown in a phytochamber under a long-day regime (16 h daylight with an intensity of 200 μmol m⁻² s⁻¹ and temperature 20 °C; 8 h night with 16 °C; 60% humidity). After 2 weeks, seedlings were transferred into 15 × 15 × 15 cm pots and grown under the same conditions until flowering. The day of pollination was monitored using the morphology of the stigma and anthers according to the Waddington scale (W10) (Waddington *et al.*, 1983) as we established previously (Kovacik *et al.*, 2020; Nowicka *et al.*, 2021b). Seeds were collected from the center of the spike at 4, 8, 16, 24, and 32 days after pollination (DAP).

Isolation of nuclei and flow sorting

Nuclei were isolated from root apical meristem (RAM), embryo, and endosperm tissues. For isolation of root nuclei: 70 roots of seedlings at 2 d after germination were cut ~1 cm from the apex and collected in a drop of distilled water. Next, roots were drained on a cellulose tissue paper, rinsed in 10 mM Tris buffer pH 7.0, fixed with 2% (v/v) formaldehyde/Tris buffer for 20 min on ice, and washed three times for 5 min each with Tris buffer also on ice. Root apices were excised ~1 mm from the tip and homogenized in 500 μl of LB01 buffer (15 mM Tris-HCl pH 7.5, 2 mM NaEDTA, 0.5 mM spermine, 80 mM KCl, 20 mM NaCl, and 0.1% Triton X-100) for 13 s at 15 000 rpm using a Polytron PT1300D homogenizer (Kinematica AG).

For isolation of embryo nuclei, ~100 embryos were manually dissected from seeds at 8 DAP, using an SZX16 binocular microscope (Olympus). First, seeds were peeled (manual removal of hulls) and placed on a Petri dish in a drop of 1× phosphate-buffered saline (PBS) (Kovacik *et al.*, 2020). Dissected embryos were collected into a 1.5 ml Eppendorf tube containing 200 μl of 1× PBS and kept on ice until the sampling was finished. Tubes were low-speed centrifuged (1 min, 2000 g), PBS was removed, embryos were rinsed in Tris buffer, fixed with 2% (v/v) formaldehyde/Tris buffer for 20 min on ice, and washed three times for 5 min with Tris buffer also on ice. Embryos were homogenized with a pellet pestle in the same Eppendorf tubes with 500 μl of LB01 buffer. For 16 DAP and older seeds, at least 50 embryos were manually dissected using a binocular microscope. Embryos were collected into a small beaker containing PBS and kept on ice. Subsequently, the material was rinsed in Tris buffer, pre-fixed with 4% (v/v) formaldehyde/Tris buffer for 30 min by vacuum infiltration on

ice, followed by fixation with the same solution for 30–40 min without a vacuum also on ice, and washed in Tris buffer. Samples were chopped in 2 ml of LB01 buffer with a razor blade on a Petri dish.

For isolation of endosperm nuclei, ~80 of the whole peeled seeds from 4 and 8 DAP endosperm samples were gathered into a small beaker kept on ice. Seeds were rinsed in Tris buffer, pre-fixed with 4% (v/v) formaldehyde/Tris buffer for 20 min on ice, fixed without vacuum for 40 min, and washed. Samples were chopped with a razor blade in 2–3 ml of LB01 buffer on a Petri dish. For endosperm samples at ≥16 DAP, ~60 whole peeled seeds with embryos removed were collected into a small beaker, cut with the razor blade into 1 mm thick transversal slides, pre-fixed for 30 min, then fixed for 40 min. Samples were chopped with a razor blade in 3–4 ml of LB01 buffer on a Petri dish.

For flow sorting of nuclei, the crude homogenates of all samples were double-filtered first through a 50 µm and then a 20 µm pore size mesh. Nuclei suspensions were stained with 2 µg ml⁻¹ DAPI. Approximately 500 nuclei for each C-value were flow-sorted into a 2 µl drop of sorting buffer (100 mM Tris-HCl pH 7.5, 50 mM KCl, 2 mM MgCl₂, 0.05% Tween-20, and 5% sucrose) on poly-llysine (Menzel Gläser, J2800AMNZ) or superfrost Plus (Menzel Gläser, J1810AMNZ) microscopic slides using a FACSaria II SORP flow cytometer and sorter (BD Biosciences, Santa Clara, CA, USA). Slides were air-dried for 1 h at room temperature and stored at -20 °C until use.

Mitotic chromosome preparations

Metaphase chromosomes were prepared from synchronized root tips (Lysák *et al.*, 1999). Briefly, germinated seedlings were transferred into Hoagland's nutrient solution containing 2 mM hydroxyurea for 18 h. Then the roots were washed in distilled water and cultured in hydroxyurea-free Hoagland's solution for 5.5 h. To accumulate cells at metaphase, the roots were treated for 2 h with Hoagland's solution containing 2.5 µM amiprofos-methyl (A0185, Duchefa Biochemie). Subsequently, the root tips were fixed in ice-cold 90% acetic acid for 10 min followed by three washes in 70% ethanol and stored in 70% ethanol at -20 °C. Chromosomes were prepared using the drop technique (Danilova *et al.*, 2012). In brief, maceration of root tips was performed at 37 °C for 57 min using an enzyme mixture consisting of 4% (w/v) cellulase Onozuka R-10 (Yakult Pharmaceutical Industry, 150422-01) and 1% (w/v) pectolyase Y23 (Duchefa, 9033-35-6) in KCl buffer (75 mM KCl, 7.5 mM EDTA, pH 4). The quality of chromosome spreads was evaluated using a phase-contrast microscope (Primo Star, Zeiss), and the slides with at least five metaphases were used for fluorescence *in situ* hybridization (FISH). Before a hybridization step, the slides were pre-treated with pepsin (10 µg ml⁻¹ in 10 mM HCl) at 37 °C for 10 min, then rinsed in 2× SSC followed by RNase A treatment (described below).

Fluorescence *in situ* hybridization

Three combinations of the following probes were used in the double- or triple-color FISH experiments. For detecting barley centromeres, a synthetic 28-mer oligonucleotide (5'-AGGGAGA-3')₄ probe labeled at the 5' end with Cy3 or Cy5 (Eurofins) was used. The probe targets a centromeric retroelement-like element *CEREBA* conserved among cereal centromeres (Hudakova *et al.*, 2001). For detecting the telomeres, we used a synthetic 28-mer oligonucleotide probe (5'-CCCTAAA-3')₄ corresponding to the Arabidopsis-type telomeric repeat and labeled at the 5' end with Cy3 or Cy5 (Eurofins). The 5S *rDNA* probe was amplified from cv. Compana genomic DNA with the primers 5'-GGATGCGATCATACCAGCAC-3' and 5'-GACATGCAACTATCTATTTGT-3' using biotin-dUTP or digoxigenin-11-dUTP (both Roche, 11093070910 and 11093088910) during PCR. The 45S *rDNA* probe was labeled with biotin-dUTP or digoxigenin-11-dUTP from the pTa71 plasmid containing a 9.1 kb fragment of

rDNA sequence from bread wheat (Gerlach and Bedbrook, 1979) using nick translation kits (both Roche, 11745824910 and 11745816910) according to the manufacturer's instructions.

FISH was performed as described (Karafiátová *et al.*, 2013; Nowicka *et al.*, 2020), with the following modifications. Preparations were air-dried at room temperature, rinsed in 2× SSC, treated with RNase A (50 µg ml⁻¹ in 2× SSC; Thermo Fisher, EN0601) for 30 min at 37 °C, and washed with 2× SSC and 1× PBS. Subsequently, slides were post-fixed with 4% formaldehyde/1×PBS for 15 min and washed with 1× PBS. A hybridization mixture contained a cocktail of two or three probes, each with a final concentration of 400 ng µl⁻¹, and 1 µg of sheared salmon sperm DNA (Invitrogen, AM9680), 50% (v/v) deionized formamide, 10% (v/v) dextran sulfate, and 2× SSC. For biotin-dUTP- and digoxigenin-11-dUTP-labeled probes, the hybridization mixture was heated for 4 min at 95 °C, cooled on ice, and denatured again together with target DNA on slides for 4 min at 80 °C. For oligo-probes, the step of hybridization mixture pre-denaturation was skipped. Biotin-dUTP was detected either by (i) streptavidin-Cy3 (1:500, Molecular Probes, SA1010) or (ii) goat anti-avidin conjugated with biotin (1:100, Vector Laboratories, NC9256157) followed by avidin conjugated with Texas Red (1:1000, Vector Laboratories, NC9172942). Digoxigenin-dUTP was detected either with (i) an anti-digoxigenin antibody conjugated with fluorescein isothiocyanate (FITC, 1:200 Roche, 11207741910) or (ii) a mouse anti-digoxigenin antibody (1:250, Roche, 11333062910) followed by application of a goat anti-mouse antibody conjugated with Alexa Fluor 488 (1:200, Molecular Probes, A32723). The preparations were counterstained with DAPI in Vectashield (Vector Laboratories, H-1200-10).

ImmunoFISH

Slides were air-dried at room temperature, post-fixed with 4% formaldehyde/1× PBS for 15 min, and washed with 1× PBS. Immunostaining was carried out as described (Jasencakova *et al.*, 2000) with minor modifications. In brief, preparations were incubated with the rabbit anti-barley-αCENH3-specific primary antibody (1:200; Sanei *et al.*, 2011) at 4 °C overnight and the secondary goat anti-rabbit-Alexa Fluor 488 (1:300, Molecular Probes, A11008) at 37 °C for 90 min. Before FISH, slides were fixed in 3:1 ethanol/acetic acid for 10 min, followed by 10 min fixation with 3.7% formaldehyde/1× PBS. Slides were washed with 1× PBS. FISH steps were performed as described above, excluding pepsin and RNase A treatment.

Microscopy

The images were taken with an AxioImager Z2 upright microscope (Zeiss, Oberkochen, Germany) equipped with a pE-4000 LED illuminator light source (CoolLED, Andover, UK), motorized four-position excitation filter wheel, laser-free confocal spinning disk device (DSD2, Andor, Belfast, UK), and a ×100/1.4 NA Oil M27 Plan-Apochromat (Zeiss) objective. Image stacks of 40–80 slides depending on the C-value of the nucleus, on average, with a 0.2 µm z-step were acquired separately for each fluorochrome using the appropriate excitation [DAPI λ=390/40 nm, green fluorescent protein (GFP) λ=482/18 nm, red fluorescent protein (RFP) λ=561/14 nm, Cy5=640/14 nm] and emission (DAPI λ=452/45 nm, GFP λ=525/45 nm, RFP λ=609/54 nm, Cy5=676/29 nm) filters. For fluorescence detection, the 4.2 megapixel sCMOS camera (Zyla 4.2) was used and the iQ 3.6.1 acquisition software (both Andor) was used to drive the microscope.

Image analysis

The images were converted into .ims format with Imaris File Converter 9.2.1 (Bitplane, Zurich, Switzerland) and exported as maximum intensity projection (mip) tif files with Imaris 9.7 software (Bitplane). For

visualization of the surface and shape of the nuclei, the Imaris 9.7 function ‘Surface’ was used for rendering the DAPI-stained nucleus surface and to obtain 3D nucleus images. Then, functions ‘Slide viewer’ and ‘Section view’ were applied to visualize inside the nucleus. For determination of the nucleus area, perimeter, and circularity, the nucleus area (NA) and perimeter (NP) of the X–Y middle slide view tif images were measured in FIJI (ImageJ2; <https://imagej.net/software/fiji/>) calibrated with an internal size control. The nucleus circularity index (NCI) was calculated according to the formula: $NCI = 4\pi \times NA / (NP)^2$ (Ankam et al., 2018).

To construct the karyotype, chromosomes were paired based on the chromosomal position of *rDNAs* and *CEREBA*. The karyotype was prepared in Adobe Photoshop 6.0 (Adobe Systems Corporation, San Jose, CA, USA). Individual chromosomes were classified according to Fukui et al. (1994) and Kapusi et al. (2012). For FISH signal scoring, the number of FISH signals per nucleus was quantified in FIJI with the ‘Multipoint’ tool using mip tif images. Quantitative analysis of CENH3 co-localization with *CEREBA* was performed in FIJI calibrated with an internal size control using fluorescent intensity ‘Plot Profile’ for both correlated signals.

Total fluorescence intensity measurements of all CENH3 and *CEREBA* per nucleus were done in FIJI using mip tif images. For each nucleus, 2–10 regions of interest (ROIs) defined manually with a constant size of $3.5 \times 3.5 \mu\text{m}$ were evaluated. For green and red channels, the same ROIs were analyzed, and for each of them the fluorescence intensity ratio of CENH3/*CEREBA* was calculated. For the DAPI channel ($3.5 \times 3.5 \mu\text{m}$), ROIs located in the middle of the nucleus were evaluated.

For Rab1 configuration analysis, Imaris applications ‘Surface’ and ‘Spot detection’ were used for rendering the nucleus surface and modeling the centromere/telomere arrangements, respectively. The space in the nucleus occupied by centromeres and telomeres was measured using Imaris ‘Measurement point’ in polygon mode. The detailed Imaris-based image analysis workflow is described separately (Randall et al., 2022). The Imaris statistic output files reporting on the distance between centromeres and telomeres were exported for each nucleus separately.

Image data normalization and statistical analysis

Scored numbers of FISH signals were normalized to the number of signals per nucleus at the G_1 phase (Supplementary Fig. S1). Hence, for the number of *5S major rDNA* loci, scoring values were divided by two or by three for embryo and endosperm data, respectively. In the case of *5S minor* and *45S rDNA* loci, raw data were divided by four and six for embryo and endosperm, respectively. For *CEREBA*, data were normalized to 14 and 21 for embryo and endosperm, respectively. Distances between centromeres and telomeres were expressed as a ratio to the nucleus diameter (ND).

All scoring and measurement, raw and normalized data were tested for Gaussian distribution. To return to Gaussian distribution, data expressed as percentages were first arcsine transformed. Next, relevant comparisons were carried out by two-way ANOVA (factor 1=C-value, factor 2=DAP) and post-hoc Duncan’s multiple ranges ($P \leq 0.05$) test. To evaluate the statistical differences between embryo and RAM samples, one-way ANOVA (factor 1 tissue) was applied. Pearson’s correlation coefficient analysis was used to visualize relationships among the measured and evaluated parameters (NCI, NA, NP, and co-localization between CENH3/*CEREBA*). Statistical analyses were performed in Statistica v. 12 (Statsoft Inc.) or Minitab v. 18 (Minitab). Boxplots were drawn using the ggplot GUI online tool (<https://shiny.gmw.rug.nl/ggplotgui/>).

Results

Endoreduplication affects the morphology of barley embryo and endosperm nuclei

We isolated G_1 (2C/3C), G_2 (4C/6C), and endoreduplicated (8C/ ≥ 12 C) nuclei from barley embryo and endosperm tissues

(embryo/endosperm C- values, respectively) at 4, 8, 16, 24, and 32 DAP as described (Nowicka et al., 2021a), and analyzed their morphology. Nuclei from highly dividing RAM tissues were used as somatic control. Based on our initial assessment, we noted differences in nuclear shape and therefore calculated the nucleus circularity index (NCI) (Ankam et al., 2018) using nucleus area (NA) and nucleus perimeter (NP) values (Materials and methods; Fig. 1A, B; Supplementary Figs S2, S3).

The 2C and 4C embryo nuclei had a nearly ideal circular shape (NCI ≥ 0.91) during the whole of seed development, but the NCI of endoreduplicated (8C) nuclei from 24 and 32 DAP was significantly reduced to ~ 0.75 (two-way ANOVA; Fig. 1B; Supplementary Fig. S2D). Hence, the circularity of the embryo nuclei depended on the degree of endoreduplication but not the number of DAP. In contrast, NCI of endosperm nuclei was influenced not only by the C-value but also by DAP. The NCI of 3C and 6C nuclei was ~ 0.89 from 4 to 16 DAP, then reached its maximum of ~ 0.95 at 24 DAP and decreased to 0.82–0.88 at 32 DAP. Endoreduplicated endosperm nuclei exhibited an ellipsoid shape with NCIs between 0.75 (12C at 8 DAP) and 0.67 (24C at 24 DAP), and the ellipticity increased during seed maturation and desiccation (Fig. 1A, B; Supplementary Fig. S2D). Interestingly, rendering of the surface of endoreduplicated endosperm nuclei revealed grooves of variable dimensions that were not observed in the nuclei with lower C-values (Fig. 1C; Supplementary Fig. S4).

Loss of sister chromatid cohesion at *5S rDNA* loci of endoreduplicated nuclei

The altered morphology of barley endoreduplicated seed nuclei stimulated us to also explore the chromosome organization. As detection of single-copy sequences in barley interphase nuclei is not possible using current cytology tools, we focused on the arrangement of major tandem repetitive regions *5S rDNA*, *45S rDNA*, and *CEREBA* centromeric repeats using FISH (Fig. 2A, B).

The genome of cv. Compana contains a cytologically distinguishable single large *5S rDNA* cluster at the bottom arm of chromosome 2H (hereafter *5S major*) and two smaller clusters at the bottom arms of chromosomes 3H and 7H (hereafter *5S minor*; Fig. 2A–C). In G_1 (2C) and G_2 (4C) nuclei of the embryo samples up to 16 DAP and root samples, we observed two separate *5S major rDNA* signals, which suggests SC cohesion during the G_2 phase and separation of the two homologous chromosomes in both G_1 and G_2 . However, in embryo nuclei from older (24 and 32 DAP) seeds, 4C nuclei contained mostly three to four *5S major* FISH signals and 8C nuclei contained five to seven such signals, indicating a reduced SC cohesion at *5S major* (Fig. 2D; Supplementary Fig. S5A). G_1 (3C) endosperm nuclei showed mostly three *5S rDNA major* FISH signals, but G_2 (6C) and once-endoreduplicated (12C) nuclei displayed SC separation progressing in a DAP-dependent manner. Finally, the majority of twice-endoreduplicated

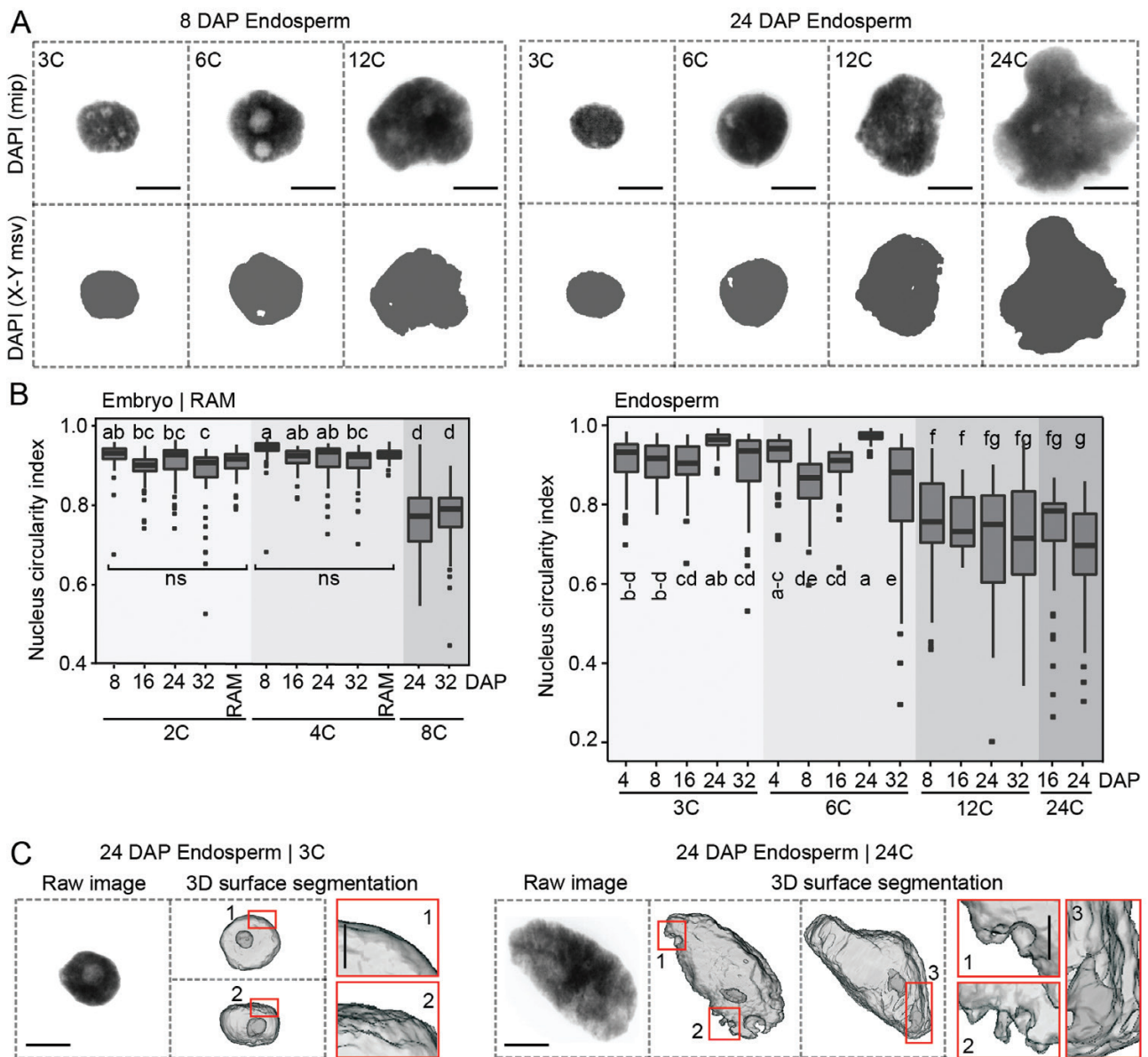


Fig. 1. Endoreduplicated barley grain nuclei have altered shape. (A) Representative DAPI-stained endosperm nuclei of different C-values collected at 8 and 24 days after pollination (DAP). The upper panels show 3D maximum intensity projections (mip) and the lower panels their 2D X-Y middle slide view (msv). Scale bars=10 μ m. (B) Boxplots showing the nucleus circularity index (NCI) for nuclei of different tissues, C-values, and DAP. Root apical meristem (RAM) nuclei were used as the vegetative tissue control. NCI was calculated using the following formula $NCI=4\pi \times NA/(NP)^2$ (Ankam et al., 2018). Original data for NA and NP are depicted in [Supplementary Fig. S2](#). The lower and upper hinges of the boxplots correspond to the first and third quartiles of the data, and the black lines within the boxes mark the median. Whiskers mark 10% and 90% intervals. A total of 75 nuclei were measured in three microscopic slides. Black squares represent outliers. Different letters indicate significant differences ($P \leq 0.05$, two-way ANOVA, factor 1=C-value, factor 2=DAP, followed by Duncan post-hoc test). The summary of ANOVA is presented in [Supplementary Fig. S2D](#). Statistical significance between embryo and RAM samples was evaluated with one-way ANOVA, ns, not significant ($P_{2C}=0.453$, $P_{4C}=0.101$). (C) Example images of 24 DAP 3C and 24C DAPI-stained endosperm nuclei presented in 3D mip (left panel) and their surface reconstructions using Imaris software (right panels). Insets display in more detail the absence (3C) and presence (24C) of nuclear grooves. Scale bars=10 μ m (main) and 2 μ m (insets). Additional images are presented in [Supplementary Fig. S4](#).

endosperm (24C) nuclei had 21 FISH signals at 24 DAP, corresponding to full SC separation at *5S rDNA major* (Fig. 2C, D; [Supplementary Fig. S5](#)). Statistical analysis by ANOVA showed that the *5S rDNA major* SC separation in embryo and en-

dosperm significantly increased with rising C-values, developmental progression (DAP), and as a result of an interaction between both factors ([Supplementary Fig. S5](#)). The same trend was observed for *5S rDNA minor loci* ([Supplementary Fig. S6](#)).

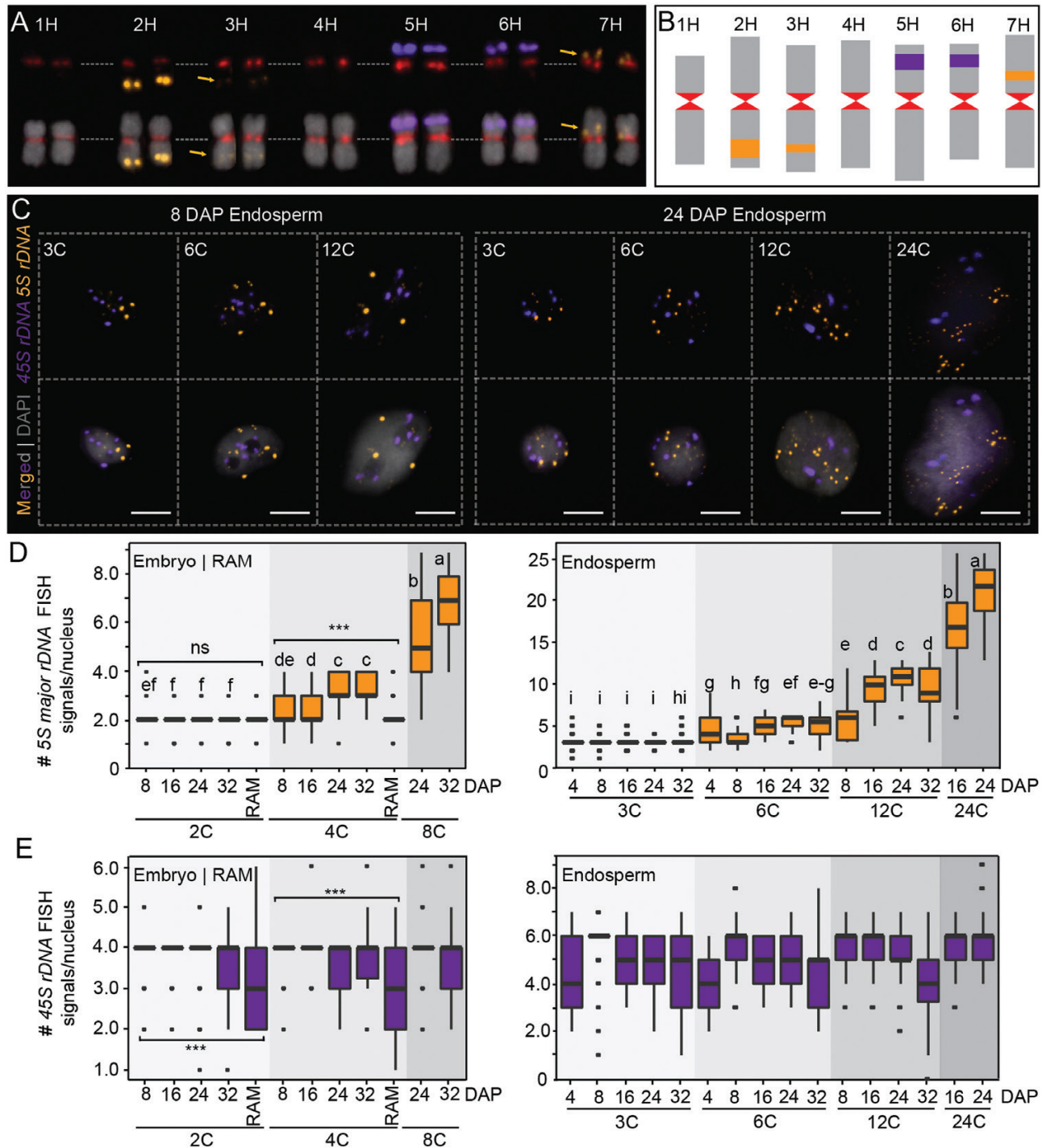


Fig. 2. Sister chromatid cohesion at 5S and 45S rDNA loci in barley seed nuclei. (A) Karyotype of cv. Compana showing localization of 5S rDNA, 45S rDNA, and CEREBEA centromeric repeats on metaphase chromosomes by FISH. DNA was counterstained with DAPI. Arrows indicate 5S minor rDNA loci. Scale bar=10 μ m. (B) Ideogram of cv. Compana (based on A). (C) Representative endosperm nuclei with different C-values collected at 8 and 24 DAP after FISH with 5S (orange) and 45S (violet) rDNA probes. The larger and brighter 5S rDNA signals correspond to the 5S major loci. DNA was stained with DAPI (gray). Scale bars=10 μ m. (D, E) Boxplots showing the number of (D) 5S major and (E) 45S rDNA FISH signals per nucleus for different tissues, C-values, and DAP. Root apical meristem (RAM) nuclei were used as the vegetative tissue control. The lower and upper hinges of the boxplots correspond to the first and third quartiles of the data, and the black lines within the boxes mark the median. Whiskers mark 10% and 90% intervals. At least 75 nuclei from three microscopic slides were scored. Black squares represent outliers beyond the whiskers. Different letters indicate significant differences ($P \leq 0.05$, two-way ANOVA, factor 1=C-value, factor 2=DAP, followed by Duncan test). No significant differences were found for the 45S rDNA ($P > 0.05$). The summary of ANOVA is presented in [Supplementary Figs S5B and S7A](#). Statistical significance between the embryo and RAM samples was evaluated with one-way ANOVA, *** significant at $P \leq 0.001$, ns, not significant ($5S P_{2C} = 0.771$). Normalized data ([Supplementary Fig. S1](#)) for 5S major and 45S rDNA signals are provided in [Supplementary Figs S5C and S7B](#), respectively.

Analogous analysis of the *45S rDNA*, located on barley chromosomes 5H and 6H (Kapusi *et al.*, 2012), revealed a lower than expected number of FISH signals. This suggests a persistent SC cohesion and tendency toward *45S rDNA* clustering (Fig. 2C, E; Supplementary Figs S5A, S7). Neither C-value nor DAP affected this pattern (two-way ANOVA, $P > 0.05$, no significant differences for single factors and their interaction, Supplementary Fig. S7). Hence, the organization of *45S rDNA* loci remained relatively intact, suggesting a locus-specific control of SC alignment in endoreduplicated barley seed nuclei.

Decondensation of CEREBEA and reduction of CENH3 in endoreduplicated nuclei

After FISH with *CEREBEA* repeats, we observed on average 12 signals at 8 DAP and 11 signals at 32 DAP in 2C and 4C embryo nuclei (Fig. 3; Supplementary Fig. S8A). The average number of signals increased significantly to ~14–17 after endoreduplication (8C). In 3C and 6C endosperm nuclei, the average number of *CEREBEA* foci ranged from nine to 17 at different DAPs. In 12C and 24C nuclei, the *CEREBEA* signals appeared less compact, often splitting into several smaller foci,

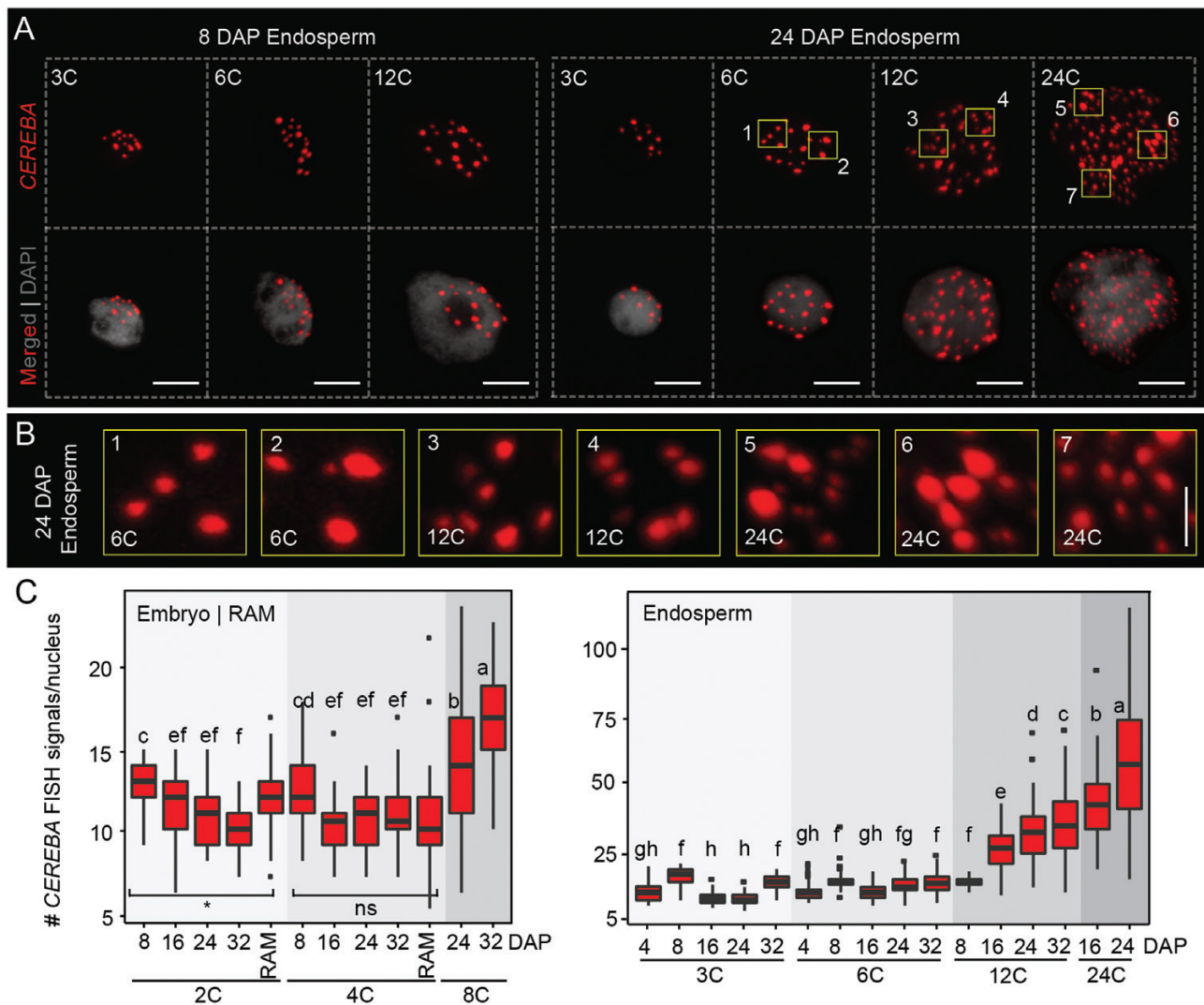


Fig. 3. *CEREBEA* organization in barley seed nuclei. (A) Representative endosperm nuclei of different C-values collected at 8 and 24 DAP after FISH with *CEREBEA* centromeric repeat (red). DNA was stained with DAPI (gray). Insets are enlarged in (B). Scale bars=10 μ m. (B) Insets (1–7) marked in (A) show the variable size of *CEREBEA* FISH signals in the 6C–24C endosperm nuclei. Scale bar=2 μ m. (C) Boxplots showing the number of *CEREBEA*-FISH signals per nucleus for different tissues, C-values, and DAP. Root apical meristem (RAM) was used as the vegetative tissue control. The lower and upper hinges of the boxplots correspond to the first and third quartiles of the data, and the black lines within the boxes mark the median. Whiskers mark 10% and 90% intervals. At least 75 nuclei from three microscopic slides were evaluated. Black squares represent outliers beyond the whiskers. Different letters indicate significant differences ($P \leq 0.05$, two-way ANOVA, factor 1=C-value, factor 2=DAP, followed by Duncan test). The summary of ANOVA is presented in Supplementary Fig. S8B. Statistical significance between embryo and RAM samples was evaluated with one-way ANOVA, * significant at $P \leq 0.05$, ns, not significant ($P_{4c} = 0.147$). Normalized data (Supplementary Fig. S1) are provided in Supplementary Fig. S8C.

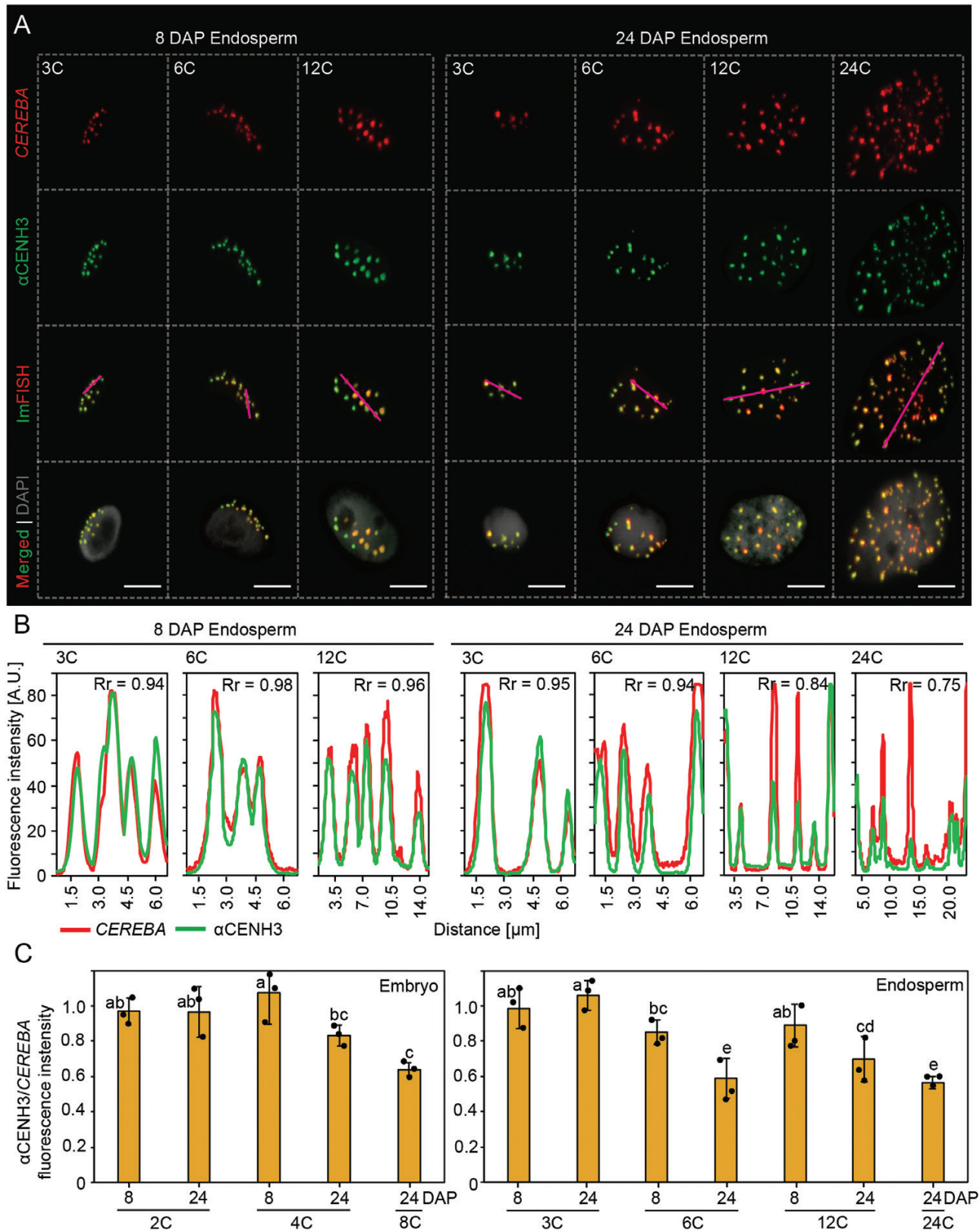


Fig. 4. Loss of HvCENH3 signals in endoreduplicated nuclei of seed tissues. (A) Representative endosperm nuclei of different C-values collected at 8 and 24 DAP after immunostaining followed by FISH (ImFISH) for barley αCENH3 (green) and CEREBBA (red). DNA was stained with DAPI (gray). Scale bars=10 μm. (B) Fluorescence intensity plot profiles (y-axis; arbitrary units, A.U.) showing the quantified co-localization of HvCENH3 and CEREBBA

signals. Intersects used for quantification are highlighted by a pink line in the ImFISH images in (A). R_r displays Pearson's co-localization coefficient. Data for embryos are presented in [Supplementary Fig. S9](#). (C) α CENH3/*CEREBA* fluorescence intensity signal ratio (based on [Supplementary Fig. S10A](#)) measured for the same-size squared regions of interest (ROIs). Values are means (\pm SD) from three biological replicates (microscopic slides) marked as black spots, each with at least 100 measured ROIs. Different letters indicate significant differences ($P \leq 0.05$, two-way ANOVA, factor 1=C-value, factor 2=DAP, followed by Duncan test). The summary of ANOVA is shown in [Supplementary Fig. S10B](#). DAPI fluorescence measurements are presented in [Supplementary Fig. S10C](#).

and this trend was more pronounced with increasing DAP ([Fig. 3B, C](#)). Two-factor ANOVA revealed an additive effect of DAP in combination with C-value on the number of *CEREBA* foci in both embryo and endosperm nuclei ([Supplementary Fig. S8B, C](#)). The high number of *CEREBA* signals most probably indicates relaxation of centromeric repeats or a larger distance between individual sister chromatids at the centromeric region.

To understand whether a reduced compaction of the centromeric regions would prevent centromere maturation, we set out to measure the levels of CENH3 in different types of nuclei. For this, we performed *CEREBA* and barley α CENH3 immunofISH in 8 and 24 DAP embryo and endosperm nuclei, measured the fluorescence signal intensities over an intersecting line, and calculated their Pearson correlation ([Fig. 4A, B](#); [Supplementary Fig. S9](#)). This indicated that all *CEREBA* foci also contain a CENH3 signal, but the latter appeared to be weaker with increasing C-value in 24 DAP endosperm nuclei (Pearson correlation 0.95 in 3C and 0.75 in 24C). To quantify this interesting observation, we measured signal intensities within ROIs of fixed size and calculated the α CENH3/*CEREBA* ratio ([Fig. 4C](#); [Supplementary Fig. S10](#)). Since it was previously shown that the α CENH3 immunosignal reflects the amount of CENH3 ([Lermontova et al., 2006](#)), we measured both FISH and immunosignals in ROIs and calculated the α CENH3/*CEREBA* ratio. In both embryo and endosperm tissues, there was a significant reduction of α CENH3 relative to *CEREBA* repeats in endoreduplicated nuclei at 24 DAP ([Fig. 4C](#)). Interestingly, this was an effect not only of the C-value but also of DAP as, for example, 6C and 12C nuclei had significantly more α CENH3 at 8 DAP than at 24 DAP ([Fig. 4C](#); [Supplementary Fig. S10C](#)). Thus, the decondensation of centromeres occurring in endosperm nuclei correlates with a lesser loading of α CENH3.

Loss of Rabl chromosome configuration in seed endoreduplicated nuclei

In the light of the massive changes in chromosome organization, we asked whether barley seed nuclei retain a Rabl configuration. For this, we imaged the 3D distribution of FISH signals targeting the *CEREBA* and telomeric repeats in 8 and 24 DAP embryo and endosperm nuclei ([Figs 5, 6](#)). Besides nuclei with a typical Rabl configuration, we observed several types of nuclei with dispersed and non-polar centromeric and telomeric signals. To quantify the degree of signal dispersion versus clustering, we measured the shortest distance of each centromere signal to the next telomere signal and expressed

it relative to the diameter of the nucleus ([Fig 5A, B](#); image processing workflow as described in [Randall et al., 2022](#)). In the 2C and 4C embryo nuclei with a typical Rabl organization, the average, relative distance between centromere and telomere clusters was \sim 30–40% of ND. In 8C nuclei with more dispersed signals, the relative distance was only \sim 12% of ND. Assessing the distance distribution among all samples, ANOVA revealed that the C-value (but not DAP) affected the relative positioning of centromeres and telomeres in embryo nuclei ([Supplementary Fig. S11A](#)). Similar patterns were found in endosperm nuclei, but with an effect of C-value, DAP, and a combination thereof ([Fig. 5B](#); [Supplementary Fig. S11A](#)).

In addition, we noted that centromeric and telomeric signals are occasionally located away from the nuclear periphery, which might be another indication of altered chromosome organization. To quantify this reorganization, we measured the shortest distance of centromeric and telomeric FISH signals to the nuclear periphery, defined by the boundary of DAPI staining ([Randall et al., 2022](#)). We confirmed that centromeres and telomeres became more dispersed towards the interior of the nucleus in endoreduplicated embryo and endosperm nuclei, with a gradual relocation depending on the C-value and DAP ([Fig. 5A, C](#); [Supplementary Fig. S11B](#)). Furthermore, to quantify the dispersion of telomeres and centromeres, we calculated the volume occupied by connected centromere signals and the same for telomeres. We expressed these values relative to the volume of the nucleus to provide an estimate of the spatial dispersion ([Fig. 5A, D](#)). In the 2C and 4C embryo nuclei, these domains occupied 18–26% of the nuclear volume but this increased to 44–45% in 8C nuclei. Statistical analysis showed that the C-value (for centromeres and telomeres) and DAP (only for telomeres) influenced the expansion of the signals ([Supplementary Fig. S11C](#)). In endosperm, centromeres and telomeres covered 27–35% of the nuclear volume of 3C and 6C nuclei at 8 DAP. With increasing C-value and DAP, they dispersed over the nuclear volume even more and reached 68% and 70% of nuclear space, respectively, with 27% overlap in 24C endosperm nuclei at 24 DAP. In endosperm nuclei, the dispersion increased with the C-value, DAP, and their combination ([Supplementary Fig. S11C](#)).

Based on the above observations, we defined three arbitrary categories of nuclear organization: (i) Rabl; (ii) intermediate; and (iii) non-Rabl, with a median shortest centromere to telomere distance of 42, 23, and 7%, respectively ([Fig. 6A, B](#)). We quantified frequencies of these categories over the experimental points ([Fig. 6C](#)). The Rabl configuration was present in \geq 85% ($n=21$ of 25) of 2C and 4C embryo nuclei and in 77.3%

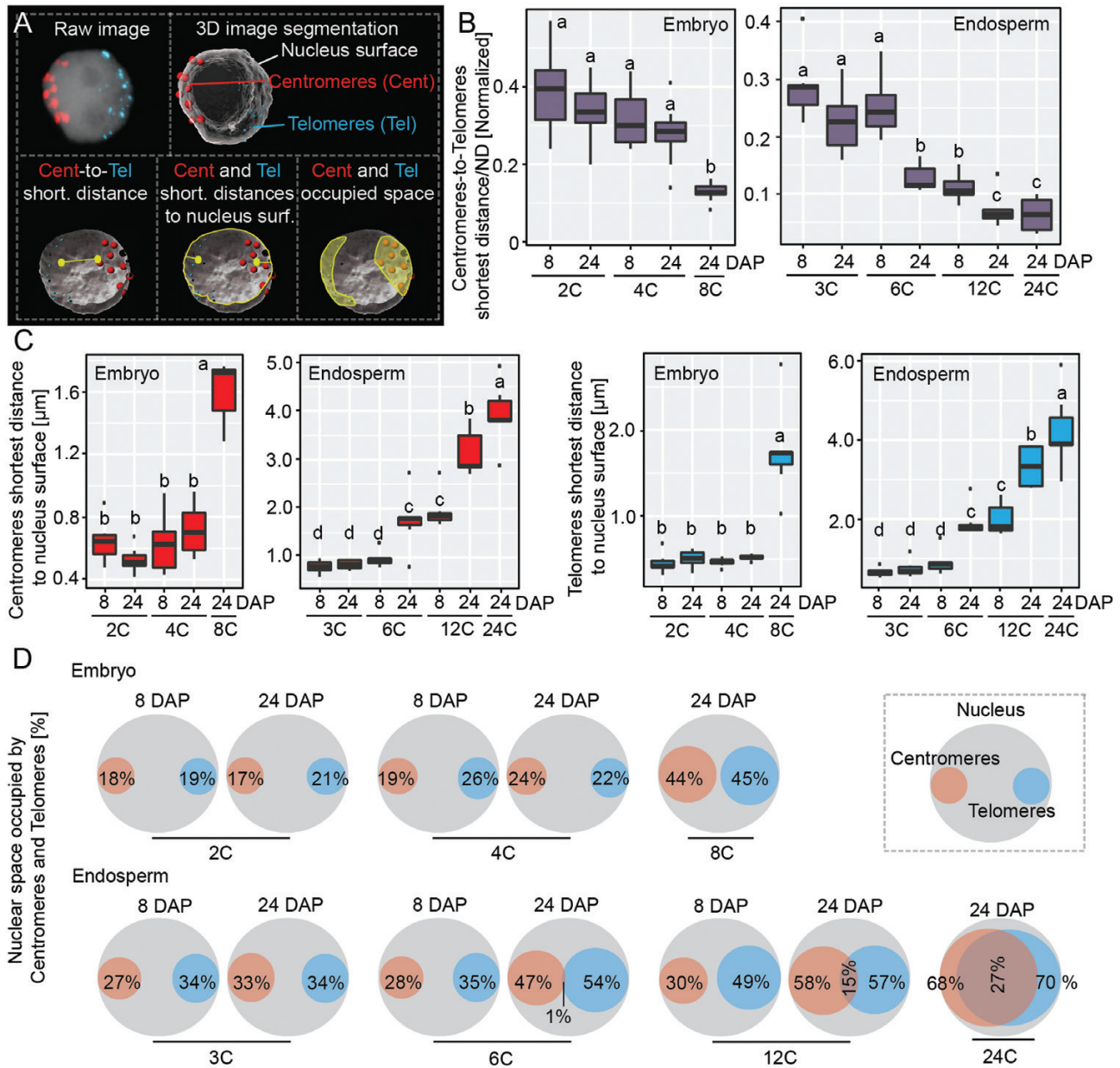


Fig. 5. Endoreduplication disrupts the Rab1 chromosome organization in barley nuclei. (A) Schematic overview of the processing of the raw images and quantified parameters applied for centromere and telomere positioning in the interphase nucleus. (B) Boxplots showing the shortest distance between centromeres and telomeres normalized to nucleus diameter (ND). The lower and upper hinges of the boxplots correspond to the first and third quartiles of the data, and the black lines within the boxes mark the median. Whiskers mark 10% and 90% intervals. Black squares represent outliers beyond the whiskers. The measurements were performed in Imaris software after FISH signal segmentation and nucleus surface rendering. Ten randomly selected nuclei of each C-value/time point were used for the analysis. Different letters indicate significant differences ($P \leq 0.05$, two-way ANOVA, factor 1=C-value, factor 2=DAP, followed by Duncan test). The summary of ANOVA is presented in [Supplementary Fig. S11A](#). (C) Boxplots showing the shortest distance of centromeres and telomeres to the nucleus surface. Data acquisition, plot organization, and statistics were performed as described in (B). The summary of ANOVA is presented in [Supplementary Fig. S11B](#). (D) Venn diagrams show the percentage of nuclear space occupied by centromeres and telomeres. The measurements were performed in Imaris software after FISH signal segmentation, nucleus surface rendering, and manual measuring of the nucleus territories occupied by centromeres and telomeres. Ten randomly selected nuclei of each C-value/time point were used for the analysis. The summary of ANOVA is presented in [Supplementary Fig. S11C](#).

($n=19$ of 25) of 8C nuclei. The Rab1-type nuclei were substituted by the intermediate type and the proportion of the non-Rab1 type remained very low (20%; $n=5$ of 25). In endosperm,

the Rab1 configuration appeared in the majority (64%; $n=16$ of 25) of 3C and 6C nuclei at 8 DAP. With increasing C-value and DAP, the proportion of nuclei with an intermediate and

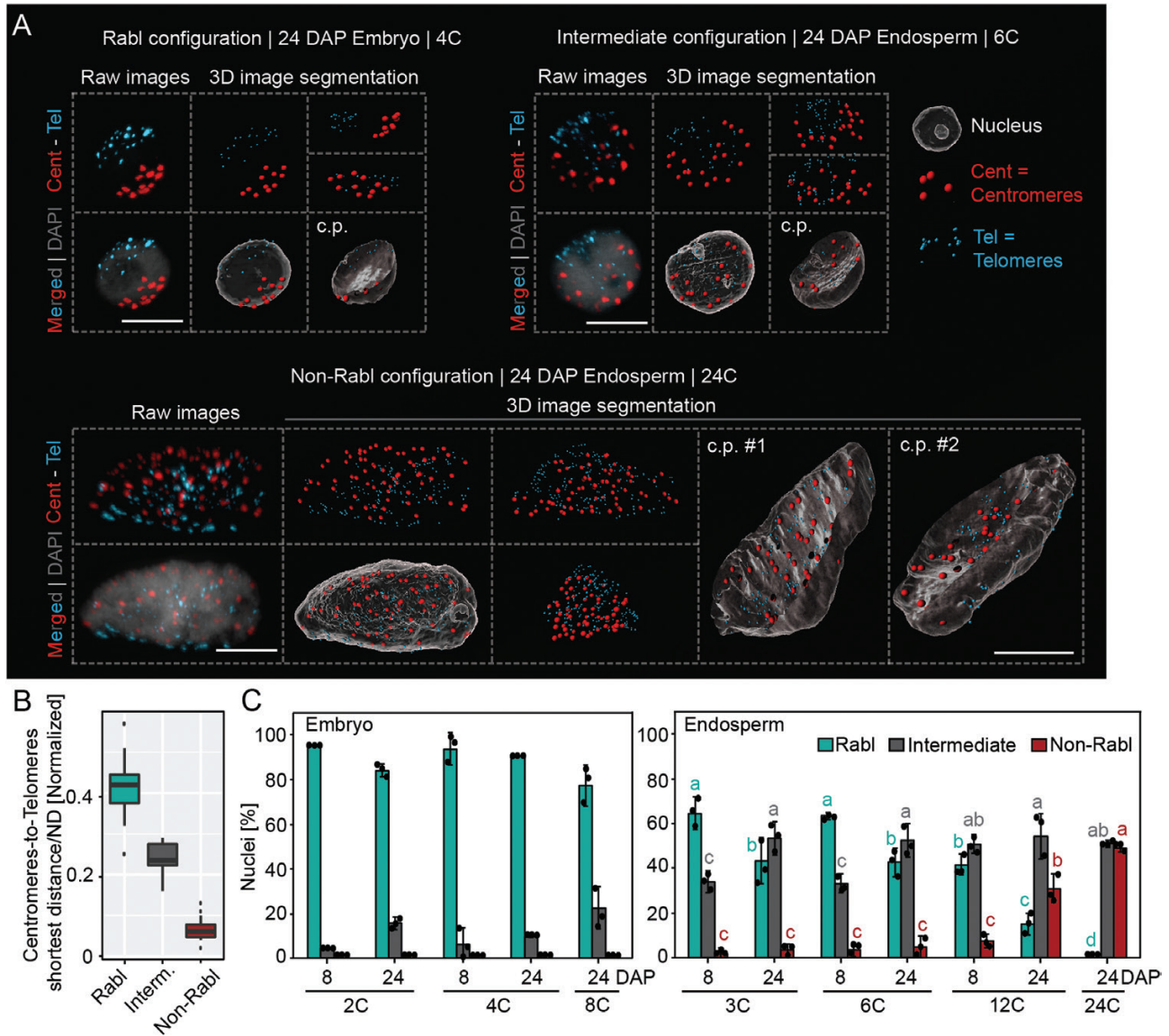


Fig. 6. Three phenotypes of chromosome organization at interphase. (A) Raw images show representative embryo and endosperm nuclei of different C-values revealing Rabl, intermediate, and non-Rabl chromosome organization as determined based on FISH with *CEREBA* (red) and telomeric (blue) probes. DNA was stained with DAPI (gray). The 3D image segmentation pictures of the surface of the nucleus and FISH signals allow visualization of the spatial distribution of the centromeres and telomeres within the nucleus. Clipping planes (c.p.) represent sections through the 3D modeled nuclei. Scale bars=10 μ m. (B) Recognition of the three chromosome organization phenotypes based on Fig. 5B. Interm.=intermediate. (C) Percentage of nuclei with Rabl, intermediate, and non-Rabl chromosome organization. Values are means (\pm SD) from three biological replicates (microscopic slides), each with at least 25 evaluated nuclei and indicated as a black spot. The same letters indicate samples that do not show significant differences ($P < 0.05$, two-way ANOVA, factor 1=C-value, factor 2=DAP, followed by Duncan test). There were no significant differences between the embryo samples. The summary of ANOVA is shown in Supplementary Fig. S11D.

non-Rabl organization became dominant. For instance, 12C endosperm nuclei showed an almost 3-fold reduction in Rabl nuclei from 8 DAP (42%, $n=10$ of 25) to 24 DAP (15%, $n=4$ of 25). In parallel, non-Rabl organization increased from 8% ($n=2$ of 25) at 8 DAP to 31% ($n=8$ of 25) at 24 DAP. In the extreme case of 24 DAP 24C endosperm, there were nuclei only with non-Rabl (49%, $n=13$ of 25) and intermediate (51%, $n=14$ of 24) organization. Statistical analysis confirmed that the Rabl

organization was lost with increasing C-value, DAP, and their combination (Supplementary Fig. S11D).

Discussion

Here, we revealed a remarkable plasticity in the morphology of nuclei and arrangements of interphase chromosomes in nuclei

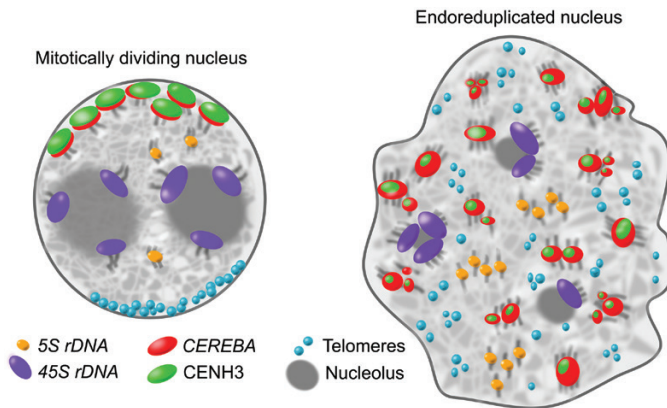


Fig. 7. Graphical summary of the major findings. Dividing nuclei have a round shape; adherent sister chromatids keep an equal amount of CENH3 histone and organize chromosomes according to a Rabl pattern. Endoreduplication alters the nuclear shape and causes positional loss of sister chromatid cohesion and loss of histone CENH3. In addition, they show a non-Rabl chromosome organization.

from developing barley embryo and endosperm tissues (Fig. 7). Our study shows that the tissue type, level of endoreduplication, and the age after pollination are the major determinants of the observed differences.

Chromosome organization has been explored in actively dividing meristematic and somatic tissues of barley, which contain mostly spherical nuclei with a smooth surface (Němečková et al., 2020). These nuclei are from cells that are either mitotically cycling or resting in the G_0/G_1 phase (Jasenčakova et al., 2000). Surprisingly, endoreduplicated endosperm nuclei adopted a very irregular shape, with channels lacking DNA staining, suggesting invagination of the nuclear membrane (Fig. 1). Similar shapes have been reported for endoreduplicated nuclei of several distantly related plants including *Allium cepa*, *Narcissus*, *Pisum sativum*, or *Solanum lycopersicum* (Collings et al., 2000, and references therein; Bourdon et al., 2011, 2012). This suggests that the effect of endoreduplication on the shape of the nucleus and particularly the regularity of its boundary is potentially widespread, consistent with the proposal that complex surface structures may be typical for nuclei of high ploidies (Pirrello et al., 2014). It is assumed that the grooves and invaginations may keep the necessary nucleus to cytoplasm surface ratio (Bourdon et al., 2012). Our work shows that invaginations are not a pure effect of endoreduplication in barley and that the seed developmental stage, tightly linked to its physiological state, plays a role. Some nuclear surface irregularities could be a result of metabolic activity in embryo and endosperm cells, possibly due to filling of cells with active and/or storage compounds or due to the altered cytoskeleton impacting the integrity of the nuclear envelope. This phenotype could also be linked to programmed cell death that is typical for the endosperm of most cereals (Young et al., 2000).

The hallmark of the Rabl configuration is the centromere and telomere clustering at opposite nuclear poles. However,

>130 years after its discovery (Rabl, 1885), the principles of this organization remain a matter of debate (Santos and Shaw, 2004). In some plants, the Rabl configuration was long thought to be the only type of genome organization. However, an increasing number of studies suggest tissue-specific variation in chromosomal organization (Fujimoto et al., 2005a; Idziak et al., 2015; Němečková et al., 2020; Shan et al., 2021). Some cells lose the Rabl pattern soon after entering the interphase, whereas others retain the organization throughout the interphase and until the next mitosis (Cowan et al., 2001). Nuclear genome size and chromosome length were postulated as two possible factors conferring the Rabl configuration (Santos and Shaw, 2004). While this holds for many species, some plants with giant genomes lack Rabl organization (Fujimoto et al., 2005a). Also, there are striking differences in genome organization between some closely related species. A well-described example are *Brachypodium* species, where *B. distachyon* shows a Rabl configuration in root nuclei while its relative *B. stacei*, with a similar genome size but twice as many chromosomes, does not (Idziak et al., 2015). This suggests that genome size alone cannot serve as a universal rule defining the Rabl organization. Recently, it was proposed that the Condensin II complex plays a major role in 3D interphase genome organization, and that an incomplete set of its subunits favors a Rabl-like pattern across the tree of life (Hoencamp et al., 2021). Applicability of this classification for the organization of plant chromosomes still requires investigations because all plants sequenced to date contain a full set of Condensin II subunits, in spite of their diverse chromosome organization (Fujimoto et al., 2005b; Schubert, 2009).

So far, barley has been considered as a species with a strict Rabl chromosome organization. We showed that there is variability in the chromosome configuration in barley seed tissues that is affected by the tissue type, seed developmental stage (days after pollination), and strongly by endoreduplication (C-value) and combination of the latter two factors. In contrast, Rabl organization was maintained in the embryo and endosperm nuclei of bread wheat (Wegel and Shaw, 2005), which could be due to analysis of younger tissues that contained only a small portion of endoreduplicated nuclei or, less likely, due to genuine species-specific differences. Importantly, correlation between loss of Rabl organization and degree of endoreduplication favors models suggesting that Rabl configuration is established and reinforced during mitotic cell divisions (Santos and Shaw, 2004). Our data show that the amount of nuclei with Rabl decreases not only with the number of DNA replications (that are not followed by mitosis), but also with the time since the last replication (Fig. 6). However, which molecular factors ensure relatively stable clustering of centromeres and telomeres in between divisions remains currently unknown.

The other observed changes in chromosome organization add to the little-explored organization of endoreduplicated nuclei of cereal seeds (Wegel and Shaw, 2005; Wegel et al., 2005; Bauer and Birchler, 2006). Here, repositioning of centromeres and telomeres from the nuclear envelope more into the nuclear space

may contribute to loss of Rabl configuration (Fig. 5) (Santos and Shaw, 2004). Another observed alteration in chromosome organization was related to absence of SC cohesion at *5S rDNA* loci (Fig. 2). Although we cannot draw any conclusions about the organization of singly-copy sequences, our data suggest that SCs are absent at least in some parts of the endoreduplicated barley chromosomes. This is reminiscent of the loss of SC cohesion along chromosome arms in Arabidopsis nuclei with a C-value of 4C or more (Schubert *et al.*, 2006). At centromeric regions, we found an increasing number of *CEREBA* foci in endoreduplicated nuclei (Fig. 3), which is similar to Arabidopsis (Schubert *et al.*, 2006; Baroux *et al.*, 2017). This suggests a relaxed control of heterochromatin compaction at centromeres upon endoreduplication in barley, which is in contrast to the situation in maize (Bauer *et al.*, 2006). We also observed reduction in centromeric histone CENH3 in endoreduplicated nuclei (Fig. 4). This is to be expected because CENH3 loading occurs in G₂ phase, that is skipped in the endoreduplication cycle (Lermontova *et al.*, 2007). Furthermore, data from Arabidopsis show that CENH3 is not produced during endoreduplicative S-phase (Lermontova *et al.*, 2011). Interestingly, we found a significant replication-independent loss of CENH3 in nuclei of the same C-value in later versus earlier seed developmental stages.

What the significance of the manifold changes in endoreduplicated barley nuclei is remains currently unknown. Speculatively, it could be linked with transcriptional reprogramming and a boost in synthesis of specific storage compounds in endosperm (Sabelli and Larkins, 2009). Furthermore, it could be related to a loss of mitotic activity and onset of the cellular trajectory towards programmed cell death that occurs in large parts of cereal endosperm (Nowicka *et al.*, 2021a).

In conclusion, our study highlights previously underappreciated dynamics in chromosome organization of barley embryo and endosperm nuclei upon endoreduplication. The most notable change is the progressive loss of polar chromosome organization and the disruption of centromere and telomere clusters. This shows that the Rabl chromosome arrangement is not a general rule for barley, and that mitosis may function as a mechanism reinforcing this organization. In general, these data help in understanding the principles and dynamics of genome organization during the course of plant development.

Supplementary data

The following supplementary data are available at [JXB online](#).

Fig. S1. Schematic drawing of G₁ diploid and triploid cells.

Fig. S2. Geometrical characteristics of flow-sorted embryo and endosperm nuclei.

Fig. S3. Pearson correlation coefficient analysis between nuclear geometry parameters.

Fig. S4. The complex shape of endoreduplicated nuclei.

Fig. S5. Sister chromatid organization for the *5S major rDNA* locus in barley seed nuclei.

Fig. S6. Sister chromatid organization for the *5S minor rDNA* loci in barley seed nuclei.

Fig. S7. Sister chromatid organization for the *45S rDNA* loci in barley seed nuclei.

Fig. S8. *CEREBA* organization in barley seed nuclei of different C-values and DAP.

Fig. S9. Co-localization of CENH3 and *CEREBA* signals in barley embryo nuclei.

Fig. S10. Fluorescence measurements of α CENH3, *CEREBA*, and DAPI signals.

Fig. S11. Statistical analysis supporting the Rabl chromosome configuration study.

Acknowledgements

We thank, Dr A. Doležalová for sharing the immunoFISH protocol and anti- α CENH3 antibody, E. Jahnová for technical assistance, and Z. Bursová for plant care. The authors thank COST Action no. CA 16212 'INDEPTH' for training in Imaris software.

Author contributions

AP and AN: design; AN, LF, MK, and JZ: performing experiments; MS: flow sorting of the nuclei; AN: data analysis and figure preparation; CB: providing expertise in microscopic image processing analysis by Imaris; AP and AN: writing, with contributions from all authors. All authors approved the final version of this article.

Conflict of interest

The authors declare that they have no conflict of interest in relation to this work.

Funding

This research was funded by the Czech Science Foundation grants 18-12197S and 21-02929S (to AP), Purkyně Fellowship from the Czech Academy of Sciences to AP, and the European Regional Development Fund project 'Plants as a tool for sustainable global development' (no. CZ.02.1.01/0.0/0.0/16_019/0000827).

Data availability

All data supporting the findings of this study are available within the paper and within its supplementary data published online.

References

- Ankam S, Teo BKK, Pohan G, Ho SWL, Lim CK, Yim EKF. 2018. Temporal changes in nucleus morphology, Lamin A/C and histone methylation during nanotopography-induced neuronal differentiation of stem cells. *Frontiers in Bioengineering and Biotechnology* **6**, 69.
- Baroux C, Fransz P, Grossniklaus U. 2004. Nuclear fusions contribute to polyploidization of the gigantic nuclei in the chalazal endosperm of Arabidopsis. *Planta* **220**, 38–46.

- Baroux C, Pecinka A, Fuchs J, Kreth G, Schubert I, Grossniklaus U.** 2017. Non-random chromosome arrangement in triploid endosperm nuclei. *Chromosoma* **126**, 115–124.
- Bauer MJ, Birchler JA.** 2006. Organization of endoreduplicated chromosomes in the endosperm of *Zea mays* L. *Chromosoma* **115**, 383–394.
- Bourdon M, Coriton O, Pirrello J, Cheniclet C, Brown SC, Poujol C, Chevalier C, Renaudin JP, Frangne N.** 2011. In planta quantification of endoreduplication using fluorescent *in situ* hybridization (FISH). *The Plant Journal* **66**, 1089–1099.
- Bourdon M, Pirrello J, Cheniclet C, et al.** 2012. Evidence for karyoplasmic homeostasis during endoreduplication and a ploidy-dependent increase in gene transcription during tomato fruit growth. *Development* **139**, 3817–3826.
- Collings DA, Carter CN, Rink JC, Scott AC, Wyatt SE, Strömberg Allen N.** 2000. Plant nuclei can contain extensive grooves and invaginations. *The Plant Cell* **12**, 2425–2439.
- Cowan CR, Carlton PM, Cande WZ.** 2001. The polar arrangement of telomeres in interphase and meiosis. Rabl organization and the bouquet. *Plant Physiology* **125**, 532–538.
- Danilova TV, Friebe B, Gill BS.** 2012. Single-copy gene fluorescence *in situ* hybridization and genome analysis: Acc-2 loci mark evolutionary chromosomal rearrangements in wheat. *Chromosoma* **121**, 597–611.
- Fransz P, de Jong JH, Lysak M, Castiglione MR, Schubert I.** 2002. Interphase chromosomes in *Arabidopsis* are organized as well defined chromocenters from which euchromatin loops emanate. *Proceedings of the National Academy of Sciences, USA* **99**, 14584–14589.
- Fransz P, Soppe W, Schubert I.** 2003. Heterochromatin in interphase nuclei of *Arabidopsis thaliana*. *Chromosome Research* **11**, 227–240.
- Fujimoto S, Ito M, Matsunaga S, Fukui K.** 2005a. An upper limit of the ratio of DNA volume to nuclear volume exists in plants. *Genes and Genetic Systems* **80**, 345–350.
- Fujimoto S, Yonemura M, Matsunaga S, Nakagawa T, Uchiyama S, Fukui K.** 2005b. Characterization and dynamic analysis of *Arabidopsis* condensin subunits, AtCAP-H and AtCAP-H2. *Planta* **222**, 293–300.
- Fukui K, Kamisugi Y, Sakai F.** 1994. Physical mapping of 5S rDNA loci by direct-cloned biotinylated probes in barley chromosomes. *Genome* **37**, 105–111.
- Gerlach WL, Bedbrook JR.** 1979. Cloning and characterization of ribosomal RNA genes from wheat and barley. *Nucleic Acids Research* **7**, 1869–1885.
- Grob S.** 2020. Three-dimensional chromosome organization in flowering plants. *Briefings in Functional Genomics* **19**, 83–91.
- Hoencamp C, Dudchenko O, Elbatsh AMO, et al.** 2021. 3D genomics across the tree of life reveals condensin II as a determinant of architecture type. *Science* **372**, 984–989.
- Hudakova S, Michalek W, Presting GG, Hoopen R, Santos K, Jasencakova Z, Schubert I.** 2001. Sequence organization of barley centromeres. *Nucleic Acids Research* **29**, 5029–5035.
- Idziak D, Robaszekiewicz E, Hasterok R.** 2015. Spatial distribution of centromeres and telomeres at interphase varies among *Brachypodium* species. *Journal of Experimental Botany* **66**, 6623–6634.
- Jasencakova Z, Meister A, Walter J, Turner BM, Schubert I.** 2000. Histone H4 acetylation of euchromatin and heterochromatin is cell cycle dependent and correlated with replication rather than with transcription. *The Plant Cell* **12**, 2087–2100.
- Kapusi E, Ma L, Teo CH, Hensel G, Himmelbach A, Schubert I, Mette MF, Kumlehn J, Houben A.** 2012. Telomere-mediated truncation of barley chromosomes. *Chromosoma* **121**, 181–190.
- Karafiátová M, Bartoš J, Kopecký D, Ma L, Sato K, Houben A, Stein N, Doležel J.** 2013. Mapping nonrecombining regions in barley using multicolor FISH. *Chromosome Research* **21**, 739–751.
- Kovacic M, Nowicka A, Pecinka A.** 2020. Isolation of high purity tissues from developing barley seeds. *Journal of Visualized Experiments* **164**, e61681.
- Lermontova I, Schubert V, Fuchs J, Klatte S, Macas J, Schubert I.** 2006. Loading of *Arabidopsis* centromeric histone CENH3 occurs mainly during G₂ and requires the presence of the histone fold domain. *The Plant Cell* **18**, 2443–2451.
- Lermontova I, Fuchs J, Schubert V, Schubert I.** 2007. Loading time of the centromeric histone H3 variant differs between plants and animals. *Chromosoma* **116**, 507–510.
- Lermontova I, Koroleva O, Rutten T, Fuchs J, Schubert V, Moraes I, Koszegi D, Schubert I.** 2011. Knockdown of CENH3 in *Arabidopsis* reduces mitotic divisions and causes sterility by disturbed meiotic chromosome segregation. *The Plant Journal* **68**, 40–50.
- Lysák MA, Čhalíková J, Kubaláková M, Šimková H, Künzel G, Doležel J.** 1999. Flow karyotyping and sorting of mitotic chromosomes of barley (*Hordeum vulgare* L.). *Chromosome Research* **7**, 431–444.
- Misteli T.** 2020. The self-organizing genome: principles of genome architecture and function. *Cell* **183**, 28–45.
- Němečková A, Koláčková V, Vrána J, Doležel J, Hřibová E.** 2020. DNA replication and chromosome positioning throughout the interphase in three-dimensional space of plant nuclei. *Journal of Experimental Botany* **71**, 6262–6272.
- Nowicka A, Tokarz B, Zwyrtková J, et al.** 2020. Comparative analysis of epigenetic inhibitors reveals different degrees of interference with transcriptional gene silencing and induction of DNA damage. *The Plant Journal* **102**, 68–84.
- Nowicka A, Kovacic M, Tokarz B, Vrána J, Zhang Y, Weigt D, Doležel J, Pecinka A.** 2021a. Dynamics of endoreduplication in developing barley seeds. *Journal of Experimental Botany* **72**, 268–282.
- Nowicka A, Sahu PP, Kovacic M, Weigt D, Tokarz B, Krugman T, Pecinka A.** 2021b. Endopolyploidy variation in wild barley seeds across environmental gradients in Israel. *Genes* **12**, 711.
- Olsen O-A.** 2001. Endosperm development: cellularization and cell fate specification. *Annual Review of Plant Physiology and Plant Molecular Biology* **52**, 233–267.
- Pecinka A, Schubert V, Meister A, Kreth G, Klatte M, Lysak MA, Fuchs J, Schubert I.** 2004. Chromosome territory arrangement and homologous pairing in nuclei of *Arabidopsis thaliana* are predominantly random except for NOR-bearing chromosomes. *Chromosoma* **113**, 258–269.
- Pfeifer M, Kugler KG, Sandve SR, et al.** 2014. Genome interplay in the grain transcriptome of hexaploid bread wheat. *Science* **345**, 1250091.
- Pirrello J, Bourdon M, Cheniclet C, Bourge M, Brown SC, Renaudin JP, Frangne N, Chevalier C.** 2014. How fruit developmental biology makes use of flow cytometry approaches. *Cytometry* **85A**, 115–125.
- Prieto P, Santos AP, Moore G, Shaw P.** 2004. Chromosomes associate premeiotically and in xylem vessel cells via their telomeres and centromeres in diploid rice (*Oryza sativa*). *Chromosoma* **112**, 300–307.
- Rabl C.** 1885. Über Zelltheilung. *Morphologisches Jahrbuch* **10**, 214–330.
- Randall R, Jourdain C, Nowicka A, et al.** 2022. Image analysis workflows to reveal the spatial organization of chromatin and chromosomes. *Nucleus* **13**, 277–299.
- Roudier F, Ahmed I, Berard C, et al.** 2011. Integrative epigenomic mapping defines four main chromatin states in *Arabidopsis*. *The EMBO Journal* **30**, 1928–1938.
- Sabelli PA, Larkins BA.** 2009. The development of endosperm in grasses. *Plant Physiology* **149**, 14–26.
- Sanei M, Pickering R, Kumke K, Nasuda S, Houben A.** 2011. Loss of centromeric histone H3 (CENH3) from centromeres precedes uniparental chromosome elimination in interspecific barley hybrids. *Proceedings of the National Academy of Sciences, USA* **108**, E498–E505.
- Santos AP, Shaw P.** 2004. Interphase chromosomes and the Rabl configuration: does genome size matter? *Journal of Microscopy* **214**, 201–206.
- Schubert I, Shaw P.** 2011. Organization and dynamics of plant interphase chromosomes. *Trends in Plant Science* **16**, 273–281.
- Schubert V.** 2009. SMC proteins and their multiple functions in higher plants. *Cytogenetic and Genome Research* **124**, 202–214.

- Schubert V, Klatte M, Pecinka A, Meister A, Jasencakova Z, Schubert I.** 2006. Sister chromatids are often incompletely aligned in meristematic and endopolyploid interphase nuclei of *Arabidopsis thaliana*. *Genetics* **172**, 467–475.
- Sequeira-Mendes J, Aragüez I, Peiró R, Mendez-Giraldez R, Zhang X, Jacobsen SE, Bastolla U, Gutierrez C.** 2014. The functional topography of the Arabidopsis genome is organized in a reduced number of linear motifs of chromatin states. *The Plant Cell* **26**, 2351–2366.
- Shan W, Kubová M, Mandáková T, Lysak MA.** 2021. Nuclear organization in crucifer genomes: nucleolus-associated telomere clustering is not a universal interphase configuration in Brassicaceae. *The Plant Journal* **108**, 528–540.
- Sreenivasulu N, Altschmied L, Radchuk V, Gubatz S, Wobus U, Weschke W.** 2004. Transcript profiles and deduced changes of metabolic pathways in maternal and filial tissues of developing barley grains. *The Plant Journal* **37**, 539–553.
- Waddington SR, Cartwright PM, Wall PC.** 1983. A quantitative scale of spike initial and pistil development in barley and wheat. *Annals of Botany* **51**, 119–130.
- Wegel E, Shaw PJ.** 2005. Chromosome organization in wheat endosperm and embryo. *Cytogenetic and Genome Research* **109**, 175–180.
- Wegel E, Vallejos RH, Christou P, Stöger E, Shaw P.** 2005. Large-scale chromatin decondensation induced in a developmentally activated transgene locus. *Journal of Cell Science* **118**, 1021–1031.
- Young TE, Gallie DR.** 2000. Programmed cell death during endosperm development. *Plant Molecular Biology* **44**, 283–301.